TACTICAL WEAPON
GACIAC
GUIDANCE & CONTROL
INFORMATION ANALYSIS CENTER

GACIAC SOAR 91-01

LASER DAMAGE IN THIN FILM OPTICAL COATINGS

Prepared by Kent J. Kogler
IIT Research Institute

Published by GACIAC
IIT Research Institute
10 West 35th Street
Chicago, Illinois 60616-3799

Approved for Public Release
Distribution Unlimited

July 1992

NOTICES

State of the Art Review. This State of the Art Review has been published by the Tactical Weapon Guidance and Control Information Analysis Center (GACIAC) as a service to the defense community. GACIAC is a DoD Information Analysis Center, administered by the Defense Technical Information Center, operated by IIT Research Institute under Contract No. DLA-900-86-C-0022. GACIAC is funded by DTIC, DARPA and U.S. Army, U.S. Navy, and U.S. Air Force Laboratories/Controlling Activities having an interest in tactical weapon guidance and control. The Director of GACIAC is Dr. Robert J. Heaston. The Contracting Officer is Ms. Cheryl Montoney, DESC, Dayton, Ohio. The Contracting Officer's Technical Representative is Mr. Chalmer D. George, and the Alternate Representative is Mr. H.C. Race, AMC Smart Weapons Management Office, ATTN: AMSMI-SW, Redstone Arsenal, Alabama 35898-5222.

REPORT DOCUMENTATION PAGE

Form Approved
OMB No. 0704-0188

1. AGENCY USE ONLY (*Leave blank*)	2. REPORT DATE	3. REPORT TYPE AND DATES COVERED
	July 1992	State of the Art Review; 1984-1989.

4. TITLE AND SUBTITLE
Laser Damage in Thin Film Optical Coatings

5. FUNDING NUMBERS
DoD-DLA900-86-C-0022
PE 65802
PR 1.0

6. AUTHOR(S)
Kent J. Kogler

7. PERFORMING ORGANIZATION NAME(S) AND ADDRESS(ES)
IIT Research Institute/GACIAC
10 West 35th Street
Chicago, IL 60616-3799

8. PERFORMING ORGANIZATION REPORT NUMBER
GACIAC SOAR 91-01

9. SPONSORING/MONITORING AGENCY NAME(S) AND ADDRESS(ES)
U.S. Army Missile Command
Attn: AMSMI-SW
Redstone Arsenal, AL 35898-5222

10. SPONSORING/MONITORING AGENCY REPORT NUMBER

11. SUPPLEMENTARY NOTES
This document is available only from GACIAC, IIT Research Institute, 10 West 35th Street, Chicago, IL 60616-3799 (410948)

12a. DISTRIBUTION/AVAILABILITY STATEMENT
Approved for public release; distribution is unlimited.
This document is available only from GACIAC, IIT Research Institute, 10 West 35th Street, Chicago, IL 60616-3799. (410948)

12b. DISTRIBUTION CODE

13. ABSTRACT (*Maximum 200 words*)

This document has been prepared in the interest of aiding optical designers select laser damage resistant coatings for optical elements to be employed in military systems using lasers or encountering lasers used as weapons or countermeasures. It provides an extensive data base of damage thresholds for oxide, fluoride and chalcogenide single layer and multilayer coatings. The data base is supported by a detailed description of how the coatings were synthesized and how the measurements were performed to collect the damage threshold data. The basis from which the information was collected covers a period from 1984 through 1989.

The material reviewed includes investigation of causes of damage in optical coatings and approaches to reducing or eliminating damage mechanisms with the objective of raising damage thresholds. The information should be found useful in selecting coating materials and techniques for their synthesis or as a tool in evaluating the susceptibility of existing coated optical elements.

14. SUBJECT TERMS
Laser damage thresholds, Optical coatings, Thin film synthesis, Laser test procedures, Thin film, Oxides, Fluorides, Chalcogenides.

15. NUMBER OF PAGES
132

16. PRICE CODE
$100

17. SECURITY CLASSIFICATION OF REPORT	18. SECURITY CLASSIFICATION OF THIS PAGE	19. SECURITY CLASSIFICATION OF ABSTRACT	20. LIMITATION OF ABSTRACT
UNCLASSIFIED	UNCLASSIFIED	UNCLASSIFIED	UNCLASSIFIED

THIS PAGE IS INTENTIONALLY BLANK

GACIAC SOAR 91-01 JULY 1992

State of the Art Review

LASER DAMAGE IN THIN FILM OPTICAL COATINGS

Kent J. Kogler

Published by GACIAC
IIT Research Institute
10 West 35th Street
Chicago, Illinois 60616-3799

GACIAC - A DoD Information Analysis Center
Operated by IIT Research Institute, 10 West 35th Street, Chicago, Illinois 60616-3799
DoD Technical Sponsor-Joint Service Guidance and Control Committee
Members from OSD, Army, Navy, Air Force and DARPA

PREFACE

Thin film coatings find applications in a wide variety of optical components and in particular, play an important role in optical sensors employed for guidance and control. Depending on the specific application, they may be designed to minimize reflectance over a broad optical bandwidth (AR coatings), they may enhance or replace metallic mirrors at a particular wavelength (HR coatings) or they may block or transmit desirable wavelength bands (passband or rejection band filters). By a proper choice of materials they may also provide a protective layer from the environment, shielding IR windows and domes from mechanical and chemical damage.

Since the laser has been introduced as a weapon for countering optically guided and controlled sensor systems, an additional performance parameter has been added to the list of characteristics defining good coating designs. The laser damage threshold of the coating material is a key parameter in determining the vulnerability of the guidance and control sensor. Due to the critical need of this information in predicting system vulnerability, a state-of-the-art review identifying thin film materials for which damage thresholds have been measured is highly desirable. To be confident the threshold is applicable to a given analysis, it is essential that the conditions of the measurement are well documented. Equally important is that the coating measured is similar in design, composition and morphology to that for which the data is to be applied. Accurate documentation of this information allows a valid comparison, an estimation of possible error, or a prediction based on established scaling laws.

The review pursued in this document attempts to compile a collection of data on the damage threshold of commonly used optical coating materials consisting of oxides, fluorides and chalcogenides. The material is organized to allow the reader quick access to damage thresholds for particular coating materials of interest with instant retrieval of the laser measurement parameters. Immediate identification of the coating synthesis process allows assessment of the relevance of the data to the coating being analyzed. The page in this document on which the data is presented is cited along with the reference from which it was extracted. The reference is summarized prior to the data presentation to describe in further detail how the coating was fabricated and specifically the damage threshold measurement technique.

The data base for the information reviewed is the "Proceedings Of The Laser Induced Damage In Optical Materials" Symposia sponsored by the National Institute of Standards and Technology, The American Society For Testing and Materials, Defense Advanced Research Project Agency and the Department of Energy. The proceedings are published annually by the U.S. Department of Commerce/National Institute of Standards and Technology. The data presented is copied directly from the symposia without alteration. In most instances, the motivation for measurement of damage thresholds has been different than that identified in this preface. However, the basic data is relevant to a variety of applications and generally would have been collected by identical techniques regardless of the application. It is the intent of this document to provide a ready and useful source of information reviewing the state-of-the-art in laser damage research in optical coatings and to provide a relevant collection of data establishing the damage threshold of commonly used optical coatings materials.

CONTENTS

FIGURES

FIGURES (Continued)

FIGURES (Continued)

FIGURES (Continued)

FIGURES (Continued)

FIGURES (Continued)

TABLES

TABLES (Continued)

1. INTRODUCTION

The application of thin film coatings in optical systems is varied and has become a necessity in achieving high performance. Typical applications involve enhancing reflectance from or transmission through an optical surface, selecting a transmitted or reflected polarization, selecting a transmitted or reflected spectral band and improving the mechanical and environmental tolerance of an optical surface. The prolific use of lasers in optics, particularly in applications in which high power densities and large pulse energies are employed, has created an interest in the study of thin film materials and designs tolerant of these levels. There is an increasing need to determine the threshold of damage, understand the mechanism of damage and to determine how damage thresholds can be increased by improving specific properties of the film and employing design principles which reduce susceptibility to damage.

Thin film materials typically exhibit characteristics which differ from their bulk counterparts. Many of these differences are due to dissimilar structure and in some cases unlike composition. These differences arise from the variety of synthesis techniques and variations thereon being used. Techniques commonly used include thermal evaporation, ion beam deposition, RF sputtering, plasma deposition, photochemical deposition, molecular beam epitaxy, the sol-gel process, chemical etching and plating. Each of these processes produces structures and sometimes chemical compositions at the atomic level which can differ from one another as well as from the bulk materials. Films deposited by thermal evaporation often grow as columns. These films contain a reasonably high evidence of defects which can be sites at which damage originates. Strain is also common in thermally evaporated coatings which can lead to cracking and delamination, particularly in layered films of more than one material. The more refractory materials, such as the oxides can only be evaporated using an electron beam or ion beam process. While these coatings are hard, adherent and amorphous, they often contain pinholes. Some techniques, such as RF sputtering, plasma deposition and molecular beam epitaxy inherently have low deposition rates creating more dense uniform coatings with fewer defects. Molecular beam epitaxy offers potential for minimizing defects by growth of single crystal films. Absence of grain boundaries and impurity absorption associated with them, as well as elimination of surface roughness replication, is

hoped to remove sources of damage initiation. Plasma deposition has found application in depositing hard durable coatings such as diamond like carbon films. Plasmas have also been used along with other processes to provide added energy at the substrate surface to increase atomic mobility reducing vacancy sites. Sol-gel processes involve chemical reactions at the substrate surface. Films synthesized by this process may have high porosity due to vaporization of solvents. Such porosity may reduce stress but also harbors contaminants.

In general, thin film materials exhibit greater absorption than their bulk counterparts, contributing to a reduced damage threshold. This higher absorption can be attributed to impurities or contaminants in the film related to the deposition process, exposure to the atmosphere, inadequate cleaning of the substrate prior to deposition or introduced in handling, shipping and storage.

In addition to properties of the material, the particular thin film design plays an important role in a coating's susceptibility to damage. In particular, the electric field inside the film or combination of films is related to the intensity of the light wave, its wavelength, the refractive indicies of the film materials and their thickness. If the film design allows the peak fields to occur at discontinuities between dissimilar materials, the potential for damage is enhanced. Designs which place the field maxima inside the layers, especially the low index layer, and minimize the field at the interfaces can substantially increase the damage threshold. This may be achieved by graded index designs and non quarter-wave designs.

The following review of the current state-of-the-art is pursued to assess damage thresholds of commonly applied thin film optical materials, to identify synthesis techniques which have potential for improving damage thresholds and to identify characteristics of thin film materials which degrade damage thresholds so that such characteristics can be avoided or corrected. The review is organized by material types. Section 2 addresses oxide coatings, Section 3 addresses fluoride coatings and Section 4 addresses chalcogenides and multilayers of chalcogenides and fluorides. Providing damage threshold data is the prime motivation. However, the relevance of the data to a particular application requires an understanding of how the measurement was made, particular details of the laser used and a description of how the film was synthesized. This information is also documented in the review. The films studied have a variety of applications including HR, AR coatings and beam splitters. In most instances, they have been synthesized specifically for the purpose of improving damage threshold or examining some particular synthesis technique, post synthesis treatment, or design as a potential means of improvement.

The data base is the Boulder Damage Symposia for the years 1984 through 1989. As an aid to finding damage threshold data for single layer coating materials or multilayers, the following index is provided. The index may be used to identify damage data corresponding to a particular process by which the coating was synthesized, a particular laser wavelength and corresponding test conditions. Comments relevant to the various test parameters considered and analyses performed in the reference article from which the data was extracted are also sited. The pages in this review on which the laser damage data appears are identified. A detailed summary of each reference follows the index and the specifics of the reference are itemized in the bibliography.

Thin Film Coating Laser Induced Damage Threshold Index (page 1 of 7)

Ref.	Materials	Test, λ (μm)	Spot Size	Test Format	PW	PRF (HZ)	Description of Synthesis	Damage Thresholds (Page)	Comments
					Physical Deposition Processes for Oxide Coatings				
1	Ta_2O_5/SiO_2 ZrO_2/SiO_2 HfO_2/SiO_2	1.06	15 μm- 2 cm	1 on n	2-85 ns	760	E-beam evaporation Thermal evaporation (CO_2 laser) Reactive evaporation	13	Varied substrate temperature, 0_2 partial pressure, substrate cleaning. Assessed improvement in damage threshold due to SiO_2 overcoat.
2	SiO_2 TiO_2 Ta_2O_5 ZrO_2/SiO_2	1.06	44 μm	1 on 1	10 ns	Single pulse	E-beam evaporation Thermal evaporation	14	Varied film thickness. Assessed effects of film thickness and SiO_2 and Al_2O_3 overcoats on damage threshold.
3	TiO_2	1.06	0.35- 1.05 mm	--	--	--	E-beam evaporation (ion assisted)	19	Varied ion discharge current deposition rate, partial pressure, and substrate temperature. Related differences in processing parameters to refractive index, absorption coefficient, and damage threshold.
4	TiO_2 ZrO_2	1.06	--	--	3 ms	Microsec subpulse peaks	Not reported	20	Studied effects of repeated pulsing on damage threshold and related damage to film microstructure; assessed improvement due to overcoat.
5	TiO_2/SiO_2 Ta_2O_5/SiO_2 ZrO_2/SiO_2	1.06 0.532	0.5- 0.8 mm	1 on 1	15 ns	Single pulse	Reactive ion plating deposition	21	RMS roughness of substrate was related to damage threshold
6	ThO_2 MgO Y_2O_3 HfO_2 Sc_2O_3 CeO_2	1.06	300- 500 μm	1 on 1 n on 1	5-14 ns	1 shot/ min	E-beam evaporation	21	Evaluated charge emission as precursor to laser induced damage; related damage threshold to substrate conductivity.

Ref.	Materials	Test, λ (μm)	Spot Size	Test Format	PW	PRF (HZ)	Description of Synthesis	Damage Thresholds (Page)	Comments
	Al_2O_3 SiO SiO_2 ZrO_2 TiO_2 ThF_4 MgF_2 YF_3 HfF_4 ScF_3 CeF_3 AlF_3 LaF_3 Na_3AlF_6 NaF ZnS								
7	MgF_2 SiO_2 TiO_2/SiO_2 ZrO_2/Ta_2O_5 Sc_2O_3/SiO_2	0.355 (tripled YAG) 1.06 0.248	1.0 mm	1 on 1	0.6 ns 1 ns 20 ns		E-beam deposition (box coater)	27	Damage threshold improvement of half wave overcoats compared at three wavelengths; λ = 1,064, 355, 248 nm.
8	HfO_2/SiO_2 ZrO_2/SiO_2 TiO_2/SiO_2	1.06	~ 1 mm	1:1 N:1 S:1 R:1	1-16 ns 10-16 ns 8 ns	Single shot 10, 15, 30 18	E-beam evaporation Ion beam sputtering Plasma plating	29	Studied effects of laser conditioning on damage threshold for different materials, deposition techniques and thin film designs.
9	HfO_2/SiO_2 ZrO_2/SiO_2	1.06	0.2 mm 4.0 cm	S:1 R:1	8 ns	18	E-beam deposition	32	Compared raster scan approach using small spot to condition film with conditioning using a larger film diameter.
10	MgF_2/Al_2O_3 Al_2O_3/ZrO_2	1.06	0.25-1.00 mm	R:1	15 ns	1	E-beam deposition	39	Studied effects of spot size on effectiveness of conditioning in improving damage threshold.

Thin Film Coating Laser Induced Damage Threshold Index (page 3 of 7)

Ref.	Materials	Test, λ (μm)	Spot Size	Test Format	PW	PRF (HZ)	Description of Synthesis	Damage Thresholds (Page)	Comments
					Chemical Deposition Processes for Oxide Coatings				
11	HfO_2/SiO_2 ZrO_2/SiO_2 Al_2O_3/SiO_2 ZrO_2	1.06	1 mm	1 on 1 n on 1	16 ns	30	Sol Gel process	48	Compared damage thresholds derived from 1 on 1 test format with those derived from n on 1 test format.
12	Al_2O_3 ZrO_2 HfO_2 SiO_2 TiO_2	1.06	--	1 on 1	16 μs 10 ns	120 Single pulse	Sol Gel (with precursor) Sol Gel (with colloid)	48	Compared damage thresholds of films prepared by spinning colloidal suspensions with films prepared by depositing a precursor.
13	ThO_2/SiO_2 ThO_2	1.06 0.350	--	--	1 ns 3 ns	Single pulse Single pulse	Sol Gel process	53	Determined damage thresholds of multi-layers deposited by spinning colloidal suspensions.
14	Al_2O_3 HfO_2 ZrO_2	1.06	--	1 on 1	10 ns	Single pulse	Chemical vapor deposition Thermal decomposition (high temp.) Thermal decomposition (low temp.) Chemically assisted deposition (low temp.)	56	Compared damage thresholds of films prepared by thermal decomposition, chemically assisted deposition, and Sol Gel process.
15	ZrO_2/SiO_2 (codeposited) ZrO_2 SiO_2	--	--	--	--	--	Ion beam sputtering	57	Stress compensation studied by adjusting mixture of components.
16	SiO_2	0.350	--	--	25 ns	30	Sol Gel process	57	Post deposition treatment (UV light, ozone) to improve damage threshold.
17	TiO_2 TiO_2/SiO_2	1.06	3 mm	1 on 1	1 ns	--	Chemical vapor deposition	58	Damage thresholds of single layer and multilayer coatings synthesized by CVD were measured.

Thin Film Coating Laser Induced Damage Threshold Index (page 4 of 7)

Ref.	Materials	Test, λ (μm)	Spot Size	Test Format	PW	PRF (HZ)	Description of Synthesis	Damage Thresholds (Page)	Comments
					Comparison of Physical and Chemical Deposition Processes for Oxide Coatings				
18	Al_2O_3 Ta_2O_5 TiO_2 HfO_2 ZrO_2	1.06	710 μm	1 on 1	7 ns	Single pulse	E-beam deposition Reactive sputtering Sol Gel	58	Effects of post annealing were studied using CO_2 laser as heat source.
19	CaF_2 SiO_2 Ta_2O_5 TiO_2 ZrO_2 HfO_2 Nb_2O_5 and multi-layers of the above with SiO_2	1.06	0.5-1.0 mm	n on 1	16 ns	6-120	E-beam deposition Sol Gel process	63	Data base being accummulated at using facility.
20	SiO_2 Doped with Ge and/or F	1.06	1 mm	N:1	16 ns	30	Plasma impulse chemical vapor deposition (PICVD)	66	Low concentrations of dopants are introduced in a CVD deposition process to create interference layers exhibiting very low defect concentrations and few contaminants.
21	Al_2O_3 SiO_2	1.06	1 mm^2	5:1	16 ns	30	Sol-gel process	67	Damage thresholds were measured on HR coatings prepared from alternating layers of colloidal suspensions.
22	ZrO_2 ZrO_2/SiO_2	1.06	2.0 mm	1-on-1 R-on-1	3 ns	Single shot	Sol-gel process including soluble inorganic binder	69	An inorganic binder was used to increase refractive index and improve abrasive resistance.

Thin Film Coating Laser Induced Damage Threshold Index (page 5 of 7)

Ref.	Materials	Test, λ (μm)	Spot Size	Test Format	PW	PRF (HZ)	Description of Synthesis	Damage Thresholds (Page)	Comments
					Other Relevent Issues for Oxide Coatings				
23	Al_2O_3/SiO_2 HfO_2/SiO_2 Sc_2O_3/SiO_2 Ta_2O_5/SiO_2 TiO_2/SiO_2 ZrO_2/SiO_2 MgF_2 Na_3AlF_6	0.790 (Alexandrite)	.380 mm	1 on 1	200 ns	30	Eight different AR coatings were acquired from seven different vendors; deposition processes were not identified	71	Studied damage thresholds of various AR coatings on sapphire substrates to optimize coatings for Alexandrite laser rods.
24	Al_2O_3/SiO_2 Sc_2O_3/SiO_2 HfO_2/SiO_2	.351 (XeF) .355 (frequency doubled dye)	.44 mm .71 mm .72 mm .44 mm	--	9 ns 26 ns 54 ns 625 ns	35 35 35 0.5	Narrowband and broadband reflectors and AR coatings were acquired from four vendors; deposition techniques were not identified	71	Determined damage threshold.
25	TiO_2 Ta_2O_5 ZrO_2 HfO_2 Al_2O_3 SiO_2	1.06	300 μm	--	14 ns		Deposition process not identified	78	Compared measured damage thresholds to absorption model and inclusion model.
26	PbF_2/ZnS Th_4F/ZnS $PbF_2/ZnSe$ $ThF_4/ZnSe$ SiO_2/TiO_2 ZrO_2/SiO_2 TiO_2/SiO_2	1.315 (atomic iodine)	2.8 mm	1 on 1	8 μs	Single pulse	HR coatings were acquired from several vendors; deposition processes were not identified	80	Coatings were procured from a variety of vendors and consisted of a variety of designs.
27	HfO_2/SiO_2 Al_2O_3/SiO_2	0.351 0.248	0.2x0.8 mm	N:1	23 ns	50	Not given	80	Measured angular dependence of damage threshold.

Thin Film Coating Laser Induced Damage Threshold Index (page 6 of 7)

Ref.	Materials	Test, λ (μm)	Spot Size	Test Format	PW	PRF (HZ)	Description of Synthesis	Damage Thresholds (Page)	Comments
					Fluoride Single Layers				
28	BaF_2	1.06 10.6	0.7 mm	1 on 1	15 ns	Single pulse	Ionized cluster beam deposition Thermal evaporation	90	Compared damage thresholds of films deposited by conventional thermal evaporation with films deposited by ion cluster beam deposition.
29	SiO_2/NaF	1.053 0.527 0.355	400 μm	1 on 1 n on 1	1 ns 1 ns 0.4 ns	Single pulse	Dual source thermal evaporation NaF dissolved in water to achieve graded index SiO_2 AR coating	92	Compared damage thresholds of porous AR coatings to multilayer AR coatings.
30	Al_2O_3 SiO_2 NaF AlF_3 MgF_2 GdF_3 LaF_3 NdF_3 YF_3	0.193	0.65 mm^2 (elliptical)		25 ns		E-beam evaporation Ion beam sputtering Thermal evaporation	92	Damage thresholds were composed relative to fabrication technique, resulting optical characteristics and microstructure.
					Chalcogenides and Chalcogenide/Fluoride Multilayers				
31	ZnSe/ThF_4	2.7 3.8	150 μm 500 μm	1 on 1	1 μs	Single pulse	Thermal evaporation	96	Studied post damage morphology to assess causes of damage. Compared films deposited with electrostatic filtering of vapor stream with films deposited with no filtering.
32	ZnSe ZnS	10.6	180 μm 200 μm	1 on 1	33 ns (1700 ns tail) 340 ns	Single pulse	Molecular beam deposition using Knudsen cells (ultra high vacuum)	98	Compared damage threshold of films deposited by UHV with damage threshold of films deposited at conventional pressures.

Thin Film Coating Laser Induced Damage Threshold Index (page 7 of 7)

Ref.	Materials	Test, λ (μm)	Spot Size	Test Format	PW	PRF (HZ)	Description of Synthesis	Damage Thresholds (Page)	Comments
33	ZnS	10.6	>6.9 mm	n on 1		100 ns (2 μs tail)	Thermal evaporation E-beam evaporation	100	Compared effects of deposition process, AR efficiency, substrate type and perfection, and substrate temperature on damage threshold.
34	Zn/ZnSe ZnS_xSe_{1-x} ZnS ZnSe	10.6	100 μm	1 on 1	32 ns (1700 ns tail)	Single pulse	Molecular beam deposition Ultra high vacuum	102	Compared multicomponent graded index films, alloyed films, and single component films of the same materials with respect to damage thresholds.
35	Th_4 Th_4F	10.6	2.73 mm (tests 1-4) 1.06 mm (tests 5-48)	n on 1	35 μs	1 Hz	Thermal evaporation E-beam deposition	105	Several AR coatings of different designs on CdTe substrates synthesized by different techniques and variables were compared and relative damage thresholds measured.
36	ZnS/BaF_2 $ZnSe/BaF_2$	1.06	59 μm	1 on 1	10 ns	Single pulse	Molecular beam deposition Ultra high vacuum	108	Evaluated effect of peak electric field at interfaces relative to impurities at interfaces in inducing damage.
					Comparison of MBE and CVD Deposition Process				
37	BaF_2 PbF_2 $(BaPb)F_2$ $PbF_2/ZnSe$ PbF_2/BaF_2 BaF_2/ZnS PbF_2/ZnS	10.6	100 μm	1 on 1	33 ns	Single pulse	Thermal evaporation-Knudsen source (ultra high vacuum) Chemical vapor deposition	110	Varied deposition rates. Varied substrate temperatures. Assessed effects of surface morphology on damage threshold.
					Other Relevent Issues for Chalcogenide/Fluoride Multilayers				
38	$ZnSe/ThF_4$	10.6	60 μm	--	230 ns	--	Deposition process not identified	113	Related damage threshold to film morphology.

2. OXIDE COATINGS

Oxide coatings have been much exploited for optical applications due to their spectral range of transmission extending from the ultraviolet to the near-infrared. They are of particular interest in laser applications due to their refractory nature and offer additional desirable characteristics such as: (1) being thermally and chemically stable and environmentally durable; (2) being excellent diffusion barriers, particularly at multilayer interfaces; (3) having been more thoroughly studied and more understandable than other compounds of interest. The oxides are generally compatible with other optical materials allowing deposition on a variety of substrates and the fabrication of multilayer stacks with other desirable thin film materials such as the fluorides. Oxides have also been used as multilayers on such stacks to improve environmental resistance and through judicious design, have been applied to adjust the electric field distribution of the light wave in the stack so as to increase its damage threshold. Certain oxides, such as Al_2O_3, are resistant to moisture and fluorine and are compatible with high index materials such as AlN, allowing multilayer AR coatings to be fabricated on excimer laser windows. These materials have been prepared with indicies of refraction which allow for production of near zero reflectance and very low losses.

To obtain oxide films of the desired stoichiometry, adhesion, environmental durability, and optical properties, a variety of synthesis techniques are employed, including thermal and electron beam evaporation, RF and ion beam sputtering, ion assisted deposition, chemical vapor deposition and the sol-gel process. Thermal and sputtering techniques commonly involve the introduction of a low pressure oxygen background to the chamber to adjust the stoichiometry. The sputtering techniques are of particular interest since they lead to dense low scatter coatings with indicies closer to bulk values. Ion assisted deposition has been explored as a means of significantly influencing film growth and resulting film properties by providing energy and momentum to the growing film by way of bombardment with a beam of ions. The ion beam increases adatom mobility and eliminates the formation of a columnar microstructure resulting in more dense, less porous films exhibiting higher refractive indicies. This process has been shown to reduce scatter, improve environmental stability, modify stress, and improve stoichiometry.

In certain applications, oxides are mixed during the film formation. For instance, it has been found to be beneficial to add a small component of SiO_2 when depositing TiO_2 films to inhibit crystallization. The microstructure of TiO_2 thin films in the absence of SiO_2 is easily

modified under the influence of heat resulting in crystallization which destroys the optical utility of the film by increasing the scattering loss and the effective extinction coefficient. Other applications of mixed oxides are the creation of indicies not inherent to optical coating materials in their pure form. By varying the oxide mixture during deposition, continuously varying or graded indicies have been achieved to realize AR coatings and HR rugate filters.

Porous silica coatings were developed in response to the need for damage resistant coatings at ultraviolet wavelengths and have been applied to optical elements of large apertures (on the order of 1 meter). Such coatings are made by a sol-gel process in which the coating is derived from a precursor material spun on the substrate and subsequent chemical reaction. Oxides other then silica may be formed from different precursor materials. Such porous films are also being applied to longer wavelength applications (1064 nm). The index of the coating can be adjusted by varying the porosity. In addition to homogeneous indicies, AR coatings can be made by continuously varying the porosity and HR and AR coatings can be made by depositing multilayers of different porosities eliminating differences of physical properties of dissimilar materials at multilayer interfaces.

Coatings fabricated by the above processes have been subjected to different types of post deposition processes such as heat treatments in air and vacuum, ion bombardment and laser annealing. Such treatments have been explored as means to improve the optical properties and damage thresholds of single and multilayer coatings. It is anticipated that such processes allow annealing of defects at which damage initiates and from which light is scattered. Improvement has been found to depend upon the material and details of the synthesis process.

Section 2.1 is a review of work performed to assess the damage thresholds of oxide coatings deposited by physical deposition processes including thermal evaporation, E-beam evaporation, RF and ion beam sputtering, and ion beam and molecular beam processes. Research performed to determine damage thresholds of coatings deposited by chemical processes are discussed in Section 2.2. In Section 2.3 damage thresholds are compared by workers who have synthesized coatings by both processes. The work reviewed in Section 2.4 does not specify how coatings were deposited, but assesses the influence of a variety of other factors on damage threshold, such as thin film design, influence of substrate, and angular dependance of the incident beam.

A variety of other issues influencing damage threshold are discussed in each reference. It has been chosen to organize the references reviewed in terms of deposition process and not to try

and combine work of various authors in categories corresponding to the many issues which influence damage threshold. The principal motivation has been to preserve the continuity of technical discussion and background provided by each author to assure credibility and relevance to the damage threshold data presented by each reference.

2.1 PHYSICAL DEPOSITION PROCESSES

The influence of the deposition process of refractory oxides and silicon dioxide on the damage threshold of single and multilayer systems has been examined by Fai Zullov, et. al. (Ref. 1). Ta_2O_5, ZrO_2 and HfO_2 were studied as materials for high index layers and SiO_2 was studied as the low index layer. A comparison was made of damage thresholds for films deposited by E-beam evaporation and films deposited by laser thermal evaporation (200 watt CO_2 laser). For the latter, absorption and the number of defects was found to increase and the damage threshold to decrease with distance in the film from the melt crater on the evaporant target. Films were deposited in a reactive oxygen environment to achieve correct stoichiometry. Laser evaporation was anticipated to avoid contamination associated with conventional evaporation. Both single layer films and HR and AR stacks were examined. Fused silica substrates were used. The influence of oxygen partial pressure during deposition, substrate temperature, laser cleaning of the substrate and damage spot size was examined. Increasing oxygen partial pressure was found to improve the damage threshold and increasing the substrate temperature was found to decrease the damage threshold of single layer coatings. The HfO_2 coatings were found to have maximum damage thresholds with large variations in thresholds from site to site. While thresholds were lower for Ta_2O_5, the spread was not as large. Laser cleaning of the substrate was found to significantly improve the damage threshold of single layer films (a factor of 10 x for ZrO_2). However, for multilayer films, the improvement diminished with the number of layers since most of the radiation was reflected in the stack before reaching the substrate surface.

The deposition of a halfwave silica overcoat was found to improve the damage threshold of multilayer films. While one possible explanation is stress compensation, another explanation is presented based on absorption of energy in the halfwave silica layer which acts also a heatsink to reduce the temperature of the underlying layer. This approach has resulted in HR ZrO_2/SiO_2 and HfO_2/SiO_2 stacks exhibiting damage thresholds close to that of pure optical glass, i.e., 400 J/cm^2. Damage thresholds for 2 cm diameter spots and 2nsec pulses at λ = 1.06 μm resulted in damage thresholds of 5 to 7.5 J/cm^2.

The following damage data presented in Figures 1 to 5 was generated using three different lasers all operating in the TEM_{00} transverse mode: (1) a passively Q-switched Nd-glass laser with pulse width of 2 to 30n sec with spot sizes of 60 microns to 2 mm (some measurements involved 2 cm spot sizes); (2) a Nd-glass laser with pulse duration of 25 nsec and focal spot size of 85 microns; (3) an acousto-optically switched Nd:YAG laser with pulse width of 85 nsec and spot size of 15 microns with energy density up to 500 J/cm^2 at the sample surface.

Damage measurements were made by scanning the samples line by line using a PRF of 760 Hz without overlapping irradiated spots producing 150 sets of data per line at constant energy density. Power was reduced in each line until no coating damage occurred. The number of damage sites was determined by examination with an optical microscope to measure damage probability as a function of energy density. In the figures, D_0 and D_1 correspond to damage probabilities of 0 and 1 respectively.

The dependence of damage threshold on film thickness was studied for E-beam and thermally evaporated coatings by Zhouling, et. al. (Ref. 2). It was found that for irradiation with a Nd:YAG laser (10n sec pulse width), SiO_2 single layer films showed no thickness dependence nor did TiO_2 and Ta_2O_5 after correcting for differences in internal field strength. However, ZrO_2 showed a thickness dependence even after correction for the standing wave field. It was also ascertained that the damage threshold improvement by using SiO_2 overcoats and Al_2O_3 undercoats has a strong dependence on film thickness. The damage threshold of ZrO_2/SiO_2 HR coatings improved by 80% with a half wave overcoat and 300% with a three wave overcoat.

The absence of thickness dependence of TiO_2, Ta_2O_5 and SiO_2 single layers is accredited to the substrate interface absorption dominating over the bulk and air-film interface absorption, that being the direct cause of laser damage. In ZrO_2, total absorption losses and impurity sizes are thought to increase with film thickness and thus the damage threshold decreases.

The improvement in damage threshold due to overcoats is related to improved surface morphology and interface structure resulting in smoother films and finer microstructure. However, their seems to be an upper limit, on the order of 3 to 3-1/2 waves, at which stress cracks the film, greatly reducing the damage threshold. For undercoated AR coatings, improvements are thought to be related to a better film-substrate interface.

Data on deposition method, refractive index and absorption is provided in Table 1. The data presented in Tables 2 through 4 was obtained with a Q-switched Nd:YAG laser run in the TEM_{00} mode with a 10n sec pulse width and 44 micron spot size. A one on one test, format was

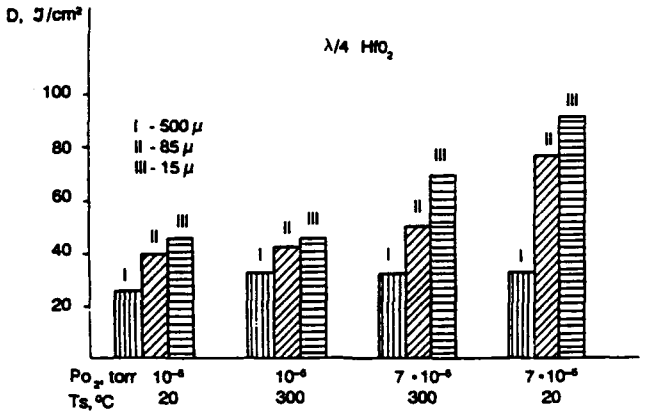

Figure 1. Dependence of damage threshold, D, of λ/4-thick HfO_2 single-layer coating on the size of radiation spot, ϕ, at different pressures of oxygen, P_{02}, in vacuum chamber, and different substrate temperatures, T_s. ϕ = 500 (I), 85 (II), 15 μm (III); $P_{01} = 1.10^{-5}$ (1,2), 7.10^{-5} Torr (3,4); T_s = 20 (1,4), 300°C (2,3).

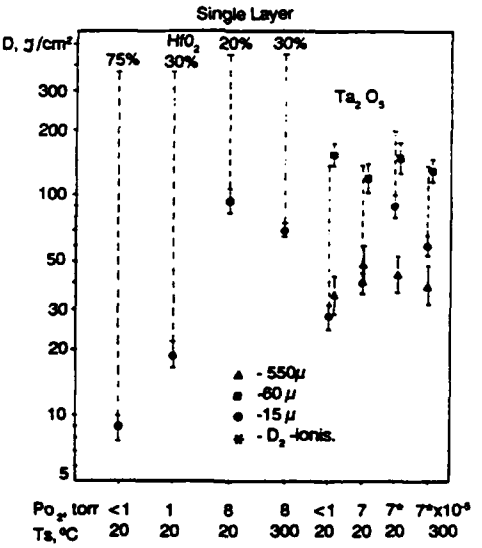

Figure 2. Dependence of damage threshold, D, of λ/4-thick HfO_2 and Ta_2O_5 single-layer coatings on the oxygen pressure, P_{02}, at different temperatures at 0 = 15 μm. T_s = 20 (1-3,5-7), 300°C (4,8); * - ionized oxygen.

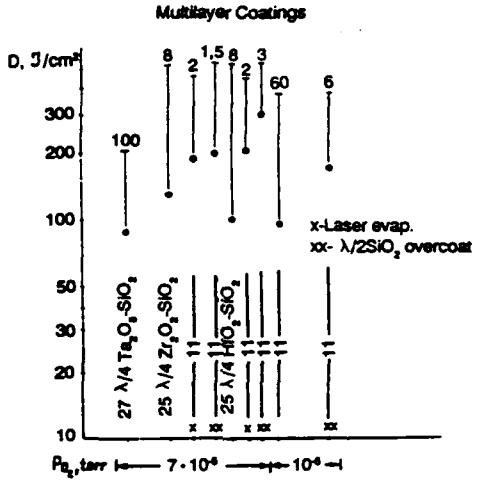

Figure 3. Damage thresholds of multilayer coatings produced by e-beam and laser (X) evaporation methods: 1-27 λ/4 Ta_2O_5-SiO_2, 2-25 λ/4 ZrO_2-SiO_2, 3-25 λ/4 HfO_2-SiO_2, (P_{O2} = 7.10^{-5} Torr), 4-25 λ/4 f_2-SiO_2 (P_{O2} = 10^{-5} Torr); **) - coatings with halfwave silica overcoat.

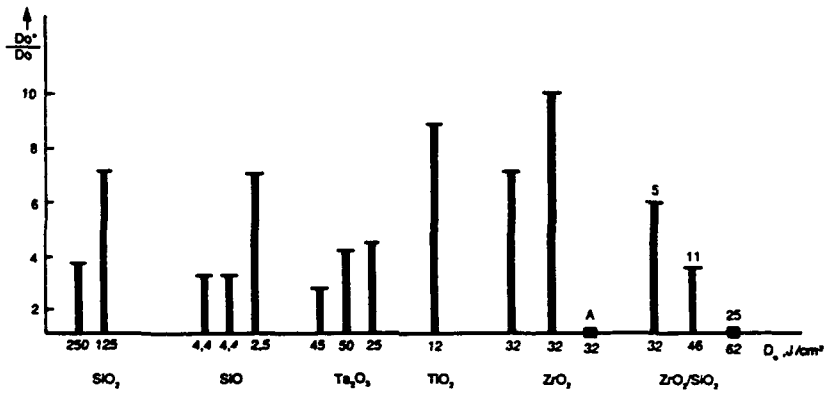

Figure 4. Increase in the damage thresholds of coatings D*/D due to preliminary treatment of substrate with CW CO_2-laser radiation (P = 100 W, 0 = 10 mm).

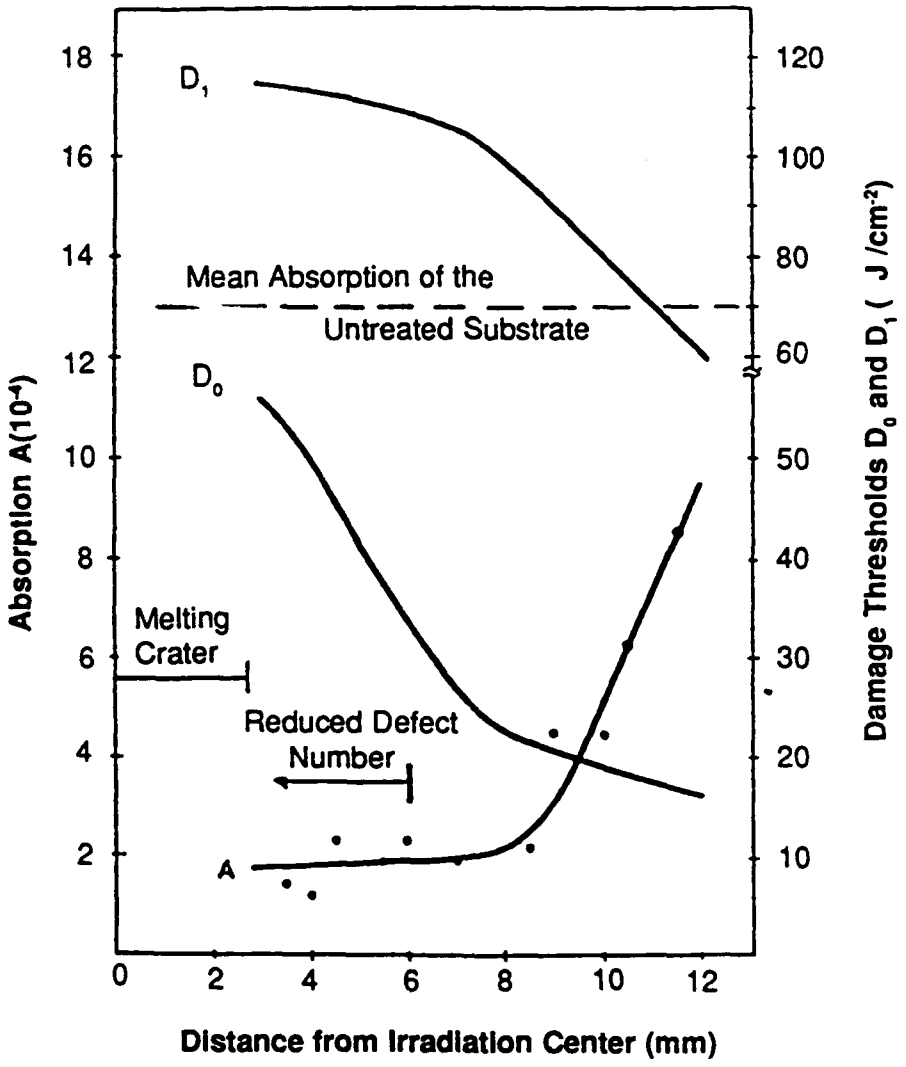

Figure 5. Distribution of absorption and damage threshold of quarter-wave single-layer TiO_2 coating in CO_2-laser irradiated region.

Table 1. Absorptance, Refractive Index, and Deposition Method of the Coatings Investigated (G: K9, λ: 1.06 μm)

Material	Absorptance (10^{-4})			Refractive Index	Deposition Method
nd:	λ/2	λ	3λ/2		
SiO_2	2.1	2.3	2.0	1.46	EB evaporation T = 250°C P = (2 - 3) x 10^{-5} torr
TiO_2	8.2	8.6	9.1	2.40	
Ta_2O_5	5.0	5.6	6.8	2.00	
ZrO_2	4.1	6.8	9.9	1.90	
ZnS	15.2	19.8	23.1	2.30	R evaporation
MgF_2	4.8	7.8	Cracked	1.38	
SiO_2 overcoat of ZrO_2/SiO_2 HR	6.0	6.5	5.8	1.46	EB evaporation T = 250°C P = (2 - 3) x 10^{-5} torr
SiO_2 overcoat of TiO_2/SiO_2 HR	7.8	7.6	8.0	1.46	
Al_2O_3 undercoat of SiO_2/TiO_2 AR	7.3	6.4	6.6	1.60	

EB = Electron Beam; R = Resistance; T = Substrate Temperature; P = Deposition Pressure.

Table 2. Standing-Field Corrected Damage Threshold (Jcm^{-2}) Dependence on Film Thickness of Single Layers (10 ns-1.06 μm-Nd:YAG Laser with Spotsize-44 μm)

Material	nd: λ/8	λ/4	λ/2	3λ/4	λ	5λ/4	3λ/2
SiO_2[a]	67.1±5.2	66.3±4.6	65.0±4.2	65.7±4.1	65.2±3.8	67.9±5.5	63.8±6.1
TiO_2	18.6±6.1	19.7±6.8	17.8±3.9		18.4±3.1		16.1±3.6
Ta_2O_2	18.3±3.74	20.1±3.5	19.8±4.1		19.3±4.3		17.8±4.5
ZrO_2	40.5±5.3	35.8±4.4	28.9±3.4		20.3±3.5		10.3±2.6
ZnS	19.8±3.8	16.2±4.1	10.9±3.2		8.4±1.2		6.3±1.0
MgF_2	53.6±6.1	48.3±4.8	30.1±3.6		5.6±3.2[b]		cracked

[a] Damage threshold data without standing-field correction.
[b] Cracks induced by stresses observable before damage testing.

Table 3. Damage Threshold (Jcm^{-2}) of HR Coatings on Film Thickness of SiO_2 Overcoats (10 ns-1.06 μm:YAG Laser with Spotsize-44 μm)

HR Material	Without Overcoat	nd of Overcoat: λ/2	λ	2λ	3λ	7λ/2	4λ
ZrO_2/SiO_2	14.1±2.8	25.8±3.2	30.5±2.9	46.3±3.8	55.2±4.0	53.8±3.6	16.3±3.1
TiO_2/SiO_2	12.6±3.5	22.5±2.6	28.3±3.6	37.6±4.2	42.8±4.5	26.4±4.8	9.5±3.4

Table 4. Damage Threshold (Jcm^{-2}) Dependence of AR Coatings on Film Thickness of Al_2O_2 Undercoats (10 ns-1.06 μm-Nd:YAG Laser with Spotsize-40 μm)

AR Materials	Without Undercoat	nd: λ/2	λ	3λ/2	2λ
SiO_2/TiO_2	4.8±1.4	5.6±2.3	8.3±2.1	10.4±2.1	10.3±2.3

used with 30 to 50 irradiations on each film sample. The damage threshold corresponds to the arithmetic mean value of the highest non-damage energy density and the lowest damage energy density, corresponding to a damage probability of 50%.

In work performed by Krishna, et. al. (Ref. 3), the effect of absorption on damage threshold was evaluated. Deposition parameters such as deposition rate, oxygen partial pressure, substrate temperature and discharge current of the Heitmann type oxygen ion source were varied to synthesize TiO_2 films. The films were deposited by evaporating TiO using E-beam in a low energy ion assisted deposition process. The refractive index, absorption coefficient and damage threshold were studied as a function of the deposition parameters. Films were deposited at ambient temperature and an oxygen partial pressure of 2×10^{-4} torr. The deposition rates were 9 nm/min and 18 nm/min. Discharge current was varied between 0 and 400 mA. The physical thickness of the films was 280 nm.

Increased ion discharge current increased oxygen content of the film, improved spectral transmission and lowered absorption. The refractive index changed insignificantly with an increase in discharge current for both rates of deposition. A slightly higher absorption was found for the higher deposition rate. For both deposition rates, the index and absorption coefficient decrease with increasing wavelength. An increase in index with deposition rate was attributed to an increase in packing density. The increase in absorption at shorter wavelengths is due to the intrinsic absorption edge of the material (at 380 nm). The films deposited at 200 mA were found to have

the lowest absorption coefficient and the highest laser damage threshold. Deposition rate did not affect the optical properties significantly.

The damage thresholds reported in Table 5 were measured using a Nd:YAG laser with spot diameters of 0.35 mm and 1.05 mm. Due to the large size of the spots, no difference was noted in damage threshold for either spot size.

Table 5. Measured Laser Damage Thresholds Studies

Rate of deposition: 9 nm/min Working pressure: 2×10^{-4} torr Laser used: Nd:YAG		
Discharge current (mA)	k (650 nm)	Power density J/cm^2
0	0.007	3.6
50		3.6
100	0	3.7
150		3.6
200	0	4.6
250	0	3.9
400	0.001	3.7

The damage threshold of refractory oxide films exposed to high energy pulses from a Nd:glass laser was measured by Zhengxiu, et. al. (Ref. 4). Single layer TiO_2 and ZrO_2 films were exposed to 3 m sec pulses having several hundred subpulse peaks of microsecond duration. It is thought that the laser induced damage in these films is due mainly to the amplitude of the pulse peak, however, repeated pulses accelerate the damage process. TiO_2 films were found to have degraded damage thresholds for repeated pulsing. The acceleration of damage by the repeated pulses depends on the intrinsic properties of the thin film. The damage threshold is related to the film structure, the smaller the grain, the higher the damage threshold. For ZrO_2 films, it was found that the damage threshold was also sensitive to the crystal structure being highest for cubic crystallinity and lowest for monoclinic crystallinity.

As in the work performed by Zhouling, et. al. (Ref. 2), it was found that overcoating of TiO_2/SiO_2 multilayers improved their damage threshold, the improvement being attributed to a

smoother surface morphology. Again, an upper limit of 2-1/2 waves thickness was observed beyond which the damage threshold dropped.

The data presented in Figures 6 and 7 and Tables 6 and 7 was obtained using a Nd:glass free vibration laser with maximum output of 1000 J. Pulses of several milliseconds with several microseconds fine structure were chopped by a narrow slit of variable width to adjust the exposure time.

Table 6. The Damage Resistance of ZrO_2 Thin Films with Different Crystallinity

Crystallinity	Amorphous	Cubic	Monoclinic
Damage threshold (j/mm^2)	19	36	14

Table 7. The Damage Resistance of ZrO_2/SiO_2 HR Multilayers with SiO_2 Overcoatings of Different Thickness

Thickness of SiO_2 overcoating (λ)	0	0.5	1	1.5	2	2.5	3	3.5
Damage threshold (j/mm^2)	8	10	14	25	31	36	30	20

λ = 1.06 μm

Guenther, et. al. (Ref. 5) performed 1 on 1 damage tests on multilayer refractory oxide coatings including SiO_2, TiO_2, Ta_2O_5 and ZrO_2 deposited on glass and BK-7 optical flats by reactive ion plating deposition. RMS roughness was in the range of 3.5 nm for the glass and 1-2 nm for the BK-7 flats. Damage measurements were made at 1064 nm with a 600 mJ output and at 532 nm with 160 mJ output. Exposures were with 20 mJ single pulses of 15 nsec duration (FWHM) using 0.5 mm spot size. Damage thresholds ranged from 7 J/cm^2 to >20 J/cm^2 varying with the design and materials. A particular ZrO_2/SiO_2 coating exhibited a threshold >40 J/cm^2. Tests performed with another Nd:YAG laser delivering 75 mJ/pulse in 9.8 nsec (FWHM) with a 0.8 mm spot size on Ta_2O_5 laser mirrors exhibited damage thresholds as high as 28 J/cm^2 on several sites and thresholds as low as 2.8 J/cm^2 on other sites. Poor polish of the substrates may have been the cause of the lower thresholds.

The potential use of charge emission as a nondestructive indicator of precursory laser induced damage was investigated by Kardach, et. al. (Ref. 6). Thermal properties of the film and substrate were also related to damage threshold. Twenty-two different half wave thick oxide and fluoride coatings were deposited by E-beam evaporation onto three different substrate materials

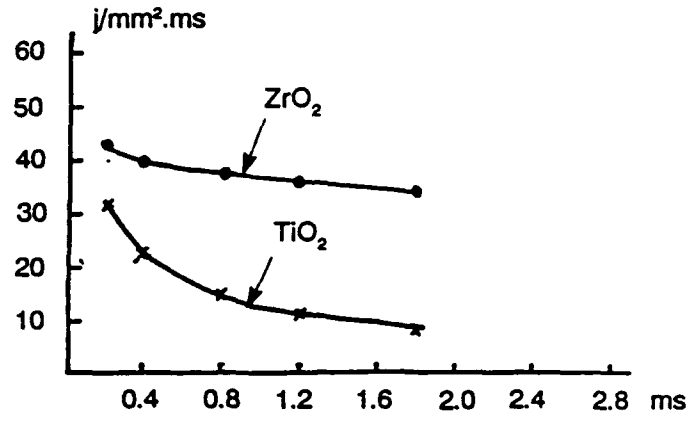

Figure 6. The Power Damage Threshold of the Optical Coating vs. Laser Acting Time.

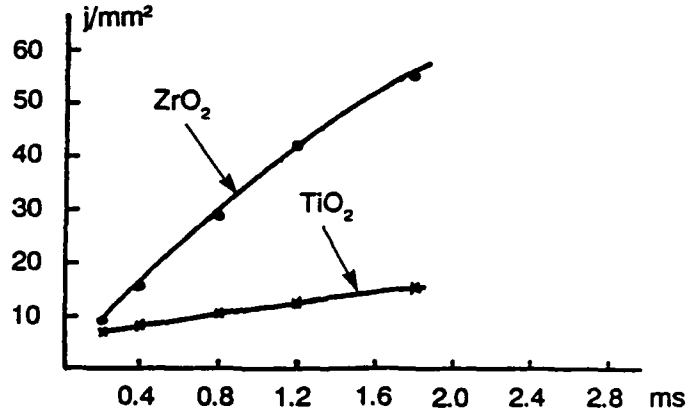

Figure 7. The Energy Damage Threshold of the Optical Coating vs. Laser Acting Time.

as identified in Table 8. Substrate surface finish was qualified as state of the art. Both 1 on 1 tests (irradiation of each site with a single pulse) and n on 1 tests (each site irradiated by several pulses) were performed with samples in 10^{-8} torr vacuum. A Q-switched Nd:YAG laser operating in the TEM_{00} mode was used with 5 nsec FWHM pulses at 1.06 micron wavelength. The spot size achieved by focussing with a 2 m focal length lens was 500 microns. The laser was fired at a constant rate of one shot per minute. A square grid of 170 target sites was irradiated on each sample. Single pulse laser damage thresholds are reported in Table 9. Three types of n on 1 experiment were performed: (1) repeated irradiation of each target site with pulses of the same energy density, (2) irradiation of a site with a series of pulses of increasing energy density until damage occurred and (3) repeated irradiation of a target at a fixed energy density for a number of shots (usually 5), continuing at steadily increasing energy density. Charged particle emission was measured with a 1 cm diameter loop of wire, positively biased at 1 KV, through which the laser was fired. Damage threshold was determined by observing plasma breakdown (sparks) with a long working distance microscope and TV camera. Post irradiation measurements using a Nomarksi microscope confirmed damage with criteria being pitting, bubbling, holes, discoloration, etc.

Table 8. Dielectric Thin Film Coatings and Substrates

DIELECTRIC THIN FILM COATINGS			
ThO_2	ThF_4	Al_2O_3	AlF_3
MgO	MgF_2	SiO	LaF_3
Y_2O_3	YF_3	SiO_2	Na_3AlF_6 (Cryolite)
HfO_2	HfF_4	ZrO_2	NaF
Sc_2O_3	ScF_3	TiO_2	ZnS
CeO_2	CeF_3		
SUBSTRATES			
Fused Silica (SiO_2)			
Sapphire (Al_2O_3)			
Calcium Fluoride (CaF_2)			

Table 9. Single Pulsed Laser Damage Threshold Measurements

	SUBSTRATES		
COATINGS	Fused Silica (SiO_2)	Calcium Fluoride (CaF_2)	Sapphire (Al_2O_3)
ThO_2	5.5 J/cm^2 (S1311) 5.0 J/cm^2 (S1350)	5.5 J/cm^2 (F5783)	8.7 J/cm^2 (A102)
MgO	4.3 J/cm^2 (S1304) 5.0 J/cm^2 (S1318)	3.2 J/cm^2 (F9858)	11.1 J/cm^2 (A173)
Y_2O_3	8.4 J/cm^2 (S1335)	8.1 J/cm^2 (F8849)	13.8 J/cm^2 (A50)
HfO_2	6.3 J/cm^2 (S1347) 4.9 J/cm^2 (S1359)	4.4 J/cm^2 (F4772)	>15.0 J/cm^2 (A10) 10.7 J/cm^2 (A46)
Sc_2O_3	3.0 J/cm^2 (S1330) 5.6 J/cm^2 (S1365)	6.8 J/cm^2 (F8838)	12.3 J/cm^2 (A137) 12.1 J/cm^2 (A150)
CeO_2	2.3 J/cm^2 (S1345) 2.2 J/cm^2 (S1367)	8.6 J/cm^2 (F5786)	13.7 J/cm^2 (A31) 9.9 J/cm^2 (A116)
Al_2O_3	5.7 J/cm^2 (S1362) 4.1 J/cm^2 (S1441)	6.8 J/cm^2 (F1716) 3.9 J/cm^2 (F6798)	4.4 J/cm^2 (A16) 7.1 J/cm^2 (A139)
SiO	3.9 J/cm^2 (S1300) 2.4 J/cm^2 (S1364)	4.4 J/cm^2 (F5792)	4.7 J/cm^2 (A111) 9.6 J/cm^2 (A119)
SiO_2	14.5 J/cm^2 (S1302) 12.3 J/cm^2 (S1342)	15.6 J/cm^2 (F1703) >17.0 J/cm^2 (F8846)	26.6 J/cm^2 (A115)
ZrO_2	2.0 J/cm^2 (S1368)	6.1 J/cm^2 (F9866)	>12.9 J/cm^2 (A35) 6.9 J/cm^2 (A112)
TiO_2	.....	3.6 J/cm^2 (F7825)	7.3 J/cm^2 (A44) 6.8 J/cm^2 (A66)
ThF_4	8.1 J/cm^2 (S1306) 3.8 J/cm^2 (S1446)	10.8 J/cm^2 (F1705) 7.4 J/cm^2 (F3756)	13.4 J/cm^2 (A5) 8.7 J/cm^2 (A170)
MgF_2	7.4 J/cm^2 (S1316) 6.1 J/cm^2 (S1389)	8.3 J/cm^2 (F2736) 4.3 J/cm^2 (F3750)	27.9 J/cm^2 (A129)
YF_3	11.6 J/cm^2 (S1326) 7.5 J/cm^2 (S1409)	6.5 J/cm^2 (F4770) 8.8 J/cm^2 (F4774)	>27.0 J/cm^2 (A121) 9.2 J/cm^2 (A131)
HfF_4	9.7 J/cm^2 (S1341) 12.3 J/cm^2 (S1397)	14.6 J/cm^2 (F1707)	10.0 J/cm^2 (A41)
ScF_3	11.1 J/cm^2 (S1363) 6.4 J/cm^2 (S1402)	8.7 J/cm^2 (F4760) 10.5 J/cm^2 (F4768)	.....
CeF_3	5.1 J/cm^2 (S1366) 10.0 J/cm^2 (S1405	8.6 J/cm^2 (F1717) 5.6 J/cm^2 (F6801)	17.2 J/cm^2 (A18) 12.0 J/cm^2 (A138)
Alf_3	19.4 J/cm^2 (S1361)	9.7 J/cm^2 (F1712) 5.4 J/cm^2 (F4767)	19.1 J/cm^2 (A15)
LaF_3	5.8 J/cm^2 (S1319) 8.5 J/cm^2 (S1424)	4.7 J/cm^2 (F7816) 4.7 J/cm^2 (F8837)	27.1 J/cm^2 (A93) 11.3 J/cm^2 (A99)
Na_3AlF_6	8.9 J/cm^2 (S1370) 7.3 J/cm^2 (S1394)	4.9 J/cm^2 (F5784) 3.7 J/cm^2 (F5787)	9.2 J/cm^2 (A90) 11.3 J/cm^2 (A103)
NaF	1.7 J/cm^2 (S1373) 1.4 J/cm^2 (S1442)	1.9 J/cm^2 (F1711) 1.8 J/cm^2 (F4766)	4.1 J/cm^2 (A105)
ZnS	1.9 J/cm^2 (S1372)	.....	4.6 J/cm^2 (A154) 5.3 J/cm^2 (A160)
Fused Silica (SiO_2) Substrate		27.7 J/cm^2 (S1434)	
Calcium Fluoride (CaF_2) Substrate		13.1 J/cm^2 (F5789)	
Sapphire (Al_2O_3) Substrate		9.4 J/cm^2 (A147)	

Scatter measurements were made on each coating before and after deposition, results being reported in Table 10. Comparative roughness of the substrate was 3 ± 1 angstroms RMS, 9 ± 8 angstroms RMS and 11 ± 8 angstroms RMS for fused silica, sapphire and calcium fluoride respectively. Precision laser calorimetric absorption measurements were made at three wavelengths as reported in Table 11.

Survivability curves, showing the probability of coating damage for a given laser energy density, were used to determine 1 on 1 pulsed laser damage thresholds. Energy density is an average for all laser shot energies in a given range (for instance 2.5 to 3.5 J/cm^2), the range depending on the sample and how laser energies were grouped. Damage probability was determined from the number of exposures to damage the coating divided by the number of

Table 10. Variable Angle Scatterometer Measurements

Thin Film (ppm)	SiO_2 Substrate		CaF_2 Substrate		Al_2O_3 Substrate	
	Uncoated	Coated	Uncoated	Coated	Uncoated	Coated
TiO_2	0.8794	1.9016	3.4652	17.542	0.0749	2.6876
HfO_2	0.3724	4.0874	28.9236	1439.5	1.9146	5.7012
CeO_2	0.4232	18.839	12.0805	759.64	0.1633	22.837
SiO_2	....	....	8.4558	33.7911	6.0399	0.0837
ZrO_2	0.6067	9.6536	....	....	0.8456	7.7232
Al_2O_3	0.2195	1.0702	....	....	0.2551	0.6962
ThO_2	....	139.33	....	....	0.0523	267.40
Sc_2O_3	0.7303	15.186	....	....	....	....
Y_2O_3	0.2833	6.7358	....	....	....	....
ThF_4	....	5.6478	12.3371	46.702	0.3498	8.7880
HfF_4	0.3851	0.9261	....	....	0.0687	0.2125
AlF_3	0.2531	1.5250	....	....	0.0629	1.6365
CeF_3	0.5109	17.961	....	....	0.2213	10.723
ScF_3	0.3829	4.6531				
YF_3	0.4319	153.76				
ZnS	0.5530	1347.8				
NaF	0.2749	71.919				
Na_3Alf_6	0.3130	0.6553				

Table 11. Thin Film Absorptance Measurements at 351, 514, and 1320 nm

Film (Half Wave at 1.06 Microns)	A_{351} (%)	A_{514} (%)	A_{1320} (%)
TiO_2	44	0.061	0.0046
MgO	9.2	6	0.21
Sc_2O_3	0.51	0.037	0..052
Y_2O_3	0.14	0.018	0.0038
HfO_2	0.33	0.037	0.0056
ThO_2	0.92	0.068	0.0015
ZrO_2	1.2	0.066	0.0038
CeO_2	27.1	2	0.0074
SiO	81	24	0.0037
ScF_3	0.25	0.041	0.0026
HfF_4	0.19	0.023	0.0023
LaF_3	0.8	0.31	0.0023
AlF_3	0.16	0.022	0.0074
ZnS	39.5	0.32	0.0078
NaF	33.0	15.0	0.0042
ThF_4	0.13	0.024	0.68
Al_2O_3	0.20	0.034	0.0022
BeO	1.1	0.14	0.0040
AlN	0.64	0.053	....
YF_3	....	....	0.0082
MgF_2	....	....	0.0084
SiO_2 Substrate	0.08	0.019	
BK-7 Substrate	2.0	0.13	

exposures in each energy range. A least square fit was made of data between zero damage and 100% damage, the damage threshold corresponding to the intercept energy density at which no damage occurs. The technique is illustrated by Figure 8.

The sensitivity of damage threshold to substrate thermal conductivity is shown in Figure 9. A trend in improved damage thresholds with higher conductivity substrates is evident, even for short (5 nsec) pulses used in this study.

Laser induced charge emission was observed both above and below the damage threshold. Data fell into distinct patterns indicating that distinct characteristics of each film material was different. The charge emission showed no distinct indicator or precursor of imminent laser induced surface damage. Charge emission decreased below detector sensitivity when a site was repeatedly irradiated indicating a cleaning effect and gradual increase to indicate accumulation of damage.

Halfwave low index overcoats, such as MgF_2 have been found by Carniglia, et. al. (Ref. 7) to improve the damage threshold of HR coatings used at some wavelengths but not at others. Improvement was found at 1064 and 248 nm but not at 355 nm. Improvements of more than 60% at 1064 nm for 1 nsec pulses were achieved by a halfwave silica overcoat on a titania/silica quarter-wave stack. A magnesium fluoride halfwave overcoat on a scandia/silica HR stack designed for 248 nm more than doubled the median damage threshold of the non-overcoated multilayer. Silica overcoats on this multilayer gave about the same improvement for high deposition temperature (250°C) but about 20% less improvement at lower deposition temperature (150°C). The damage threshold improvement cannot be explained in terms of a mechanical model. While silica is a homogenous structure and creates a compressive stress improving the damage resistance of the underlying stressed titania layer, magnesium fluoride layers have large crystalline structures and high tensile stress and are mechanically soft at temperatures as low as 150°C. Both overcoats improve damage threshold while being mechanically opposite. Neither do electric field considerations explain the improvement. The field within the HR multilayer is the same with or without the overcoat and the field within the overcoat is the highest anywhere in the coating.

At 355 nm, HR multilayers containing zirconia/tantala had 20% lower damage thresholds when overcoated with silica halfwave layers. For HR multilayers using hafnia as the high index layer, low thresholds were found with or without the silica overcoat. Scandia/silica/magnesium fluoride multilayers with magnesium fluoride overcoats exhibited the highest average thresholds, however, no multilayers of this type without overcoats were tested. To clarify whether the high threshold for the scandia multilayer was due to the magnesium fluoride overcoat or to the

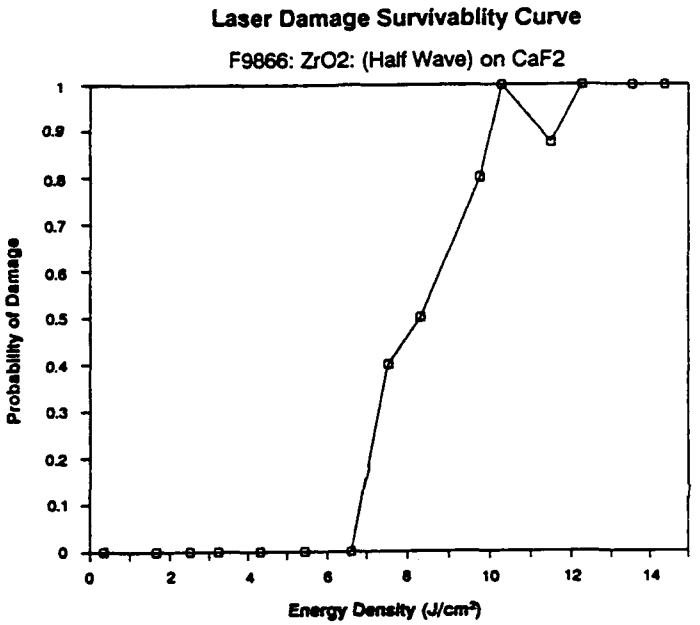

Figure 8. Laser damage survivability curve for ZrO_2 (half wave @ 1.06 μm) on CaF_2 with a damage threshold of 6.1 J/cm^2.

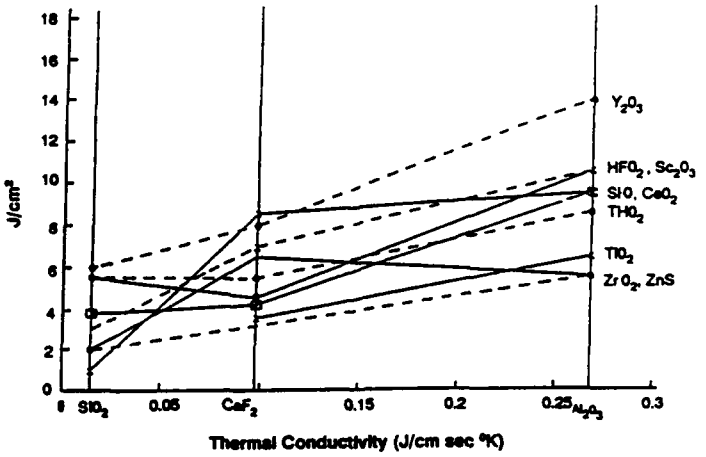

Figure 9. Laser damage thresholds of various thin film dielectric coating vs. substrate thermal conductivity.

difference between scandia and other high index layers, a set of 24 scandia/silica/magnesium fluoride 355 nm HR multilayers with different overcoats was made for damage testing. Materials were deposited in a box coater within an electron gun source on BK-7 substrates polished by a continuous-feed technique. Six substrates were deposited in each of four runs with 25 layers of scandia/silica/magnesium fluoride. Two of the resulting HR filters were overcoated with a halfwave of silica, two others with a halfwave of magnesium fluoride and the final two received no overcoat. Two runs were made at 150°C and the other two runs were made at 250°C.

Damage thresholds were measured using a frequency tripled Nd-glass laser. The 355 nm, 0.6 nsec laser pulse was focused to give a 1 mm diameter beam at the film. Each test site was irradiated with one pulse and the presence of damage determined visually using Nomarski microscopy. Precision of the threshold determination was ±10% for each part. The results are presented in Figures 10 and 11 corresponding to deposition temperatures of 150°C and 250°C, respectively. The average damage thresholds are lower than those observed using halfwave overcoats for multilayers designed for the other wavelengths (1064 and 248 nm). Neither silica nor magnesium fluoride overcoats improved the damage threshold of the 355 nm HR multilayers. Deposition temperature differences had little effect relative to the scatter in the data when comparing both overcoats to the uncoated multilayer. However, the damage threshold is higher for multilayers deposited at the higher temperature. This is consistent with results for zirconia/silica multilayers designed for other wavelengths. No cohesive explanation of the results is given. However, possible mechanisms involve differences in stress related to layer thicknesses for the three wavelengths, differences in absorption at the different wavelengths and differences in the pulse lengths of the damage test lasers. The pulses were on the order of 1 nsec for the 1064 and 355 nm lasers but were 20 nsec long for the 248 nm tests.

The results of experiments reported by Wolfe, et. al. (Ref. 8) showed that thin films of SiO_2 or HfO_2/SiO_2 deposited by conventional E-beam evaporation can be laser conditioned to significantly increase their laser damage threshold. The damage thresholds achieved are comparable to those of SiO_2 films prepared by high temperature plasma CVD. The advantage of E-beam laser conditioned films is that they may be applied to fabrication of large aperture optical components of a scale of which may not yet be achieved with plasma CVD. The conditioning effect was shown to be permanent but to be consistently observed only in HfO_2/SiO_2 films deposited by conventional E-beam evaporation. The improvement in damage threshold was found to show little dependence on the coating design (number of layers) or the size of the deposition chamber. Contrary to prior hypothesis, it was found to not be associated with removal of absorbed moisture or other

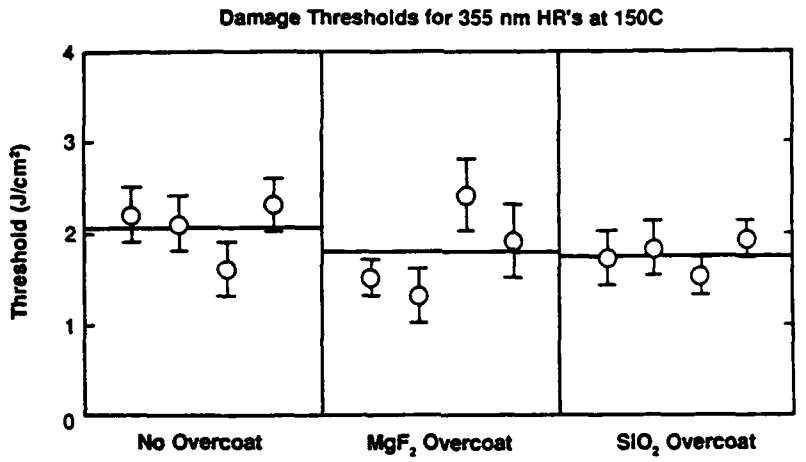

Figure 10. Laser damage thresholds for 355-nm HR's with various overcoat options coated at a temperature of 150°C. Each circle represents the damage threshold of one sample. The error bar for each sample represents the range between the lowest fluency which caused damage and the highest fluency which did not. The average damage threshold for each overcoat option is indicated by a horizontal bar.

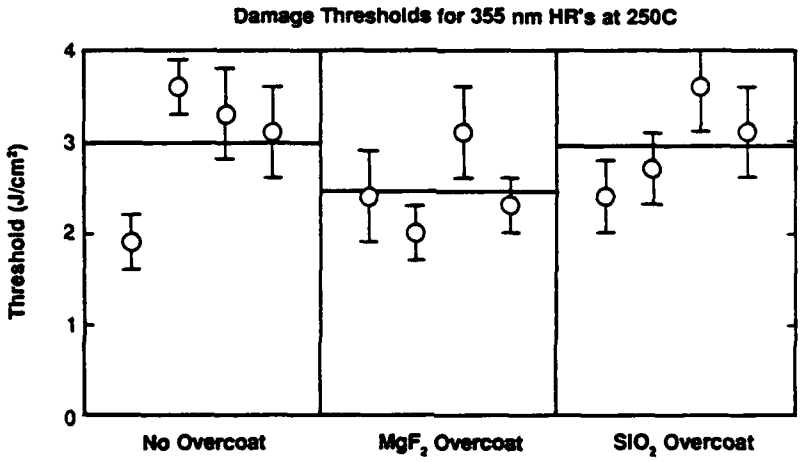

Figure 11. Laser damage thresholds for 355-nm HR's with various overcoat options, coated at a temperature of 250°C. Refer to caption for Figure 10.

atmospheric contamination, is not dependent on the number of coating layers nor transmissive or reflective characteristics of the optical design and is not associated with recrystallization within the film. It was therefore concluded that the often proposed laser cleaning or phase change mechanisms to explain laser conditioning are not the dominant mechanisms responsible for the conditioning observed in these particular films. Instead, the laser damage mechanism is attributed to the "non-equilibrium" state of E-beam deposited film. This arises from the intrinsic defects associated with the porous nature of the films. It is speculated that the intrinsic defects influence laser conditioning by way of a four step process involving: (1) photo-excitation of electrons from shallow electronic gap states into the conduction band; (2) excitation of the free carriers to high energy by acceleration under the optical electric field or by free carrier absorption; (3) subsequent transfer of the excess energy to the lattice via avalanche or an electron-phonon interaction (lattice heating); and (4) heating of the film to some critical damage temperature such as the melting or boiling point of the dielectric material.

To study the effects of laser conditioning, quarter-wave HR multilayers of HfO_2/SiO_2, ZrO_2/SiO_2 and TiO_2/SiO_2 were fabricated. Inconsistent damage thresholds were obtained for TiO/SiO_2 multilayers, thought to be due to highly absorbing suboxides of TiO_2 formed during evaporation. Therefore, only HfO_2/SiO_2 and ZrO_2/SiO_2 coatings were compared. Three different deposition techniques were also compared: E-beam evaporation, plasma plating, and ion beam sputtering. The effect of scale up from a small R&D coater to a three meter diameter production coater was assessed for the E-beam technique. Damage thresholds were compared for non-conditioned and conditioned films fabricated as described above. Damage thresholds were compared using three different 1.06 μm wavelength laser facilities: (1) a variable pulse length laser operating in a single shot mode with pulse length varying from 1 to 16 nsec; (2) a rep-rated laser operating at PRF's of 10, 15 or 30 Hz with pulse length of 10 or 16 nsec, and (3) a rep rated laser that operates at 18 Hz with a pulse width of 8 nsec. Spot size was typically greater than 1 mm diameter. Damage was defined as any visual change in sample after laser irradiation when viewed by 100X Nomarski microscope.

Four test formats were used as described by Figure 12. They differ in the number of shots, the time between shots and the range of fluences used. Unconditioned thresholds were measured using the 1:1 and S:1 formats which expose each site to only one fluence level. The 1:1 format uses a single shot per site. The S:1 uses a series of constant fluence shots on each unexposed site with time between shots determined by the PRF. Conditioned thresholds are determined by R:1 and N:1 formats. The R:1 tests use a series of shots separated by short intervals as in S:1 but the

fluence is varied from zero to a preset upper bound in a linear ramp. The N:1 uses a series of single shots, the fluence of each increased step wise up to an upper bound. Since time between shots for N:1 can be several minutes, uncertainty in threshold measurements was typically ±15%.

Results comparing unconditioned and conditioned film damage thresholds for HfO_2/SiO_2 and ZrO_2/SiO_2 are shown in Figure 13. Pulse width scaling for the material pairs is shown in Figure 14. Based on the figure, the damage threshold D_t scales with pulse length t_p approximately as $D_t \sim 7t_p^{.035}$ (unconditioned) and $D_t \sim 19t_p^{.030}$ (conditioned). The ZrO_2/SiO_2 films showed significant site to site variability in threshold measurement and only in some cases exhibited improvement by conditioning. Consistent thresholds and conditioning improvement was found for HfO_2/SiO_2 suggesting different damage mechanisms for the material pairs.

Comparison of results for the different deposition techniques and chamber size is shown in Figure 15. Best improvements due to conditioning is evident for E-beam deposited films. Results of conditioning ion beam sputtered films were inconsistent, with little improvement observed. The influence of different thin film designs on improvement due to conditioning is shown in Figure 16, where it is apparent that improvement is independent of design parameters.

The work of Kozlowski, et. al. (Ref. 9) supplements that reviewed in reference 8 and concentrates on large area conditioning. Coatings of ZrO_2/SiO_2 and HfO_2/SiO_2 designed for high reflectance at 1064, 532 and 355 nm were studied. The coatings were deposited in 1983 while the HfO_2/SiO_2 were deposited in 1989. The two principal large area conditioning methods examined were: (1) rastering a small area beam back and forth across the sample surface, and (2) illuminating a large area optic using a large aperture beam. Laser conditioning parameters examined included the fluence and the number of pulses. Preliminary conditioning tests using broadband flashlamps were also examined.

The damage tests were made using a 1064 μm Nd:YAG laser with beam diameter of 0.2 mm at 80% of the peak fluence. The pulse length was 8 nsec and the rep rate was 18 Hz. The damage threshold was taken as the lowest fluence causing a light flash at the coating surface and a visible change in surface properties as breathing on the film and observing water vapor condensation patterns to identify the damaged areas. Damage thresholds obtained using this technique were found to agree well with those obtained using a 100X Nomarski microscope. Two test formats were used: (1) S:1 employing multiple shots of the same fluence at a single site, and (2) R:1 employing multiple shots of increased (ramped) fluence at a single site. In the R:1 tests the fluence was increased at ~0.2 J/sec until damage was observed. In the S:1 tests, samples were

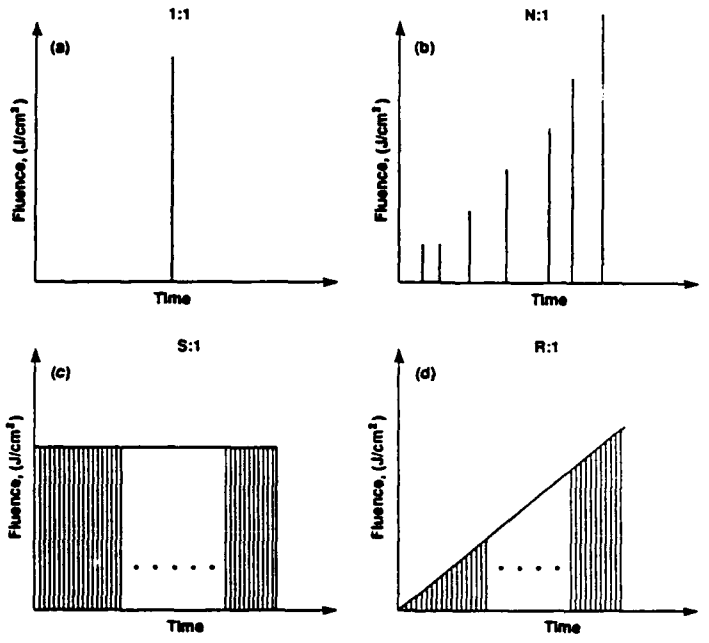

Figure 12. Four methods used to measure damage threshold: (a) single shot per site (1:1), (b) multiple shots per site with large increments in fluence between shots (N:1); (c) multiple shots per site at constant fluence (S:1), and (d) multiple shots per site with a ramped increase in fluence (R:1). Note that N:1 and R:1 tests give "conditioned" damage thresholds.

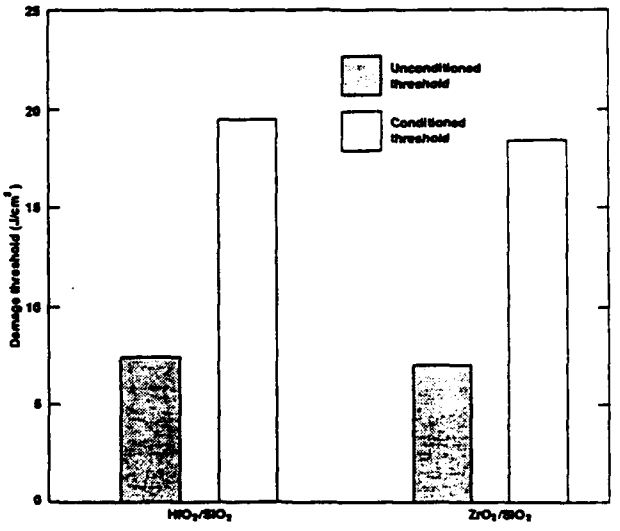

Figure 13. Comparison of unconditioned and laser-conditioned damage thresholds for HfO_2/SiO_2 and ZrO_2/SiO_2 HR quarter-wave stacks for 1 ns pulses, 1064 nm. The unconditioned values are from 1:1 tests and the conditioned values are for N:1 measurements.

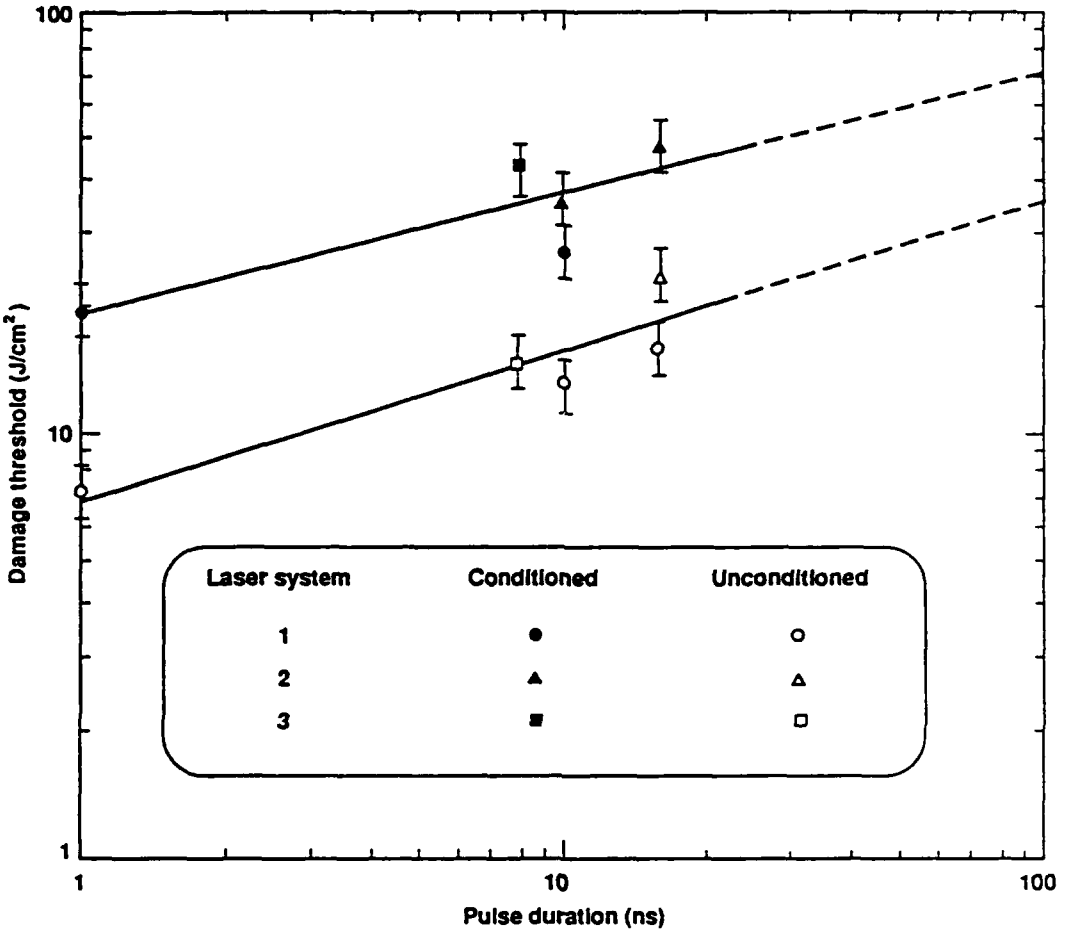

Figure 14. Measured pulselength scaling for conditioned and unconditioned damage thresholds of HfO_2/SiO_2 quarter-wave HR coatings at 1064 nm. The data are from measurements on the three different laser systems described and the solid line represents a least squares fit to the data.

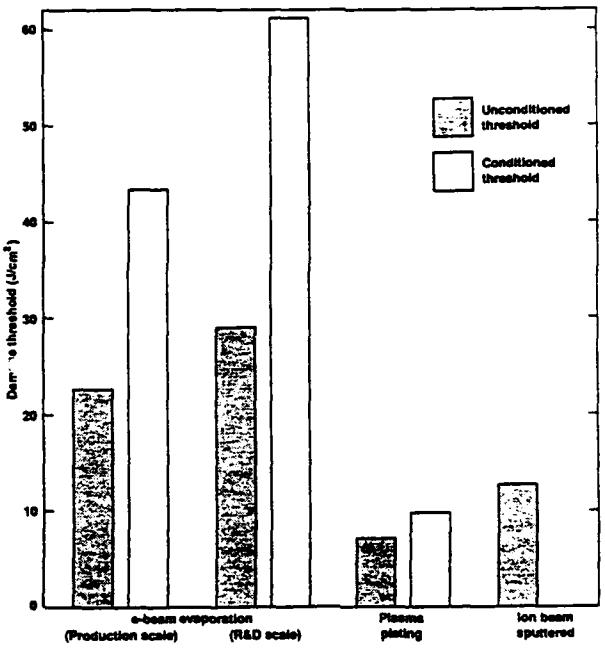

Figure 15. Unconditioned (S:1) and conditioned (R:1) damage thresholds (16 ns, 1064 nm) for HfO_2/SiO_2 HR coatings prepared by E-beam evaporation, plasma plating, and ion-beam sputtering. The E-beam data are for coatings prepared on both the small scale R & D coater and the large scale (3-diameter) production coater.

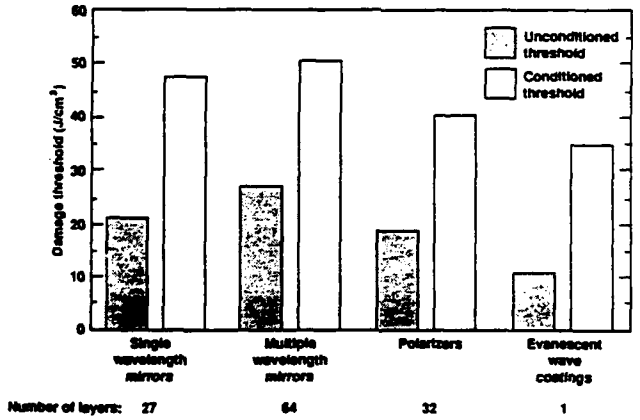

Figure 16. Comparison of conditioned and unconditioned damage thresholds for HfO_2/SiO_2 multilayer HR's, polarizer and single-layer evanescent wave coatings; all data are for 1064 nm laser irradiation. The HR data are for pulse lengths of 16 ns and the polarizer and evanescent wave coatings are for 0 ns pulses.

illuminated for ~30 seconds (~53 shots) unless damage was observed in which case illumination was stopped immediately. In nearly all S:1 tests where damage occurred, it was observed during the first couple of pulses. Threshold values reported are ±15% and each reported threshold represents the average of 1 to 4 tests. The damage tests for the two coatings are compared in Figure 17. Damage conditioning (R:1) improved thresholds of both coatings with significantly higher gain for the HfO_2/SiO_2 coating. Damage in these coatings was observed to occur at microscopic defects (<50 μm) which were smaller and of lower density then those observed in the older ZrO_2/SiO_2 coatings. Modest differences observed were not believed to influence the damage threshold. Rather, the differences were thought to indicate different types of defects, one type being more susceptible to conditioning than the other. Further difference in the coatings was exhibited by no pulse width dependence being apparent for the ZrO_2/SiO_2 coating, while the HfO_2/SiO_2 coating showed a definite dependence ($D_t = 7.1\ t_p^{0.35}$). These differences, which occur after conditioning, may indicate a change in the laser damage mechanism. Without conditioning, it is pointed out that damage thresholds are about the same for 8 nsec pulses.

To achieve conditioning of large areas, they were scanned with a 0.2 mm test beam with various raster programs as indicated by Figure 18 where the unconditioned damage threshold was determined from S:1 tests. The improvement achieved in both coatings by conditioning is illustrated in Figure 19. Conditioning increased the damage threshold of the older coating (ZrO_2/SiO_2) by a factor of 1.2 to 2.4. It is not clear which is the best raster conditioning program. It appears, however, there is no clear advantage to step conditioning. The most important conclusion reached was that for both coatings all raster conditioned programs resulted in conditioning factors less than that obtained by the ramped fluence technique (R:1).It was observed that the range of fluence over which damage probability changed from 0% to 100% depended on the conditioning history of the sample. For S:1 tests the transition range was ~10 J/cm^2 while for R:1, the range was >40 J/cm^2. Raster conditioned samples had a range intermediate to the S:1 and R:1 cases. The change in abruptness of damage threshold indicates that film properties controlling the damage threshold are not uniform across the film surface. Also since the damage threshold is not abrupt for the conditioned samples, choosing the lowest damage fluence as the threshold results in a conservative value for the conditioned damage threshold. In some areas, R:1 testing increased the threshold by a factor of >4.

The time to cover large aperture coatings with a 0.2 mm conditioning beam is restrictive. Therefore, conditioning with a larger diameter beam was investigated. Two 5 cm diameter samples of HfO_2/SiO_2 and ZrO_2/SiO_2, designed for HR at 1064 nm, were conditioned with a 4 cm

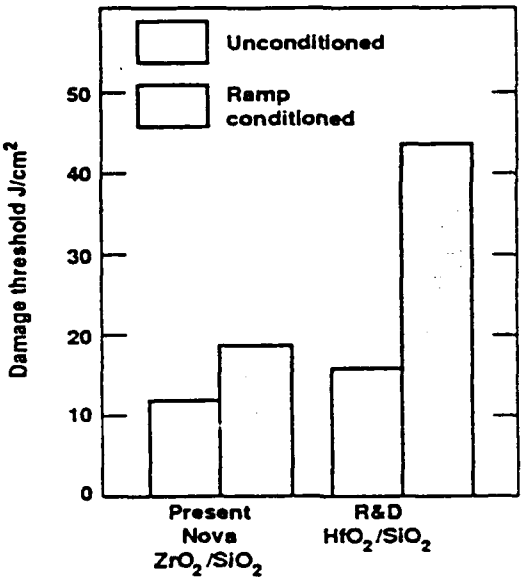

Figure 17. Unconditioned and ramp conditioned 1064 nm damage thresholds (18 Hz, τ_p=8ns) of Nova ZrO_2/SiO_2 and R&D HfO_2/SiO_2 HR coatings. Conditioning performed using damage test laser.

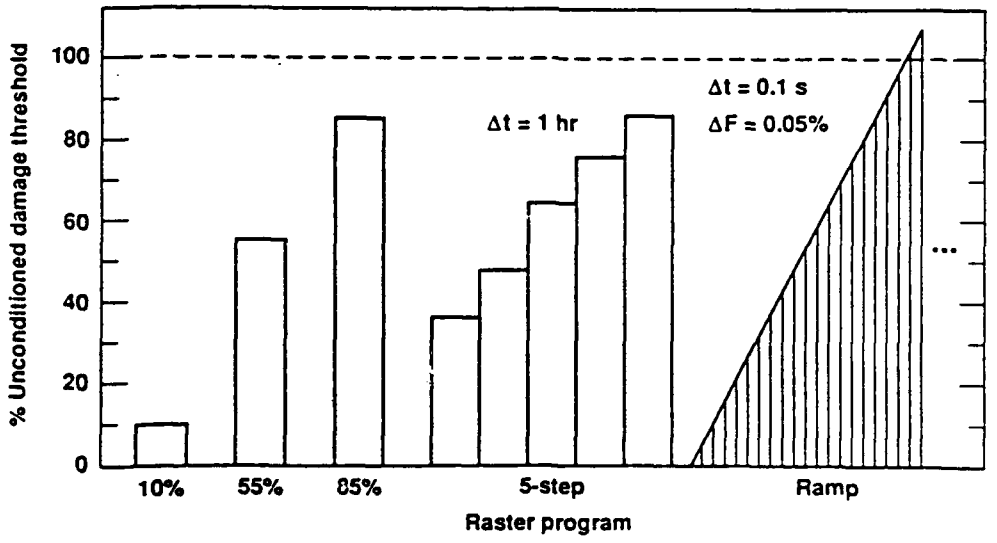

Figure 18. Laser conditioning program used in raster conditioning and ramp conditioning experiments.

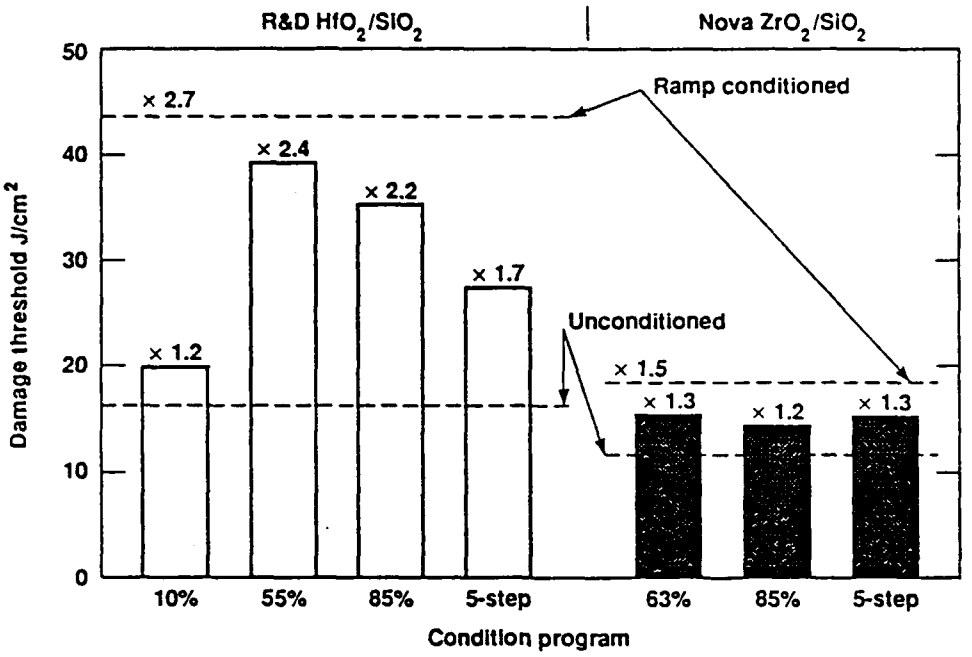

Figure 19. Conditioned 1046 nm damage thresholds (18 Hz, τ_p=8ns) of Nova ZrO_2/SiO_2 and R&D HfO_2/SiO_2 HR coatings for various raster conditioning programs. Unconditioned and conditioned thresholds are included for reference.

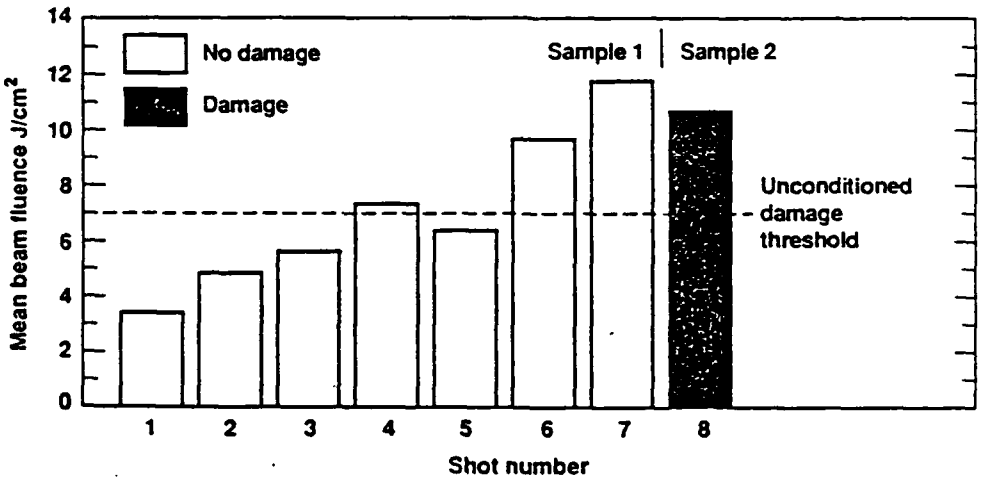

Figure 20. Beam fluence vs. shot number for large aperture Nova conditioning experiment. λ = 1064 nm, τ_p = 1 ns.

diameter spot by condensing the damage laser beam. After each shot, the sample was microscopically inspected for damage at 40X magnification using bright light illumination. At completion of the test, the samples were photographed at magnification up to 400X using Nomarski, as well as bright and dark field illumination. Data for seven shots fired is shown in Figure 20. The highest fluence (12 J/cm^2) is about 1.5 to 2 times the 1:1 damage threshold. No damage was observed until the 8th shot which was fired on the ZrO_2/SiO_2 coating with a fluence significantly above the single shot threshold (7 J/cm^2). Results show conditioning was achieved using the larger beam. To compare with damage threshold achieved by raster scanning, the HfO_2/SiO_2 sample conditioned by the larger beam was subjected to 8 nsec pulses at 18 Hz. Results shown in Figure 21 indicate damage thresholds obtained by raster scan and large beam conditioning are in the same range. However, large beam conditioning thresholds are lower than that obtained by ramp conditioning. Permanence of the large beam conditioning effect is illustrated by Figure 22 showing threshold measurements made several days after conditioning.

Flashlamp conditioning experiments were also pursued on an HfO_2/SiO_2 HR sample using 20 flashes of a xenon arc lamp at 10 J/cm^2 for each shot at a pulse length of 0.5 nsec. However, S:1 damage tests with this source did not improve the damage threshold.

The mechanism proposed for the laser conditioning phenomenon is based on the presence of sub-bandgap electronic defect levels intrinsic to the E-beam deposition process. These shallow defect levels are located below the conduction band edge. When the film is illuminated at low fluence, electrons in the defect levels are excited to the conduction band. At low fluence, the optical electric field is not sufficient to transfer enough energy to the lattice from the accelerated electrons to cause damage. In absence of illumination, the electrons then decay to deep levels from which they cannot be excited to the conduction band by higher fluence illumination.

Multilayer AR coatings of MgF_2/Al_2O_3 and Al_2O_3/ZrO_2 were fabricated by Mordaunt, et. al. (Ref. 10) using E-beam evaporation and laser tests performed to determine the effect of conditioning laser spot size and coating design on improvement in damage threshold due to conditioning. The MgF_2/Al_2O_3 coating (sample A) was deposited on an unheated BK-7 glass substrate. The Al_2O_3/ZrO_2 coating (sample B) was deposited on a heated BK-7 glass substrate. Both unconditioned and conditioned damage thresholds were measured for both samples. The unconditioned test procedure exposed each site to a single fluence. Test sites were separated by at least three times the diameter of the laser spot and each site was exposed to 25 shots or until damage was observed. The conditioned test procedure exposed each site initially to 1/2 the unconditioned threshold and then to a slowly ramped fluence until damage was observed. The

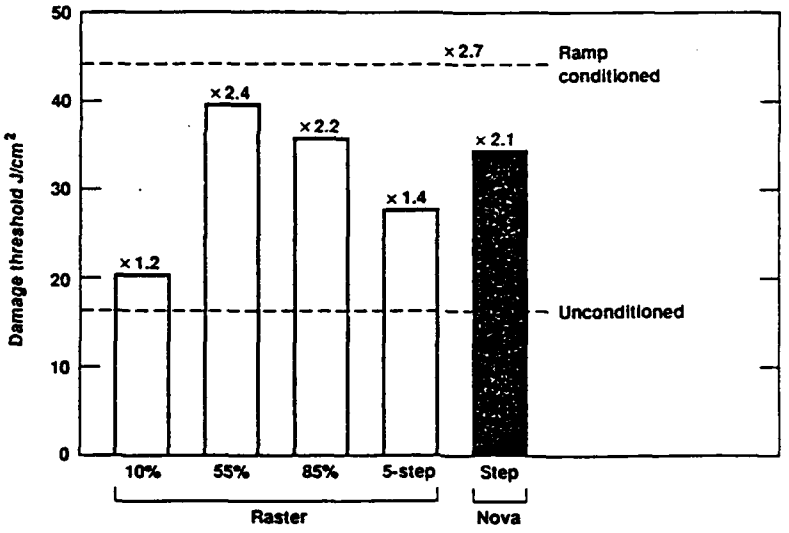

Figure 21. 1064 nm damage thresholds (18 Hz, τ_p = 8 ns) of Nova ZrO_2/SiO_2 and R&D HfO_2/SiO_2 HR coatings conditioned by raster scanning and large aperture Nova illumination.

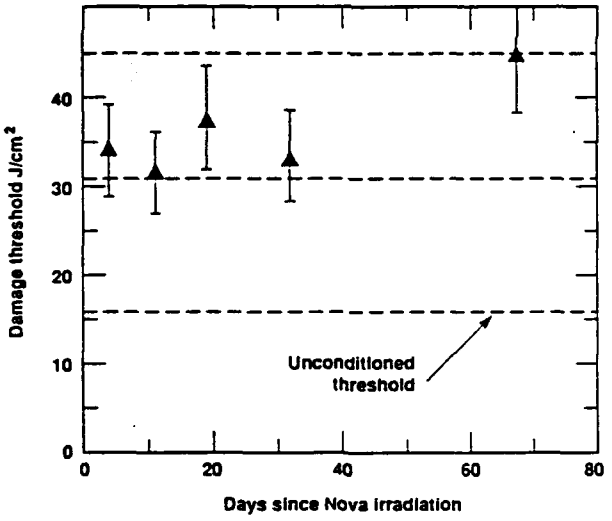

Figure 22. 1064 nm damage thresholds (τ_p = 10 ns) vs. time after conditioning for the R&D HfO_2/SiO_2 HR coatings illuminated on Nova.

sites were exposed to 25 shots at each fluence before increasing to the next fluence level. The conditioning and damage measurements were done at a wavelength of 1.06 μm with a 15 nsec pulse width. The laser PRF was 1 Hz and spot sizes of 0.25, 0.5 and 1.0 mm were used. Damage was determined using a 25X microscope and video system on line with the sample illuminated with a HeNe laser allowing observation of changes in scatter. Accuracy of all threshold measurements is ±10%.

The results of the unconditioned threshold measurements are presented in Table 12. Apparent is some dependence on spot size, particularly for the smallest spot (0.25 mm). The Al_2O_3/ZrO_2 coating has significantly higher thresholds than the MgF_2/Al_2O_3 coating. The unconditioned test results are presented in Figures 23 and 24 as a plot of test result (damage or no damage) versus fluence. Apparent is considerable overlap in the damage and nondamage fluence.

Table 12. Unconditioned Damage Threshold Measurements

Spot Size (FW in mm at $1/e^2$)	Sample A (J/cm^2)	Sample B (J/cm^2)
0.25	29.2	82.5
0.50	13.1	42.5
1.00	8.5	48.5

Conditioned sample damage thresholds are presented in Figures 25 and 26 for MgF_2/Al_2O_3 (sample A) and Al_2O_3/ZrO_2 (sample B), respectively. Approximately 20 spots per sample were tested for each spot size to allow a statistical analyses of defect distribution. Measurements on conditioned and unconditioned samples are compared in Figure 27. The conditioning increased the threshold for the smaller spot size but provided little improvement at the 1.0 mm spot size.

The standard deviation of the conditioned threshold vs. spot size is shown for both coatings in Figure 28. The deviation was largest for the smallest spot size and also was largest for the MgF_2/Al_2O_3 coating which had the lowest overall damage threshold. These results are consistent with a defect dominated damage mechanism in which the defect spacing is on the order of 1 mm.

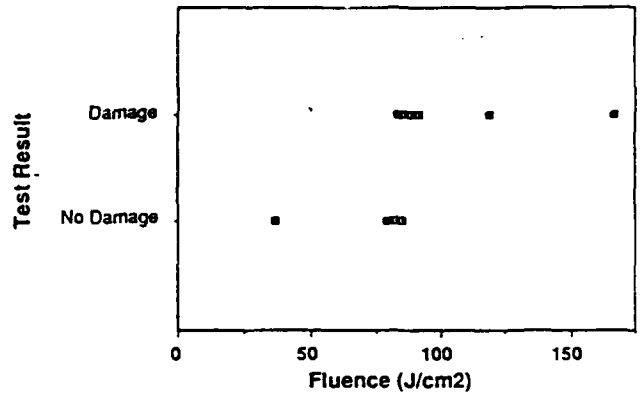

Unconditioned results for sample A with a 0.25 mm spot size.

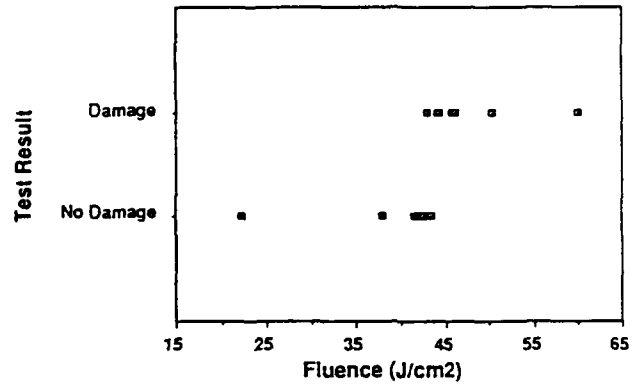

Unconditioned results for sample A with a 0.5 mm spot size.

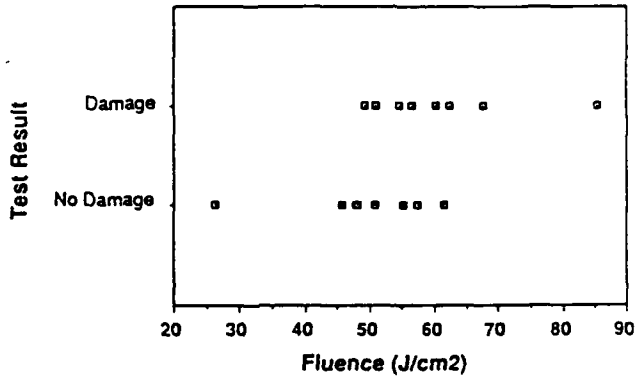

Figure 23. Unconditioned results for sample A with a 1.00 mm spot size.

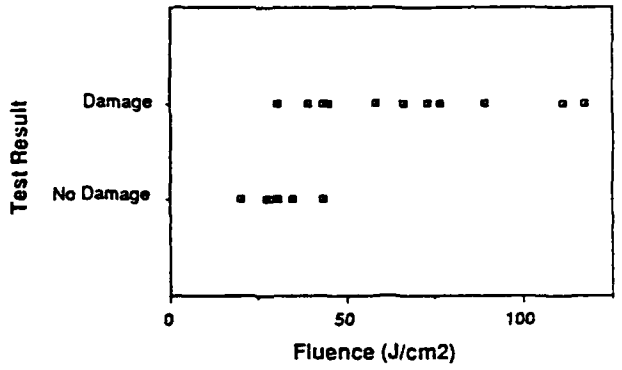

Unconditioned results for sample B with a 0.25 mm spot size.

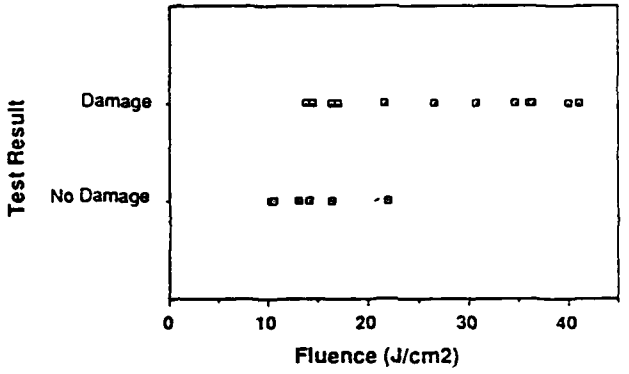

Unconditioned results for sample B with a 0.5 mm spot size.

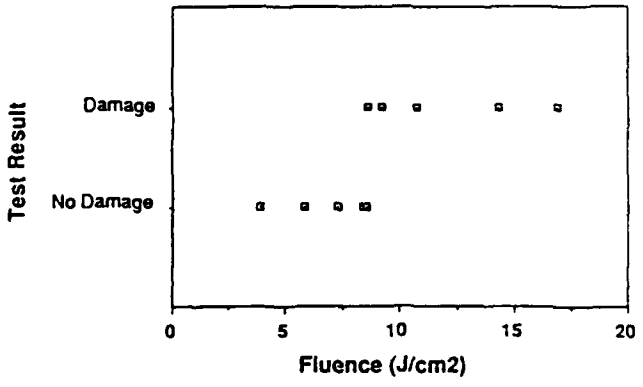

Figure 24. Unconditioned results for sample B with a 1.00 mm spot size.

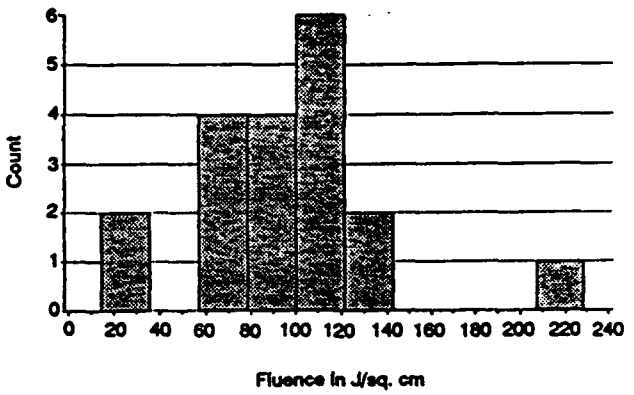

Histogram of conditioned failures for sample A with a spot size of 0.25 mm.

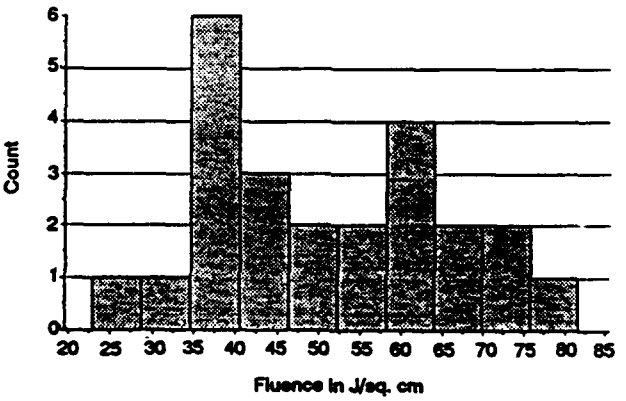

Histogram of conditioned failures for sample A with a spot size of 0.5 mm.

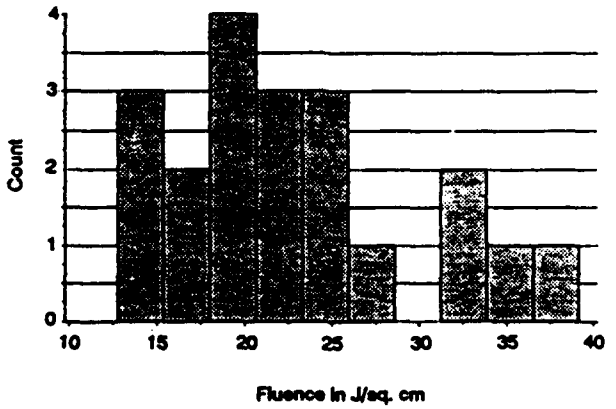

Figure 25. Histogram of conditioned failures for sample A with a spot size of 1.0 mm.

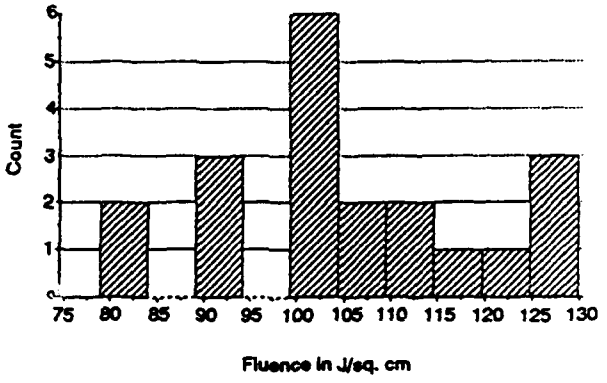

Histogram of conditioned failures for sample B with a spot size of 0.25 mm.

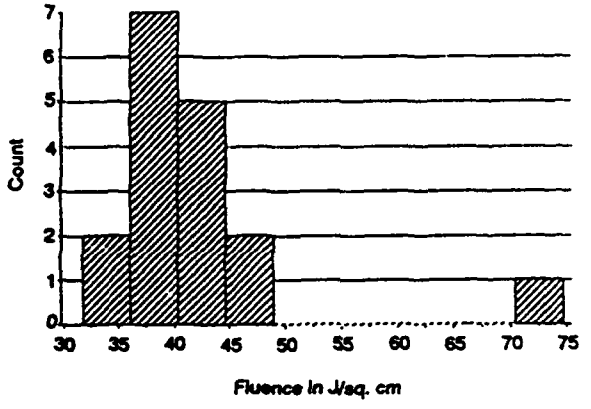

Histogram of conditioned failures for sample B with a spot size of 0.5 mm.

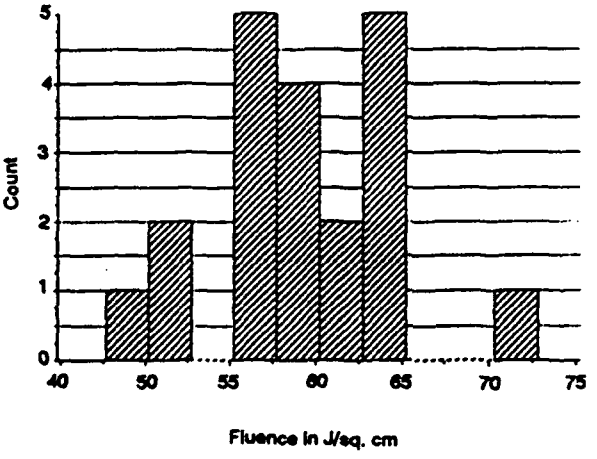

Figure 26. Histogram of conditioned failures for sample B with a spot size of 1.0 mm.

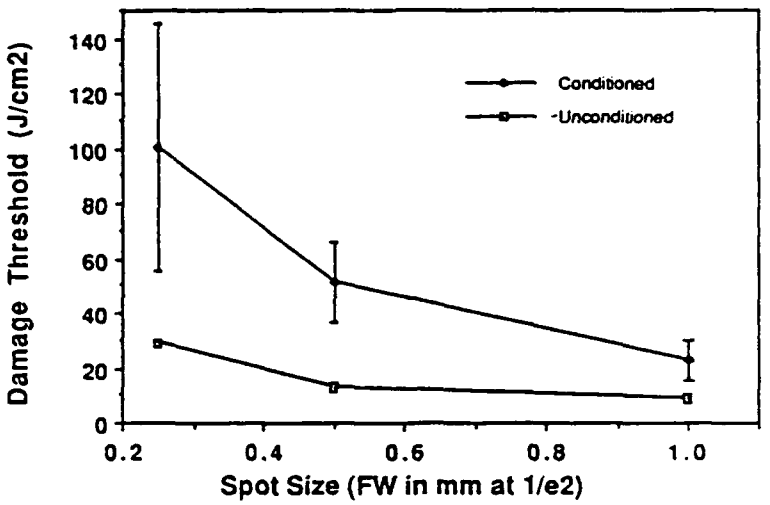

Conditioned and unconditioned performance of sample A. Comparison of the conditioned and unconditioned test results for the three different spot sizes.

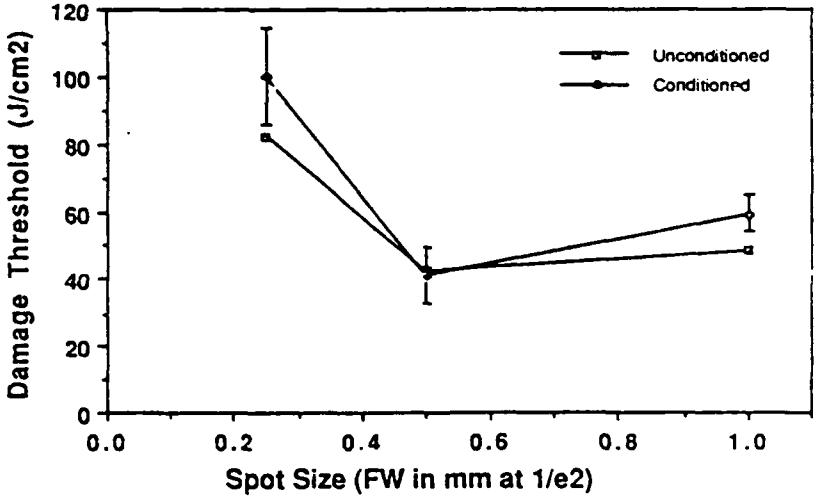

Figure 27. Conditioned and unconditioned performance of sample B. Comparison of the conditioned and unconditioned test results for the three different spot sizes.

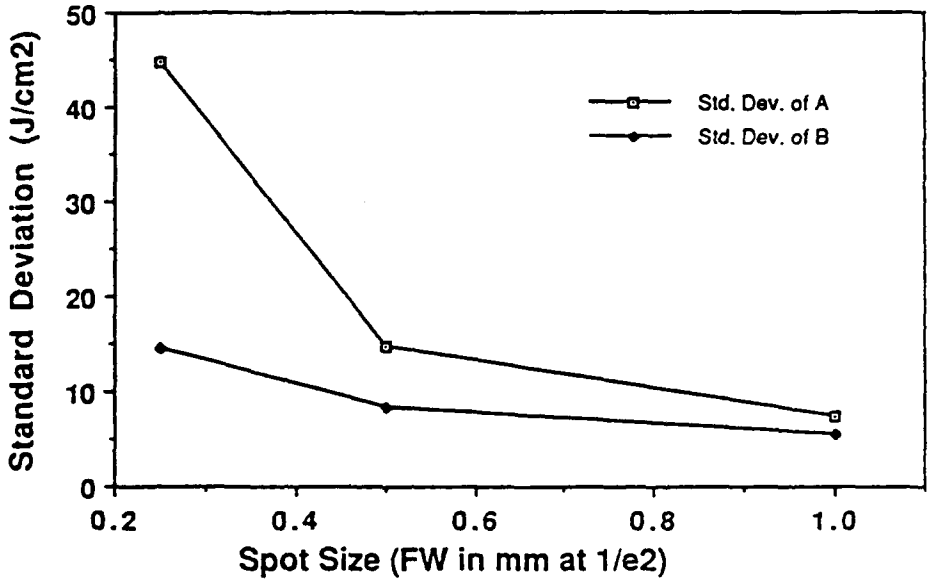

Figure 28. The standard deviation of the conditioned threshold was largest for the smallest spot size.

2.2 CHEMICAL DEPOSITION PROCESSES

In the work of Wilder, et. al. (Ref. 11) refractive oxide multilayer coatings for HR applications were fabricated by three different techniques and their damage thresholds were determined by 1 on 1 and n on 1 testing to assess the difference in the two test formats. High purity silica substrates were used. Two HR coatings (λ = 1.06 μm) consisting of a 15 layer quarter-wave design (HFO_2/SiO_2 and ZrO_2/SiO_2) were fabricated by E-beam evaporation. Sol-gel processing was used to fabricate a single layer of ZrO_2, a four layer Al_2O_3/SiO_2 and an eight layer Al_2O_3/SiO_2 multilayer structure, all designed to exhibit HR at 1.06 microns.

One on one testing involved irradiating a single location with a 1.06 μm, 16 nsec pulse at a single fluence for one minute at a rate of 30 Hz. If no damage was observed, another site was chosen and the irradiation repeated at a higher fluence. N on 1 testing involved irradiating a single site as in 1 on 1 testing. However, after the one minute exposure, the fluence is increased by 1 to 3 J/cm^2 if no damage is observed. The criterion used for identifying damage was 5% damage of the irradiated area as determined by inspection with a 100X Nomarski microscope. The area damaged was determined by measuring the size of the largest damage sites, totaling the number of sites and determining the total area of damage as a function of fluence. In the data presented in Figures 29 through 34, arrows extending above the data points indicate catastrophic damage covering at least 50% of the irradiated area.

For the E-beam films, n on 1 testing indicated higher damage thresholds (lower percent of irradiated area damaged). Both HfO_2 and ZrO_2 showed no damage up to the maximum laser fluence (50 J/cm^2). The ZrO_2 single layer fabricated by sol-gel showed a low damage threshold for both test formats, this being attributed to an iron contaminant found in the film. Consensus of the authors was that the damage threshold of the Al_2O_3 sol-gel film was greater for the n on 1 testing. However, this is not evident from the data since the n on 1 damage threshold was above the 50 J/cm^2 maximum fluence of the test laser.

The rationale for the improved damage threshold of the sol-gel films for n on 1 testing is that laser heating volatilized impurities from absorbing volumes related to the porosity of films fabricated by this technique. As impurities left over from the sol-gel process are removed, absorption is reduced and the damage threshold is increased.The lower damage threshold and higher improvement with conditioning of the MgF_2/Al_2O_3 coating was thought to be due to the former being deposited on a cold substrate and the latter being deposited on a heated substrate.In the work of Thomas, et. al. (Ref. 12), two methods of preparing sol-gel coatings were compared

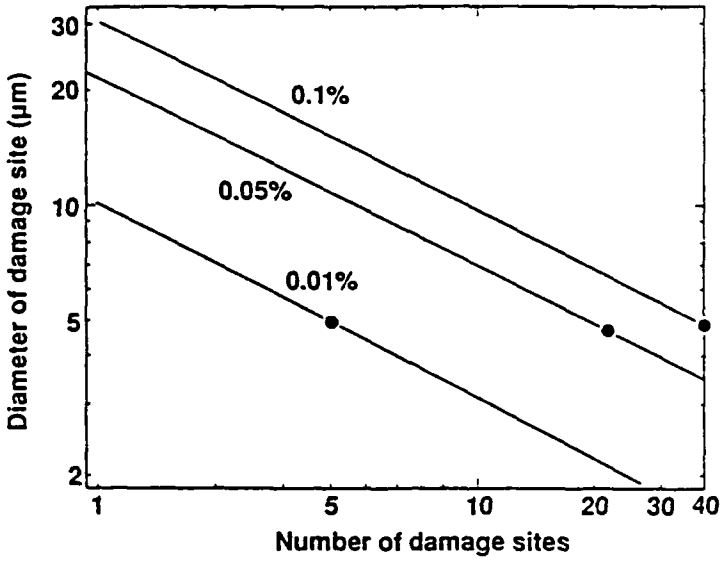

Figure 29. Damaged area of a 1 mm beam (%).

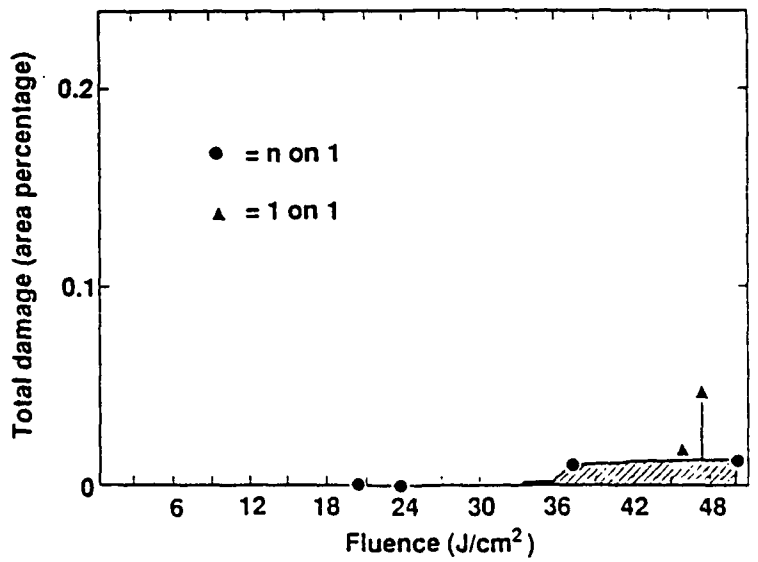

Figure 30. $[HfO_2\text{-}SiO_2]^8$ E-beam.

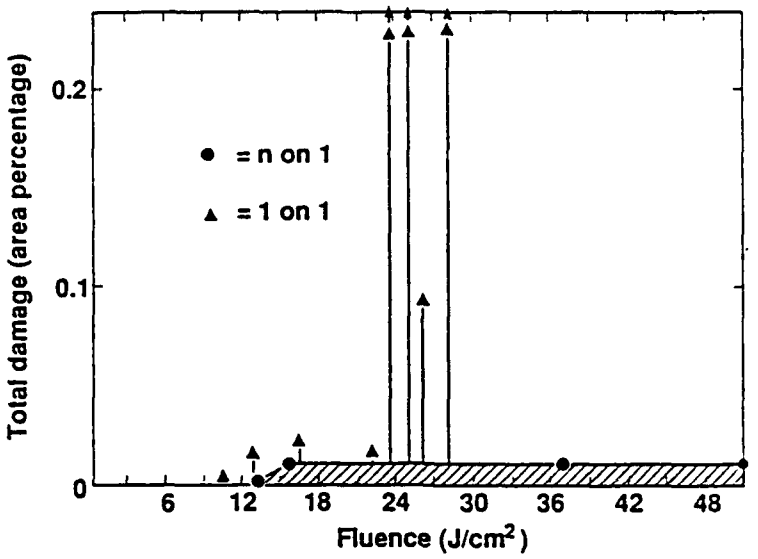

Figure 31. $[ZrO_2\text{-}SiO_2]^8$ E-beam.

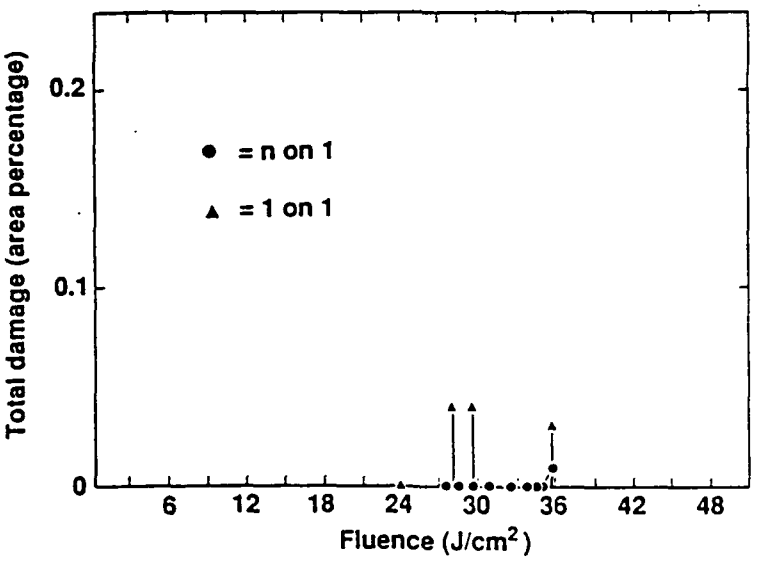

Figure 32. $[SiO_2\text{-}Al_2O_3]^4$ sol-gel.

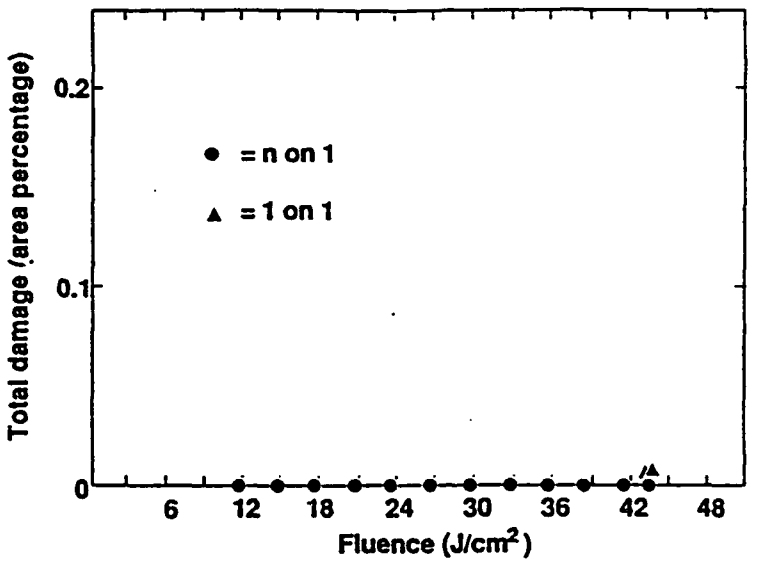

Figure 33. $[SiO_2\text{-}Al_2O_3]^2$ sol-gel.

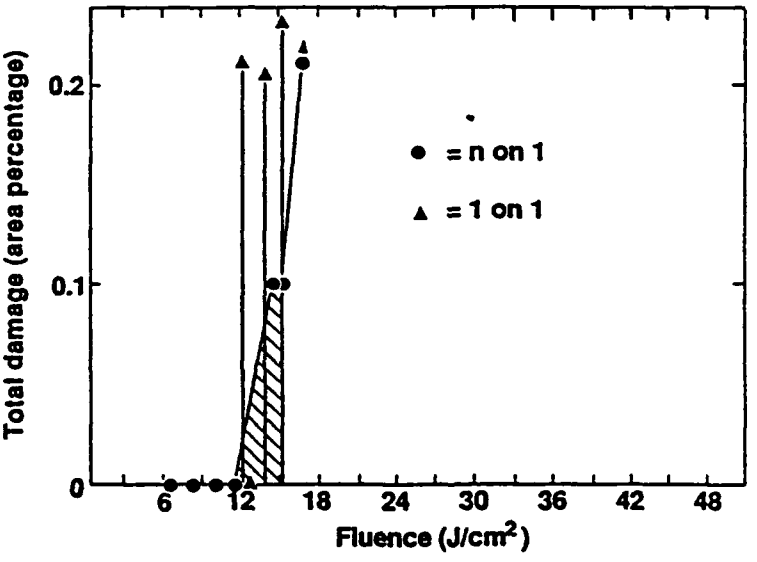

Figure 34. $[ZrO_2]^1$ sol-gel.

with respect to the damage threshold of the resulting films. The first method applied a precursor solution to the substrate with subsequent conversion of the precursor to an oxide on the substrate surface through addition of water and heat. In the second method, a colloidal suspension of an oxide is applied to the substrate with subsequent evaporation of the suspending medium at room temperature. The second method is superior to the first if multilayers are deposited since the conversion of the precursor to the oxide in the first method involves shrinkage due to the necessary removal of the residual reactive groups which creates a stress and subsequently causes crazing and peeling of the film. Single layers of Al_2O_3, ZrO_2 and HfO_2 were prepared by the first method. Using the second method, single layers of SiO_2, $Al_2O_3 \cdot H_2O$, ZrO_2, HfO_2 and TiO_2 were prepared as well as multilayers of the two best materials: $SiO_2/Al_2O_3 \cdot H_2O$. With 35 layers of the latter pair, HR mirrors with reflectance of 99% at 1064 nm were achieved. The damage threshold data presented in Table 13 was obtained with single shot pulses of 10 nsec duration and 16 nsec pulses at 120 Hz. The data presented in Figure 35 was obtained with single shot pulses of 10 nsec duration. From the table it is clear SiO_2/Al_2O_3 is the most damage resistant pair for a multilayer. Damage thresholds for the multilayer show a wide spread with average about 12 J/cm^2, well below the 30 to 40 J/cm^2 threshold found for the single layers. It is observed that the number of damage sites increases with the number of layers suggesting absorptive sites are increasing with each added layer. It is hypothesized that the damage threshold of sites decreases with coating thickness due to liberation of gases (H_2O and CO_2) when an underlying site damages. While these gases escape in a thin coating, they propagate damage in a thicker coating due to the weak particle to particle bonding in these films.

Table 13. Laser Damage Thresholds and Refractive Indices of Single Oxide Coatings

Oxide	Index	Damage at 1064 nm • J/cm^2	
		10 ns, Single Shot	16 ns, 120 Hz
SiO_2	1.20	30-40	30-40
$Al_2O_3 \cdot H_2O$	1.43	20-30	30
ZrO_2	1.55	10-20	10-15
HfO_2	1.52	15-20	15-20
TiO_2	1.75	15-20	2-5

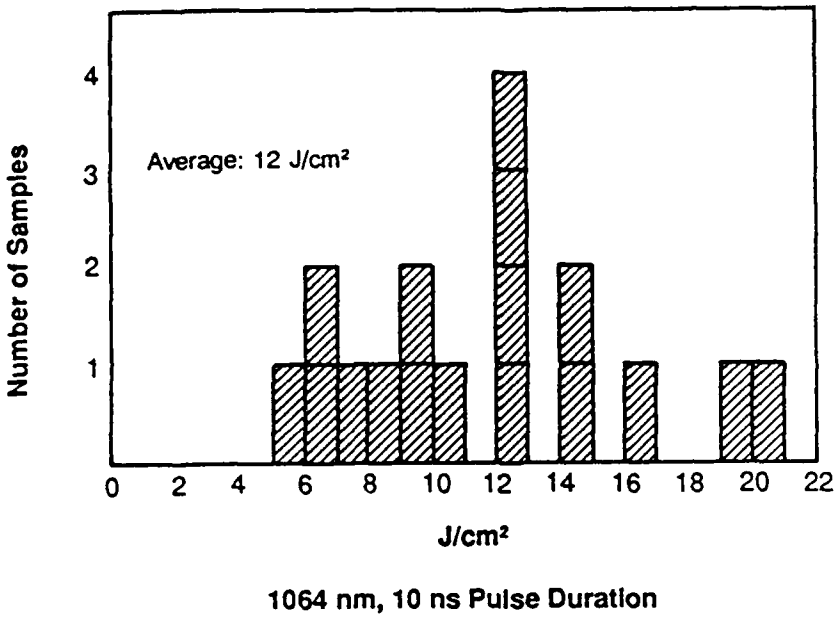

Figure 35. Laser damage thresholds of $Al_2O_3 \cdot H_2O$-SiO_2 multilayer coatings.

Further damage threshold measurements on refractory oxide multilayers synthesized by the sol-gel process were made by Floch, et. al. (Ref. 13). The second method described in Ref. 12 was used to prepare ThO_2/SiO_2 multilayer HR coatings. Coatings consisting of 21 layers exhibited reflectance of 98% at 1064 nm. By changing thickness of the layers, unstressed HR coatings could be achieved with reflection maxima varying from 0.3 μm to several microns.

The damage thresholds presented in Figures 36 and 37 corresponds to single shot pulses of 1 nsec at laser wavelength of 1064 nm. The data in Figures 38 and 39 was obtained with single shot pulses of 3 nsec at laser wavelength of 350 nm. Figures 36 and 38 present data for single layers and Figures 37 and 39 present data for ThO_2/SiO_2 multilayers. The effect of a long sol dialysis in improving damage threshold is shown. As in reference 12, damage thresholds of multilayers at 1064 nm (8.7 J/cm² average) are inferior to those of single layers (12.3 J/cm² average). At the 350 nm wavelength, the single layers and multilayers had average damage thresholds of 33.6 J/cm² and 2.6 J/cm², respectively. The low thresholds at this wavelength cannot be attributed to the ThO_2 UV cutoff (~250 nm) but are probably due to residual nitrates which exhibit absorption bands around 302 nm. This absorption could be eliminated by changing the metal precursor used to form the colloidal oxide. Another hypothesis is that absorption at 350 nm may be due to trapped parasitic organic species in the multilayers. Oxidation of these species offers hope of eliminating this absorption mechanism.

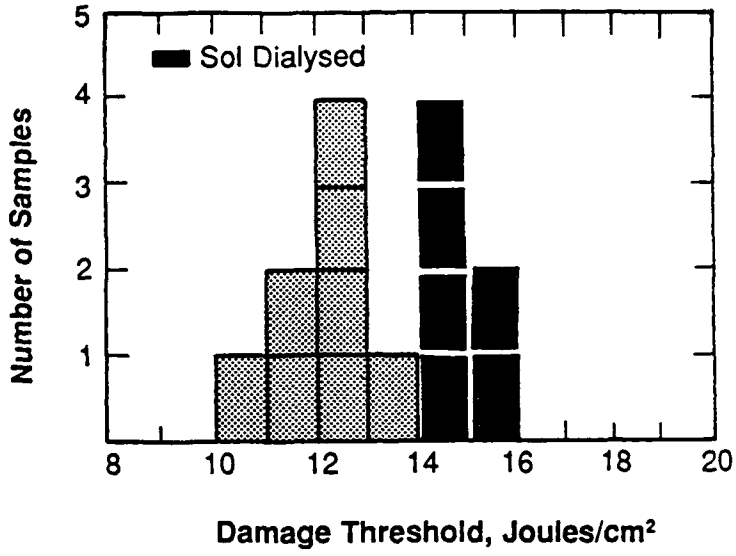

Figure 36. Radiation stability of ThO_2 coatings at 1064 nm - 1 ns.

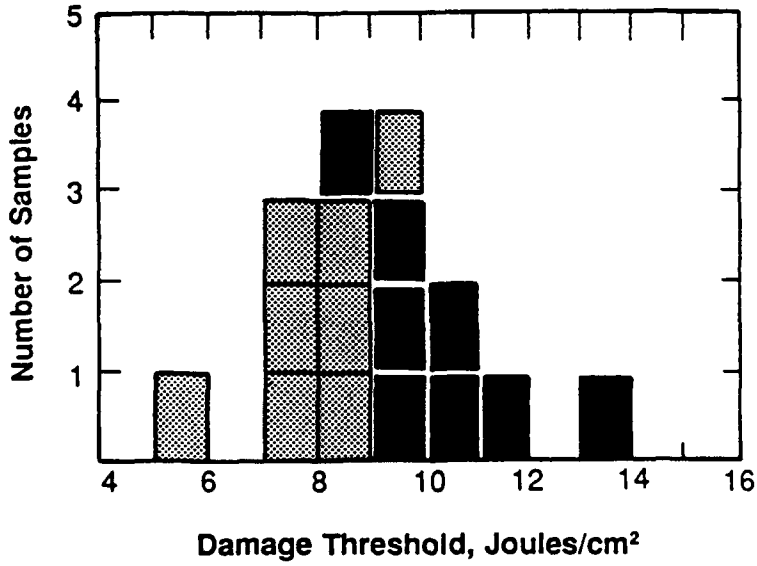

Figure 37. Radiation stability of ThO_2-SiO_2 coatings at 1064 nm - 1 ns.

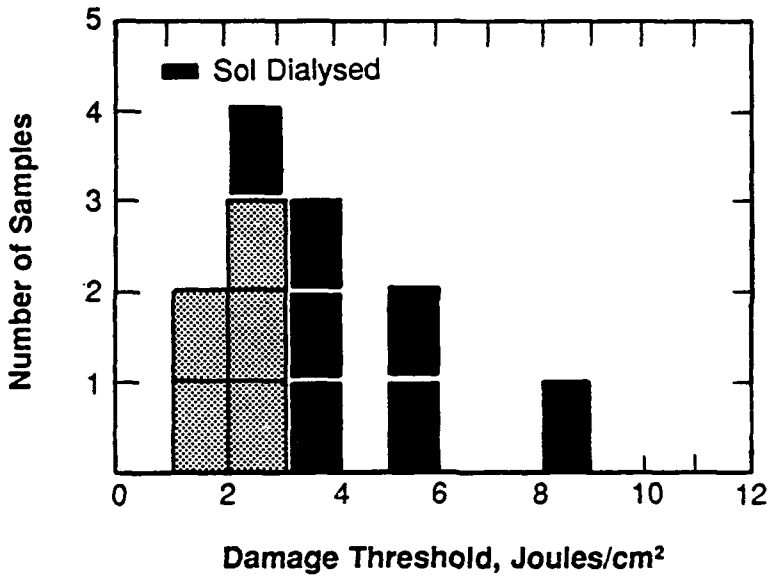

Figure 38. Radiation stability of ThO_2 coatings at 350 nm - 3 ns.

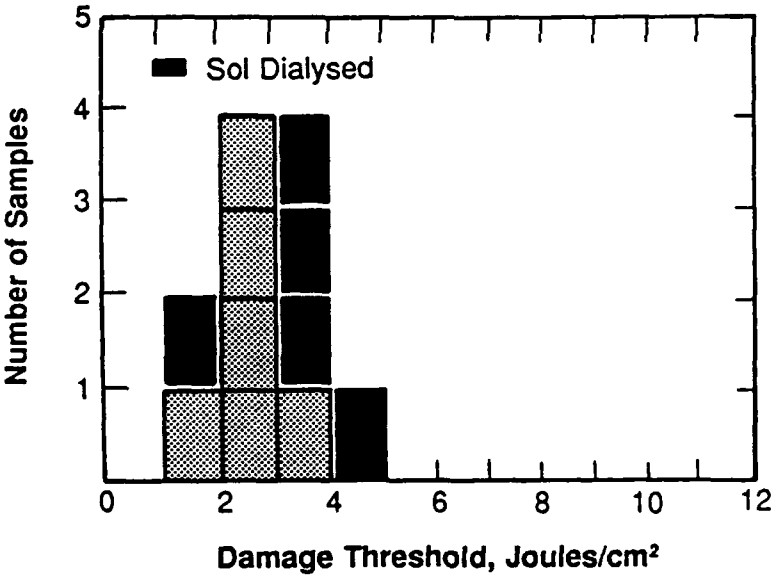

Figure 39. Radiation stability of ThO_2-SiO_2 coatings at 350 nm - 3 ns.

Brusasco, et. al. (Ref. 14) prepared single layer Al_2O_3, HfO_2 and ZrO_2 coatings by chemical vapor deposition (CVD). The reactions were achieved in a horizontal silica reactor of 140 mm diameter using Ar as the carrier gas. Three types of reactions were employed: (1) simple thermal decomposition at high temperature (400°C), (2) simple thermal decomposition at low temperature (250°C), and (3) chemically assisted deposition (CAD) at low temperature (250°C). In the latter method, tert-butanol is admitted to the reaction zone and dehydrates into water and isobutylene at the hot substrate surface. The water formed assists in the decomposition of the source material.

Damage threshold data presented in Table 14 and Figure 40 was collected from single shot 1 on 1 exposures with 10 nsec pulses at a wavelength of 1060 nm. Damage thresholds of films at this wavelength prepared by thermal decomposition at 400°C are lower than those achieved by sol-gel prepared films. Damage thresholds of these films were found to be insensitive to film thickness and deposition conditions such as flow rate, presence or absence of additional oxygen during deposition, deposition rate or post deposition treatment consisting of air annealing and treatments with H_2O_2 or O_3 and UV light suggesting chemical inertness of the damage nucleation sites. Microscopic examination of the damaged film revealed that damage begins at a multitude of sites rapidly increasing in size as the fluence increases. The damage mechanism is attributed to absorption as is apparent from transmission spectral measurements. This absorption was observed to be less in films prepared at lower temperature and for films prepared by CVD. Damage thresholds of these films were correspondingly higher. The effect of lowering substrate temperature without addition of ±-butenol was a damage threshold intermediate to high temperature and CAD films. Apparent in the data of Figure 40 is that Al_2O_3 and HfO_2 damage thresholds decrease with increasing film thickness while the ZrO_2 damage threshold tends to increase with film thickness. Damage morphology of these films exhibits a few small damage sites which do not grow significantly at fluences exceeding the threshold.

Table 14. Single Shot Laser Damage Threshold (400°C Deposition)*

Material	Threshold (J/cm^2) ± 10%
Alumina	4.0
Zirconia	7.0
Hafnia	10.0

*Single Shot Test, 1-on-1, 1060 nm, 10 ns duration.

Further evidence of improvement in damage threshold by heat treatment is given by Pond, et. al. (Ref. 15). It was found that codeposition of ZrO_2 and SiO_2 by ion beam sputtering produced films exhibiting lower absorption and lower stress than either component deposited separately by the same process. Subsequent baking at 300°C of the mixed oxides having silica fractions between 10% and 50% resulted in compressive stresses in the range of 40 to 50 kpsi as compared to 219 kpsi for ZrO_2 and 112 kpsi for SiO_2 films alone. For films with a silica fraction less than 50%, the stress after baking was tensile. For a 10% silica content, baking converted a 46 kpsi compressive stress to 23 kpsi tensile stress. Similar results were found for mixed oxide films of ZrO_2 and Al_2O_3. Unfortunately, no laser damage thresholds were measured for these films.

The work reported by Thomas, et. al. (Ref. 16) describes a post deposition treatment to improve the damage threshold of SiO_2 coatings prepared by applying colloidal silica suspensions to silica substrates. As coating thickness was increased, a drastic reduction in laser damage threshold at 350 nm was noted. The lowered damage threshold was attributed to absorptive organic entities in the pores of the coating remaining from the methanol and ethanol in which the colloid was suspended. It was found that damage thresholds could be restored to values corresponding to thinner coatings by exposure to UV and ozone in vacuum. By replacing ozone with nitrogen and placing samples in vacuum without exposure to UV it was shown that ozone and/or vacuum treatment were effective in improving the damage threshold.

The data shown in Table 15 was compiled using a 350 nm laser with a 25 nsec pulse width for 1000 shots at a rate of 25 Hz.

Table 15. Damage Thresholds Before and After Treatment

Treatment	Time	Average Damage		Number of Samples
		Before	After	
UV/O_2	15 min	12.1 J/cm^2	14.0 J/cm^2	5
UV/O_2	30 min	8.5 J/cm^2	17.7 J/cm^2	6
UV/O_2	60 min	8.4 J/cm^2	16.7 J/cm^2	4
UV/O_2	90 min	6.6 J/cm^2	10.7 J/cm^2	6
UV/N_2	60 min	7.3 J/cm^2	7.6 J/cm^2	2
UV/vacuum	60 min	7.6 J/cm^2	21.0 J/cm^2	1
Vacuum/80°C	60 min	9.0 J/cm^2	19.0 J/cm^2	2
O_3/room temperature	30 min	13.3 J/cm^2	19.3 J/cm^2	2

The application of room temperature chemical vapor deposition (CVD) to deposit TiO_2 coatings was discussed by Wilder, et. al. (Ref. 17). The objective of this work was to investigate a CVD process to assess if even higher damage thresholds (exceeding 7 to 10 J/cm^2 at 1.06 μm and 1 nsec pulse width) can be achieved than those found for other deposition techniques. Twenty-two TiO_2 coatings were deposited with optical thickness ranging from 1000 to 2500 Å and refractive index from 1.8 to 2.4. Two $TiO_2/SiO_2/TiO_2$ multilayers were deposited with total optical thickness of 5000 Å. Some scatter and nonuniformity was indicated. Water solubility suggested incomplete hydrolysis in the CVD reaction.

Damage testing was performed with a 3 mm diameter 1.06 um laser beam with 1 nsec pulses. No test site was irradiated more than once, the energy level at each site increasing until a damage threshold (± 15%) was determined by inspection with a 108X microscope. Ten coatings exhibiting the least scatter were tested. The three multilayers exhibited damage thresholds of 3.4, 3.5 and 4.4 J/cm^2. The seven single layer coatings damaged at 4.2, 5.3, 5.8, 7.8, 8.7, 9.0 and 12.9 J/cm^2. Results suggest that higher thresholds for TiO_2 films can be achieved by CVD then by more conventional deposition techniques.

2.3 COMPARISON OF PHYSICAL AND CHEMICAL DEPOSITION PROCESSES

The affect of post deposition annealing on film microstructure, optical absorption and laser damage threshold was studied by Stewart, et. al. (Ref. 18). The intent was to determine if beneficial changes (regrowth of the film structure) could be induced in dielectric films through a laser annealing process. Single layer films (1/2 wave optical thickness at 1064 nm) of Al_2O_3 and Ta_2O_5 were prepared by E-beam evaporation and reactive sputtering. TiO_2 films were prepared by a sol-gel process. Super polished ultra low scatter 1.5 inch and 2.0 inch diameter fused silica substrates were used.

To determine if laser annealing was able to remove defects by regrowth, transmission, reflection, scattering, absorption and damage measurements were made before and after the anneal. Observed changes provided information on resultant microstructure, band structure and alteration or removal of defects.

The films were annealed using a 15 kilowatt CO_2 laser at reduced power levels. Levels exceeding 25 to 50 W/cm^2 were found to degrade transmission. The beam had a uniform profile and diameter of 8.9 cm at the sample. Samples were scanned across the beam at 1.5 cm/sec. This

produced a treatment principally at the surface, though the film thickness and substrate were also affected.

For the reactively sputtered films, transmittance dropped at higher power levels and transmission maxima shifted toward longer wavelengths. The Al_2O_3 sputtered films exhibited some change in index and a shift to shorter wavelength of the UV cutoff. Changes in refractive indicies and thickness of the E-beam deposited films were also evident. The Al_2O_3 films prepared by E-beam were found to craze after annealing at the 50 W/cm^2 level.

The TiO_2 sol gel films had slightly lower transmittance after higher intensity anneals and exhibited small shifts in peak transmittance toward the UV. Scattering measurements made before and after depositing the films indicated the substrates were exceptionally smooth, however, after deposition, the scattering increased by a factor of 100. This level of scattering was not significantly affected by annealing at the 25 and 50 W/cm^2 level. Higher power level anneals crystallized the films increasing scatter by two to four order of magnitude. Measurements indicated that compressive stress increased with annealing temperature but only for the Ta_2O_5 film deposited by either E-beam or reactive sputtering. Absorption measurements taken at a wavelength of 351 nm using a laser calorimeter indicated that absorption dropped by 5 to 90% as annealing power was increased with the exception of E-beam deposited Ta_2O_5 films in which annealing increased absorption by a factor of 3.

The damage threshold data presented in Figures 41 to 43 and Table 16 was obtained using a Nd:YAG laser (1064 nm, single mode) with 7 nsec pulse duration and 710 micron spot size. One on one testing was performed at 144 sites, the criterion for damage being observable change in the film observed with a Nomerski microscope (200X). Two samples of each type annealed at 75 and 100 W/cm^2 were tested. An unannealed sample and one sample each annealed at 75 and 100 W/cm^2 were also tested.

Damage morphologies in all films remained consistent up to the 50 W/cm^2 annealing level but changed dramatically for films annealed at higher levels. E-beam deposited Ta_2O_5 films exhibited damage morphology independent of fluence for films annealed at higher power levels likely due to sensitivity of damage threshold to substrate contamination. Damage threshold of reactively sputtered Al_2O_3 films remained unchanged after annealing, even though film crystalline structure, surface appearance, scattering level, transmissivity and damage morphology changed considerably with annealing level. Based on damage morphology of the Al_2O_3 films revealing uniform round areas of complete ablation or alteration (but absence of pitting), damage was

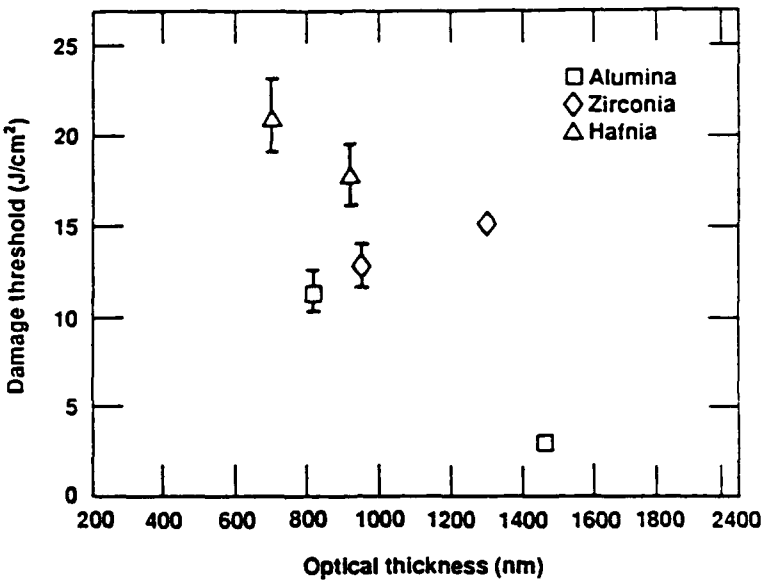

Figure 40. Laser damage thresholds measured at 1064 nm on annealed Al_2O_3 films microscopy at typical magnification of 100 times fabricated by reactive sputtering.

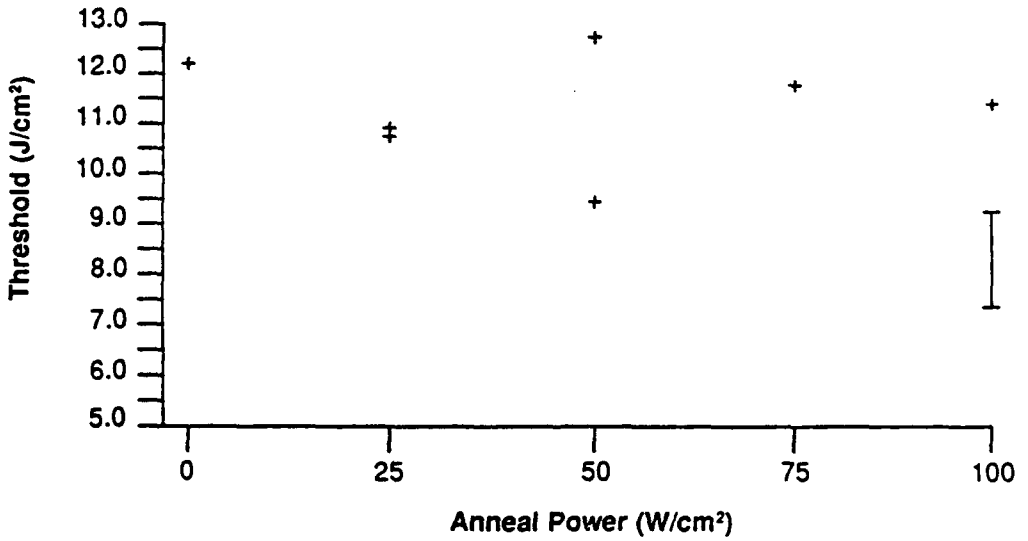

Figure 41. Laser damage threshold as a function of film thickness. Films prepared using chemical assisted deposition method.

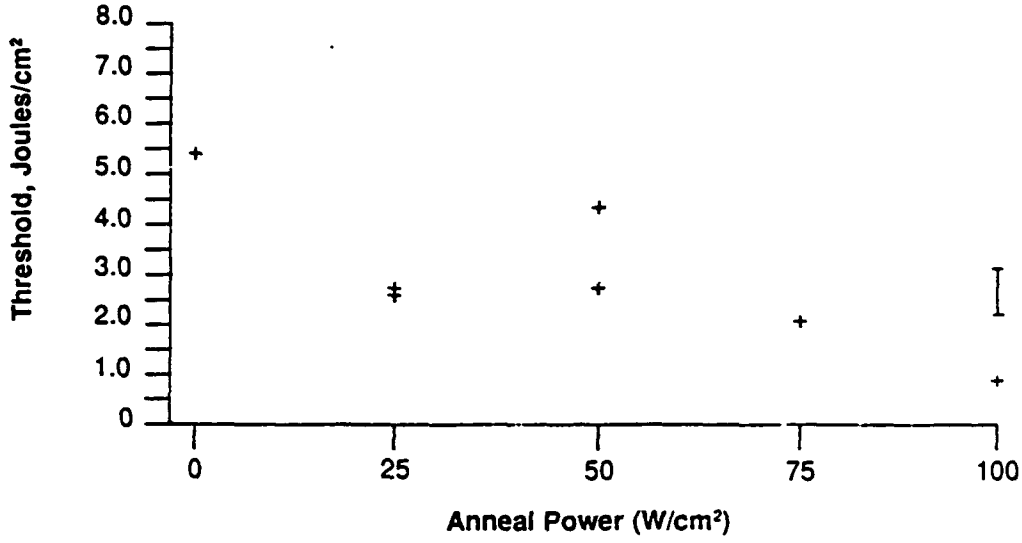

Figure 42. Laser damage thresholds measured at 1064 nm on annealed Ta_2O_5 films fabricated by reactive sputtering.

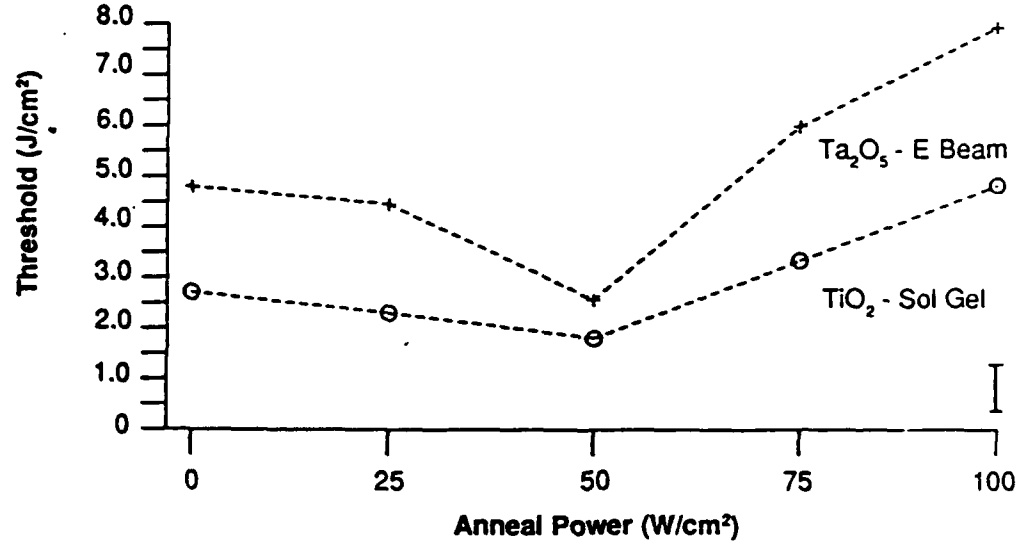

Figure 43. Laser damage thresholds measured at 1064 nm on annealed films of electron beam Ta_2O_5 and sol-gel TiO_2.

Table 16. Summary of Annealed Film Characterization Data

Annealing Power (W/cm^2)	0	25	50	75	100	
Refractive index at 500 nm	1.64	1.64	1.57	1.59	1.78	Al_2O_3, rs
	2.12	2.13	2.11	2.08	2.06	Ta_2O_5, rs
	2.01	2.01	2.03	2.02	2.06	Ta_2O_5, eb
	1.8	--	--	--	--	TiO_2, sol
Absorption at 351 nm (%)	0.192	--	0.115	--	--	Al_2O_3, rs
	0.265	0.323	0.208	--	--	Ta_2O_5, rs
	0.698	1.920	--	--	--	Ta_2O_5, eb
	8.650	8.230	8.210	--	--	TiO_2, sol
Crystal structure	Amorphous	A	A	A	A	Al_2O_3, rs
	A	A	A	Orthorhombic		Ta_2O_5, rs
	A	A	A	Orthorhombic		Ta_2O_5, eb
	A	A	A	Rutile/anatase		TiO_2, sol
Stress (MPa)	352	--	354	--	--	Al_2O_3, rs
	181	318	432	--	--	Ta_2O_5, rs
	128	261	--	--	--	Ta_2O_5, eb
	0	0	0	--	--	TiO_2, sol
Laser damage threshold at 1064 nm (J/cm2)	12.2	10.8	11.1	11.7	11.3	Al_2O_3, rs
	5.4	2.6	3.5	2.1	0.9	Ta_2O_5, rs
	2.7	2.3	1.8	3.3	4.8	Ta_2O_5, eb
	4.8	4.4	2.6	6.0	7.9	TiO_2, sol
Scattering at 633 nm (PPM/Str)	-26%	-26%	277%	1000%+	1000%+	Al_2O_3, rs
	-54%	39%	-31%	"	"	Ta_2O_5, rs
	-18%	37%	22%	"	"	Ta_2O_5, eb
	6%	-1%	-11%	"	"	TiO_2, sol
Peak temperature	20°C	380°C	660°C	900°C	1250°C	

thought to be absorption dominated. Reactively sputtered Ta_2O_5 films exhibited a trend toward reduced damage threshold as annealing power was increased. Also, the spread in fluence resulting in damage or nondamage increased with annealing power. The damage morphology was also influenced by the annealing level. For E-beam deposited Ta_2O_5 films and TiO_2 sol gel coatings, the damage threshold decreased to a low level at 50 W/cm^2 anneal and then increased for higher level anneals.

In summary, annealing at levels greater than 75 W/cm^2 caused the most significant changes in film characteristics due to crystallization. Damage thresholds and refractive index increased for some films and decreased for others. Depending on the deposition process, the resulting film structure and contaminants such as water and hydrocarbons played a key role in changes observed before and after annealing. Competing processes of water removal and densification or crystallization were thought to explain the majority of the observed phenomena. E-beam and sol gel deposited films are very porous. Annealing at higher temperatures is thought to promote growth of crystallites in these films resulting in increased damage thresholds but increased light scattering and stress. In Ta_2O_5, crystallite growth is thought to rupture pre-existing bonds increasing optical absorption. Lower absorption on Al_2O_3 films after anneal is attributed to further oxidation improving the stoichrometry. In sputtered films, the stimulation of crystallite growth by annealing was thought to be responsible for the lower damage thresholds observed and increased stress and light scattering. These films are dense as deposited and crystallite growth disrupts existing bonding patterns. The annealing can result in improved properties in some performance criteria, however, the process is relatively uncontrolled and tradeoffs are involved in performance.

A data base of laser induced average power damage thresholds at 1064 nm was compiled by Rainer, et. al. (Ref. 19) on a variety of materials using the REPTILE (Repetition Laser Experiment) Facility at Lawerence Livermore Laboratories. Data collected on AR and HR refractory oxide coatings is presented in Figures 44 to 46. Characteristics of the laser are shown in the figures. Damage is determined by comparing pre and post irradiation photographs generated by Nomarski bright field or dark field microscopy at typical magnification of 100 times.

A broad spectrum of samples were tested obtained from within Lawrence Livermore and from commercial vendors. Samples are representative of state-of-the-art technology, current optics in use in one of the laboratory's laser systems and both current and old developmental research samples. None of the results of the data bases is necessarily representative of the highest, lowest or average damage thresholds attainable for that category of coating. Moreover, in some cases they

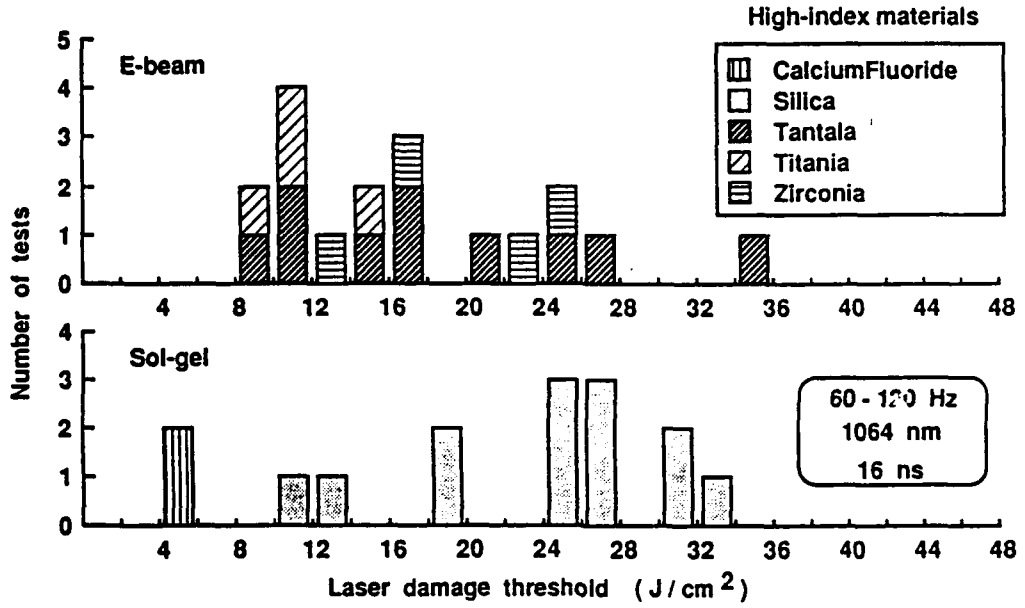

Figure 44. Distribution of laser damage thresholds of 33 E-beam- and sol-gel-deposited anti-reflective coatings. Spreads in the threshold for a particular material combination are attributable to different coating designs or deposition parameters.

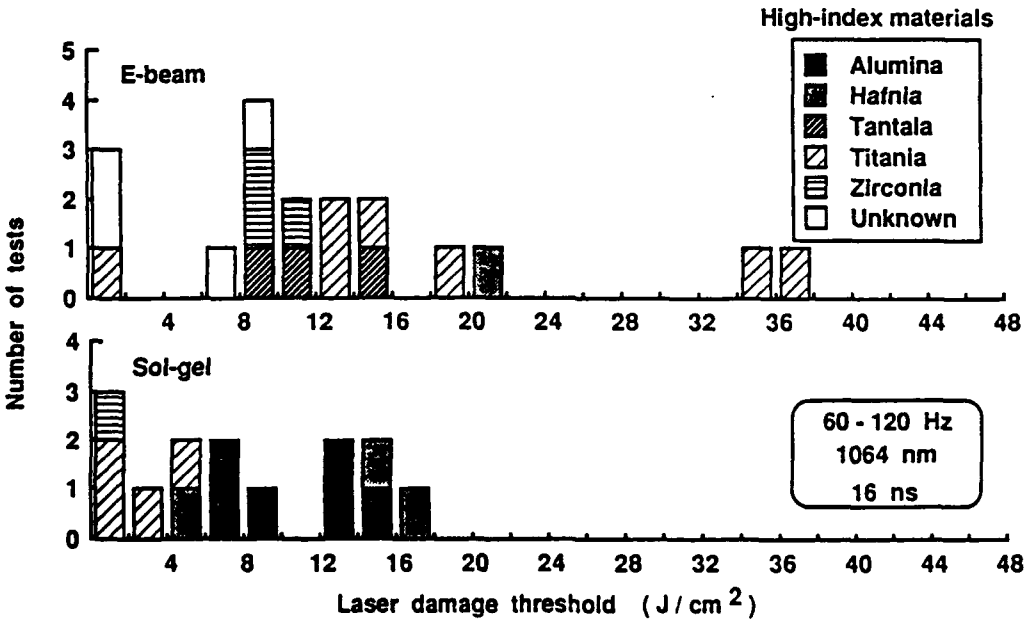

Figure 45. Laser damage thresholds of 32 E-beam- and sol-gel-deposited anti-reflective coatings. All samples are comprised of multilayer stacks of the designated high-index material and silica. Materials of some E-beam coatings were not specified by the vendors

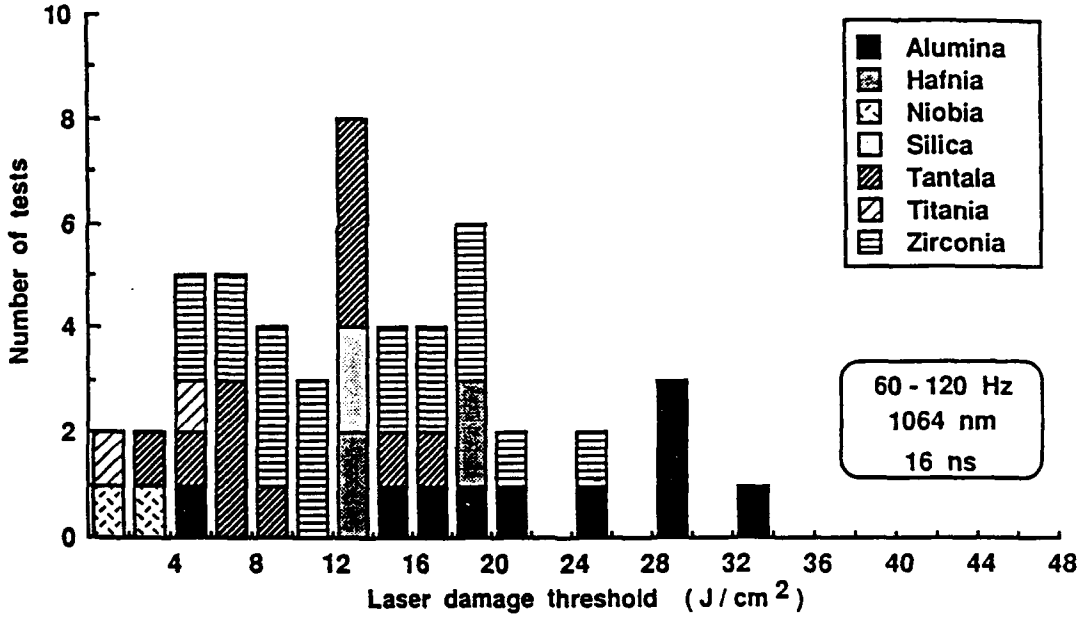

Figure 46. **Laser damage thresholds of 51 single and multiple-layer sol-gel samples of a single material. All were fabricated at LLNL on fused silica substrates. The two silica tests were for frosted type coatings. All other silica tests are listed under the AR database.**

represent evolutionary development of improved thresholds or parameter studies, which may encompass a large spread in thresholds.

In Figure 44, E-beam fabricated coatings are compared to sol gel fabricated coatings. The E-beam coatings are multilayers deposited on either fused silica or BK-7 glass substrates. The high index materials shown are combined with low index layers of SiO_2 or MgF_2 to form AR coatings of various designs. The large spread in damage thresholds is attributed to variation in coating design and deposition parameters. Tests of more samples of an optimum design for each material combination would yield tighter distribution groupings for Ta_2O_5, ZrO_2 and TiO_2 AR coatings.

The sol gel AR coatings are single and multiple layer porous coatings of primarily SiO_2. They represent a variety of processing techniques attempting to establish optimum parameters for producing high level thresholds. The spread represents improvements in the deposition process rather than intrinsic variability in the sol gel process. Substrates were fused silica, calcium fluoride and KDP crystals, the latter not having particularly clean nor well polished surfaces and correspondingly exhibiting the lowest damage thresholds. In general, the optimal sol gel deposited coatings had comparable damage thresholds to the best E-beam coatings.

Four different vendors provided 32 HR coatings on fused silica, BK-7, SiC or Cu substrates. The low index material was SiO_2 for most or all samples. As can be seen from Figure 45, the highest threshold sample was a TiO_2/SiO_2 stack developed as a research coating several years ago. Most of the stacks of this combination were variations of the optimum design.

The sol gel HR coatings are multilayer stacks of the listed materials and sol gel deposited SiO_2, all on fused silica substrates. All of these had thresholds notably lower than those of single or multiple layers of the individual constituent materials. Thresholds were lower than the best E-beam coatings.Single material tests were conducted with sol gel materials on fused silica substrates. Threshold data derived from 51 samples is shown in Figure 46. Highest thresholds were obtained with Al_2O_3 coatings, although ZrO_2, HfO_2 and Ta_2O_5 also look promising. The silica coatings in this data net were specially designed to create a frosted surface effect which may explain their somewhat lower thresholds.

High temperature (T > 850°C) plasma assisted chemical vapor deposition of fused SiO_2 and SiO_2 doped with a glass network modifier was used by Campbell, et. al. (Ref. 20) to evaluate laser damage thresholds of several thousand quarter-wave layer 1.06 μm wavelength HR coatings. By keeping the doping concentration of alternating layers low, the damage resistant characteristics of SiO_2 achieved by vapor-phase hydrolysis of $SiCl_4$ are preserved. Since the resulting material is nearly compositionally uniform, there are no distinct material interfaces with thermal-mechanical or chemical incompatibility. The chemical stoichiometry is uniformally controlled throughout the material by use of high-temperature, oxidizing deposition techniques. Dust or dirt or other particulate contamination is fully oxidized and either dissolved directly in the glass or incorporated as an insignificant low absorption, scattering center. Finally, the fused silica is a fully dense amorphous body without the high density of microstructural defects that are often produced by conventional physical vapor deposition processes.

The multilayers were deposited on the inside of a 1.7 cm diameter SiO_2 tube that also served as the reaction chamber using a plasma-impulse-CVD process developed by Schott Glaswerke. In this process, the SiO_2 tube is heated by a furnace to 800° to 1100°C. The output from a 2.45 GHz magnetron, triggered by a pulse generator, drives the deposition process. First the tube is filled with the gas reactants ($SiCl_4$, O_2), second the plasma is ignited and sustained by a pulse from the magnetron. The plasma ignited inside the tube drives a gas phase reaction between $SiCl_4$ and O_2 producing a thin amorphous deposit on the tube wall. Excellent thickness coating control is achieved by controlling reactant composition and pressure. The final step consists of pumping out product gas and continuously refilling the tube with reactants. Co-dopants of Ge and

F were used to produce the alternating different index layers. Deposition rates were 2 μm/minute over the 50 cm tube length.

Damage thresholds were measured on coatings consisting of 1000 or more layers of doped SiO_2 and compared to damage thresholds of bulk super polished fused silica. It is inferred that the coating index profile is sinusoidal with an index amplitude of 0.02 or less. Laser damage thresholds were measured on the inside diameter of the coated silica tube after sectioning length wise into four pieces. An N:1 test format was used. A 1064 nm laser beam was incident at 10 degrees using a 16 nsec pulse width and a PRF of 30 Hz. The beam was focused with a long focal length lens to a spot size of 1 mm diameter. Damage was determined by noting any change after irradiation using 100x Nomarski microscopy. Damage thresholds are compared with surface damage thresholds of super polished (Zygo) fused silica and Ge doped fused silica prepared by very high temperature CVD (1800°C) as shown in Figure 47. Damage thresholds prepared by this plasma CVD process were found to be comparable to those for super-polished fused silica surfaces.

HR multilayer coatings for 1.06 μm reflectance were prepared by Thomas, et. al. (Ref. 21) from quarter-wave thick colloidal suspensions of hydrated alumina and silica on substrates up to 8 inches in diameter. Suspensions of AlOOH and SiO_2 were prepared by the hydrolysis of distilled sec-butoxide aluminum and tetraethylsilicate, respectively. The SiO_2 suspension was prepared at 3% concentration in ethanol and diluted to 2% prior to use. The AlOOH suspension was prepared at 1% concentration in water and adjusted to pH 5 with an ion exchange resin, evaporated under vacuum to 16% and finally diluted to 4% with methanol prior to use. Coating suspensions were filtered through a 0.2 μm membrane. Thirty-two to thirty-six alternating quarter-wave layers were spin coated onto the substrate starting with the SiO_2 layer and ending with the AlOOH layer allowing 10 to 15 minutes drying time between layers.

Damage threshold measurements were made with a 1.06 μm laser using multishots at a pulse length of 16 nsec at 30 Hz. The spot size was approximately 1 mm^2, each site being irradiated for 60 seconds (1800 shots) and then inspected for damage. A new site was selected and the irradiation repeated. The damage threshold was defined as the average of the highest fluence which caused no damage and the lowest fluence which did. Damage thresholds ranging from 21 to 50 J/cm^2, with an average of 37 J/cm^2, are shown in Table 17 and exhibit no dependence on the number of layers. Damage thresholds are higher than previously reported, improvement thought to be partially due to improved cleanliness.

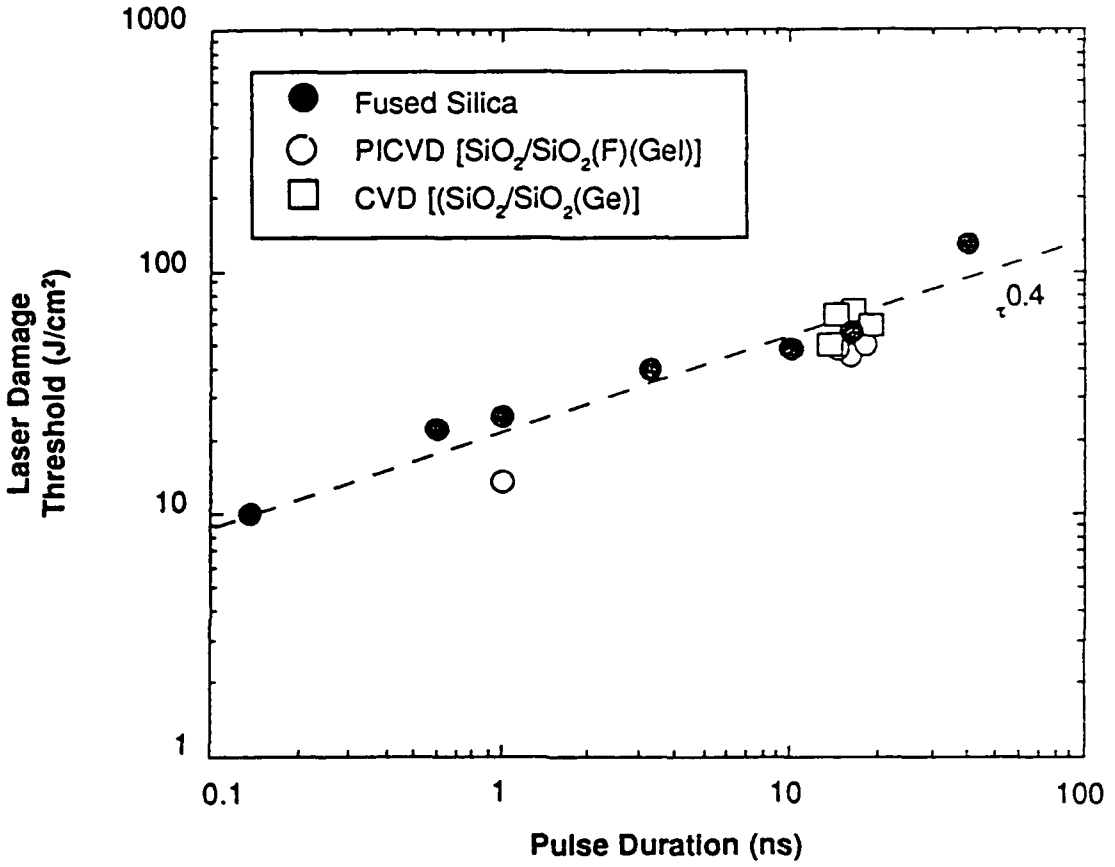

Figure 47. Measured damage threshold at 1064 nm versus pulse width for super-polished, bare fused silica and coatings prepared by either PICVD or very high temperature (~1800°C) CVD. The data for the bare fused silica are from References 15, 18, and 19. The PICVD coating samples consisted of 1000 or more quarter-wave layers of doped SiO_2. (Reference numbers stated refer to document from which data was extracted.)

Table 17. Reflectance and Damage Threshold of Several HR Coatings

Layers	Reflection at 1.06 μm (%)	Damage 1064 nm/16 ns (J/cm^2)
26	95.0	34
30	98.0	45
30	98.5	28
32	98.0	38
32	98.5	50
34	99.0	21
36	99.0	37
40	99.5	40

The objective of work performed by Floch, et. al. (Ref. 22) was to replace the AlOOH in the AlOOH-SiO_2 colloidal HR multilayer with ZrO_2 to achieve the same reflectance at 1.06 μm wavelength with fewer layers since it has a higher index. The fewer layers were also anticipated to reduce the scatter since fewer contaminants would be introduced. The zirconia suspension was prepared from recrystallized zirconium oxychloride octahydrate. The resulting colloidal suspension containing the equivalent of 12% ZrO_2 was filtered through a hydrophilic 1.0 μm teflon membrane. An SEM revealed 300 to 500 Å spheroidal particles. X-ray diffraction revealed monoclinic microcrystals.

In the colloidal suspension prepared, hydroxyl groups bound to underlying zirconia atoms were reacted with hydrolyzable zirconium compounds such as an oxychloride salt. The resulting zirconium dichloride oxide acts as a binder to increase the adhesion between adjacent particles resulting in a stronger more abrasive resistant coating. Crosslinking increases with the amount of reagent added decreasing the porosity and increasing the refractive index. The increase in index reduces the number of layers required to achieve the desired reflectance. The final binder containing coating mixture included a total of 15% zirconia, 70% colloidal and 30% in solution as a soluble zirconium oxo-hydroxo polycation.

The silica sol was prepared by the base catalyzed hydrolysis of distilled tetraethylsilicate in pure ethanol or methanol. The material was prepared at 3% silica concentration and consisted of monodispersed roughly spherical particles with a diameter of about 20 nm.

The coatings were deposited on 5 cm diameter 1 cm thick fused silica BK-7 glass substrates by spin coating at room temperature and 50 to 60% relative humidity. Hydrophilic substrate

surfaces were achieved using a $UV/O_2/H_2O_2$ ozone photoreactor. The ZrO_2 coatings applied had binder ratios ranging from 10% to 40%. Spin speed was 1500 RPM. Silica coatings were applied from a suspension in ethanol containing 3% SiO_2 in a basic medium (pH~10) at a spin speed of 1300 rpm. Coatings were air dried for 10 minutes prior to depositing the next layer.

Damage threshold measurements were made using a 1.06 μm laser with 3 nsec single shot pulses. The beam size was 2 mm in diameter. Two test formats were applied, 1 on 1 (one shot of known fluence on a selected site) and n on 1 (n shots of ramped fluence on a selected site). Each site was microscopically inspected and photographed before and after irradiation. Damage was defined as any evolutive 5 to 10 micron size alteration observable. Damage threshold was defined as the average of the highest fluence which caused no damage and the lowest fluence which did. Damage thresholds for ZrO_2 single layer coatings for both test formats are shown in Figure 48. For the 1 on 1 format, thresholds ranged from 6.3 J/cm^2 to 11.7 J/cm^2 with an average of 11.7 J/cm^2, the wide range attributed to local contamination inherent to the process. Samples with low thresholds showed only small defects in the beam area. Massive damage over the whole beam area did not occur until fluences in the range of 14 to 15 J/cm^2 were applied. In all cases, damage was observed to originate at visible artifacts. The enhancement in damage threshold due to pulse annealing (the n on 1 format) is thought to be due to a gentle desorption of volatile absorbing contaminants through coating porosity.

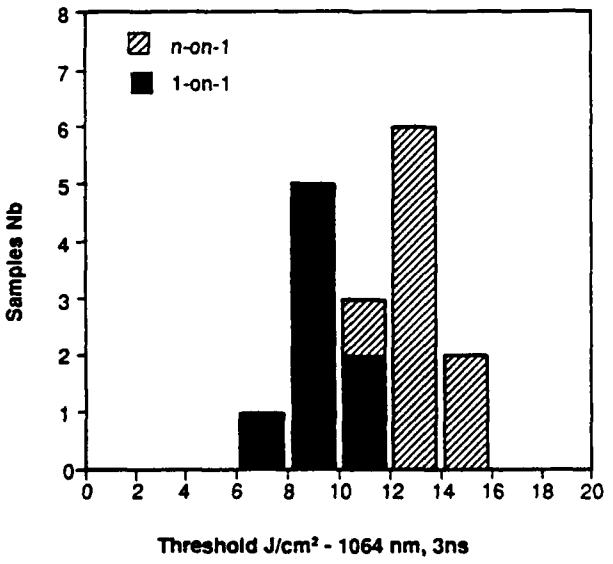

Figure 48. 1-on-1 and n-on-1 laser strength of binder-aided ZrO_2 coatings.

Damage thresholds for 17 layer HR coatings varied from 8.0 J/cm^2 to 8.8 J/cm^2 with an average of 8.2 J/cm^2. The improvement in threshold relative to the single layers was thought to possibly be to the binder covering the zirconia particles, substantially reducing their specific area, consequently decreasing their spontaneous chemical absorption which may contribute to their laser resistance. The thresholds for the laser annealed samples (n on 1 format) ranged from 10.5 J/cm^2 to 13.7 J/cm^2 with an average of 12 J/cm^2. At threshold values, damage consisted of disperse and tiny spots about 10 to 20 microns in size. For the n on 1 format, massive damage occurred at 25 to 30 J/cm^2 with catastrophic failure about 300 μm in diameter.

2.4 OTHER RELEVANT ISSUES

The damage thresholds of refractory oxides used as AR coatings for alexandrite laser rods were determined and measured by Gallegos, et. al. (Ref. 23). Eight different coatings were supplied by seven different vendors. Material combinations included: TiO_2/SiO_2, ZrO_2/SiO_2, Al_2O_3/SiO_2, Sc_2O_3/SiO_2, Ta_2O_5/SiO_2 and HfO_2/SiO_2. They were all two layer designs with half wave undercoats of SiO_2. Sapphire substrates were used and a limited number of TiO_2/SiO_2 coatings were put on alexandrite substrates. Single layer AR coatings of MgF_2 and $NaAlF_6$ were also tested for comparison. Damage thresholds were compared to those of the bare substrates. The damage thresholds for these coatings are shown in Figure 49.

The measurements were made using an alexandrite laser at a wavelength of 790 nm. with a pulse duration of 200 nsec at 30Hz for 2 seconds. The near spot diameter of the nearly Gaussian beam was 0.380 mm. TiO_2/SiO_2 on sapphire showed a marked improvement in damage threshold over the bare sapphire substrate. However, no improvement for the same coating was apparent on the alexandrite substrate suggesting that the substrate is the limiting factor.

Work described by Foltyn, et. al. (Ref. 24) showed that damage thresholds for several refractory oxide AR and HR multilayer coatings increase on the average approximately as the cube root of the pulselength for a range from picoseconds to nearly a mircosecond irregardless of wavelength. The HR multilayers included a narrow bandwidth design incorporating Al_2O_3 and SiO_2 plus Sc_2O_3/SiO_2 and a broadband design using HfO_2/SiO_2. Quarter-wave layers (At 351 nm) were used with a half wave overcoat to achieve 99% reflectance. The AR coating consisted of Al_2O_3/SiO_2. Substrates were fused silica.

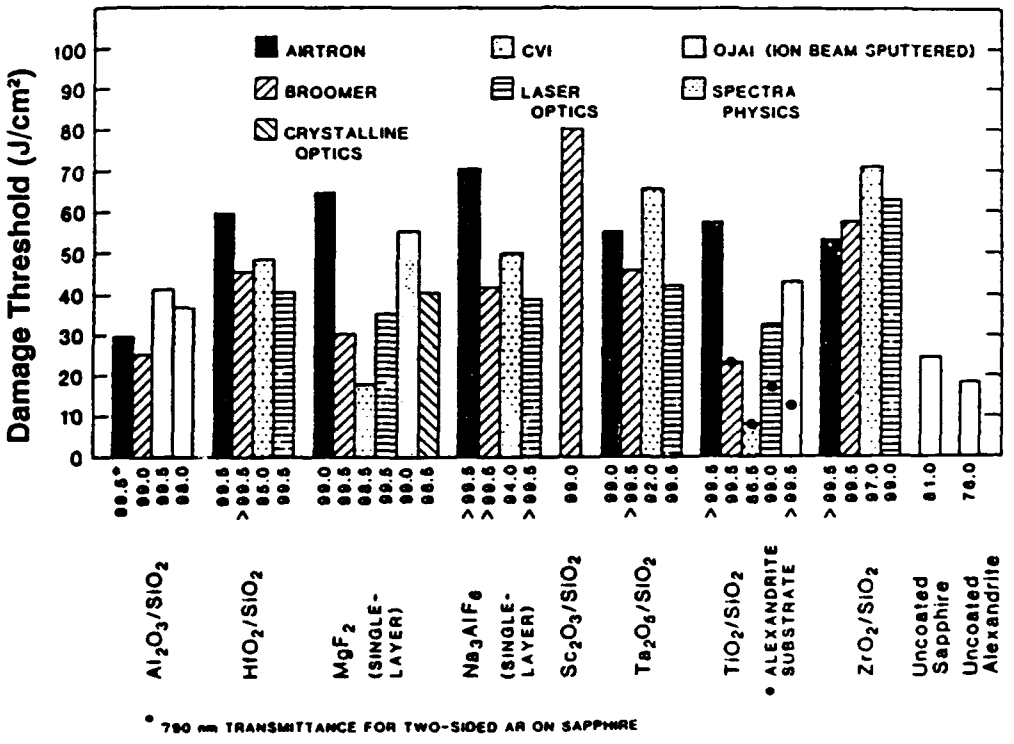

Figure 49. Damage thresholds of 790 nm anti-reflection coatings on sapphire substrates.

To achieve variations in pulse width, different lasers were used. Pulse width and other characteristics of these lasers are provided in Table 18. Between 50 and 400 sites were tested on each coating type at each pulse width. The damage probability plots presented in Figures 50 and 51 were derived using data from several samples. Three methods were used to scale results obtained at different pulse widths: method 1 compared the 0% intercept of linear regression fits to the probability data; method 2 compared lowest damaging fluence values; method 3 compared lowest fluence values producing catastrophic damage. Measured thresholds for 9 nsec pulses and scale factors (ratios of thresholds for pulses ranging from 9 to 625 nsec) appear in Table 19. Damage thresholds at all four pulse widths are summarized in Figure 52. The power law dependence for the different sample types varied from a fourth root to a square root dependence. No correlation was apparent between scaling rates and other coating properties such as index, threshold, band gap or reflectance. The nearly identical slopes after scaling for the Al_2O_3/SiO_2 HR coating shown in Figure 50 implies equivalent defect densities for both pulsewidths since spot sizes were the same. For the AR coating of the same materials shown in Figure 51, the slopes are considerably different indicating a higher defect density at shorter pulse widths. Half of the six coating types exhibited no defect density variation with pulsewidth. The other half of the coating types exhibited short pulse defect densities 2 to 6 times higher. Defect density variations were uncorrelated with scaling rates or other readily apparent coating properties.

As part of this work, scaling results at 351 to 355 nm, with thresholds normalized to 10 nsec, were compared to the above results. This comparison is shown in Table 20. The data sets of Newman, Walker and Rainer, when compared to this work, showed consistent results as indicated by Figure 53, for data sets including: (1) a quarter-wave layer tested at 355 nm with 20 psec and 27 nsec pulse width (Newman); (2) eight materials in various thickness layers tested at 353 nm with 5 nsec and 15 nsec pulse widths (Walker); and (3) five HR and four AR coatings tested at 351 or 355 nm with pulse widths of 0.6, 1.5 and 9 nsec (Rainer). From 0.6 to 625 nsec, the average scaling was $\tau^{0.32}$. For the Walker and Rainer data and above results both fast (0.5 to 0.8) and slow (0.0 to 0.2) scaling exponents were observed.

Considering other data compiled in the Table 20 summary, results are remarkably consistent over a wavelength range from 248 nm to 10.6 μm and over more than five decades in pulse width. While scaling exponents for individual tests vary widely, the average scaling rate is nearly constant from 4 to 625 psec. Thresholds improve as $\tau^{0.3\text{-}0.4}$ for picosecond pulses and continue to do so for pulse widths up to a microsecond. Based on the above, cubed root scaling as

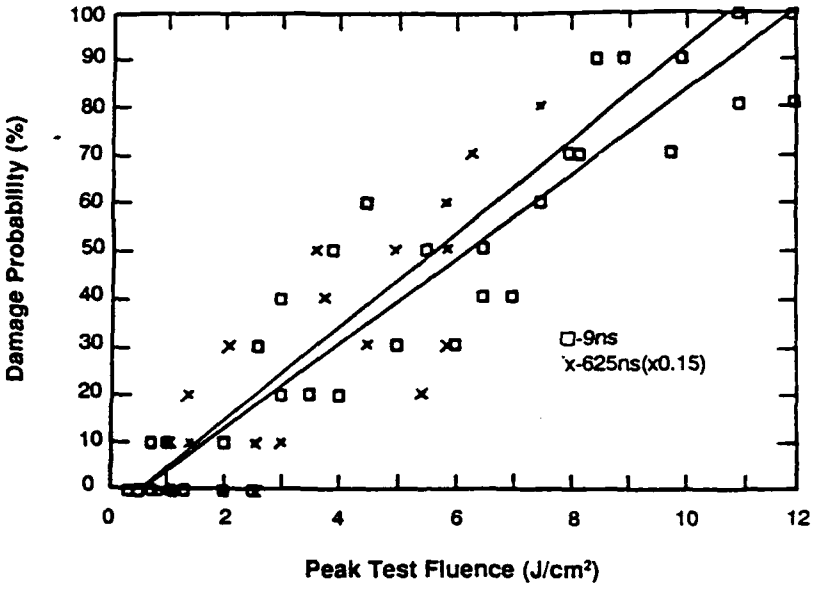

Figure 50. Damage probability plots for the Al_2O_3/SiO_2 reflectors at 9 ns and--with scaled fluency values--625 ns pulse lengths. After scaling, the slopes are nearly identical indicating equal defect densities at each pulse length.

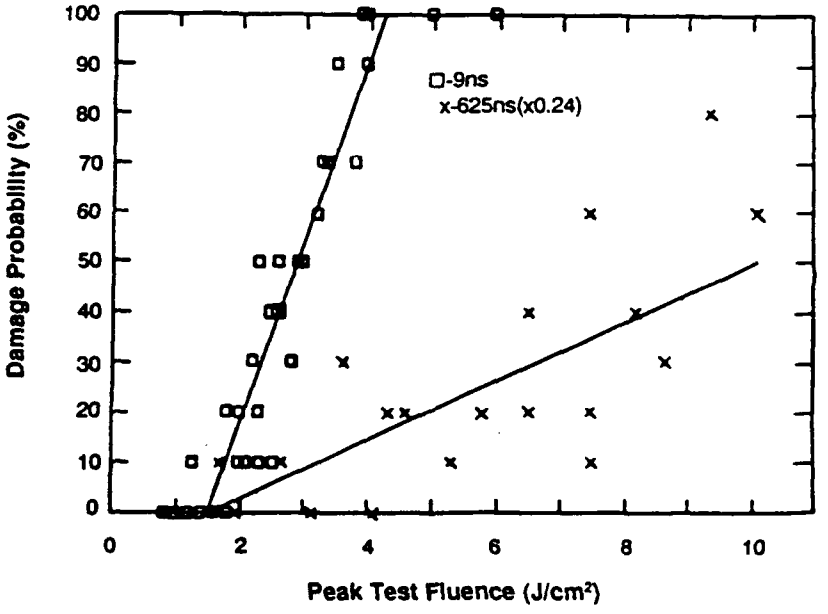

Figure 51. Probability plots for Al_2O_3/SiO_2 anti-reflection coatings. The steeper slope for 9 ns indicates a 6X higher density of defects for the shorter pulses.

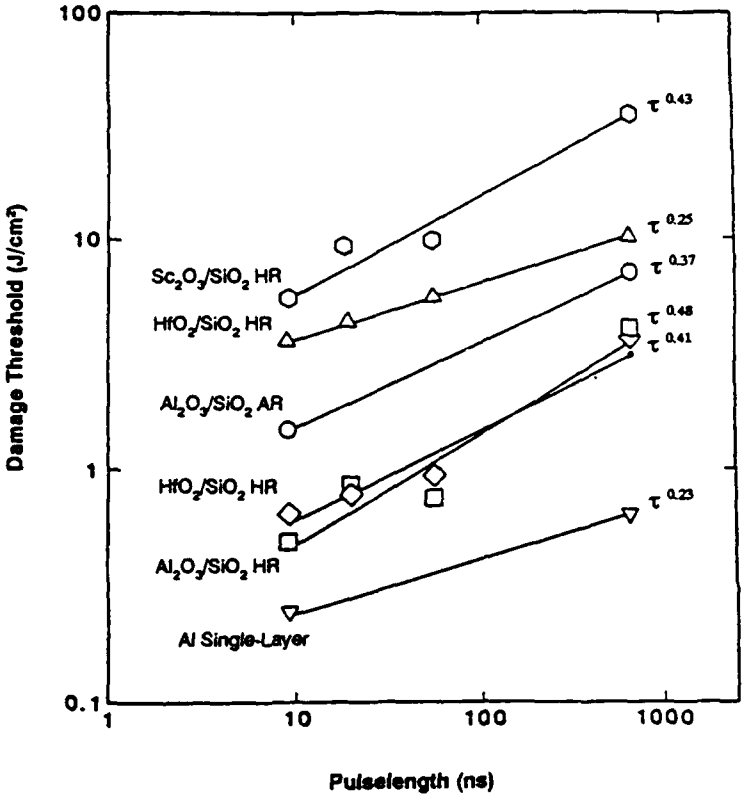

Figure 52. Damage thresholds at 9, 26, 54, and 625 ns pulse lengths for six different 351 nm coating types. Slopes of the lines, which represent best linear regression fits to the data, indicate that thresholds scale at rates ranging from fourth-root to square-root of the pulse length.

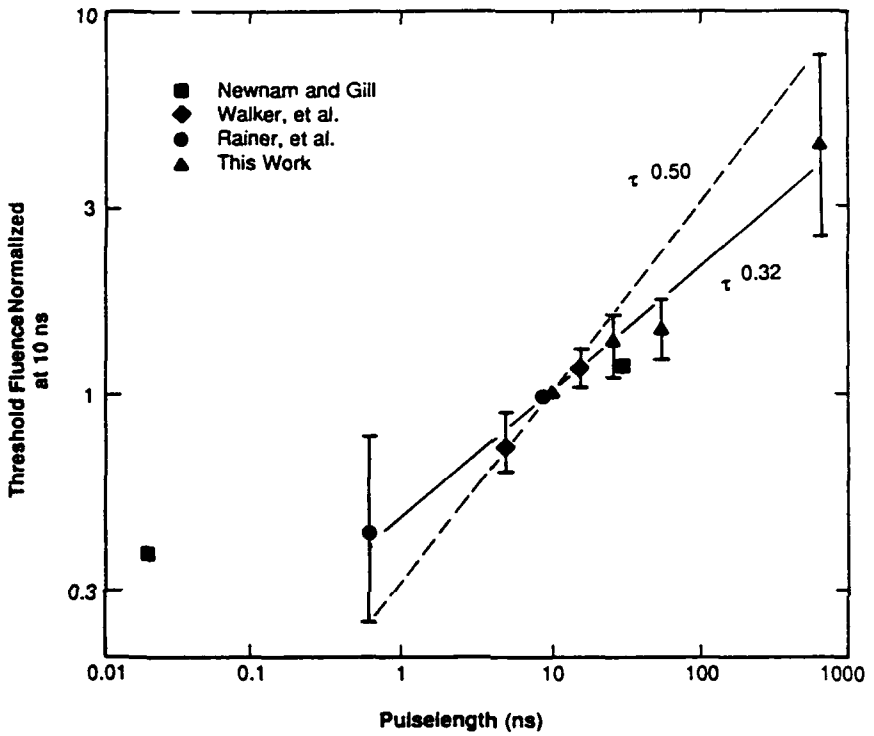

Figure 53. Results of this work plus three other 351 to 355 nm data sets (References 2 to 4). All thresholds are normalized to 10 ns. Symbols represent average scaling for each data set; error bars represent extreme scaling values for each set. Solid line indicates the weighted average scaling for the range 0.6 to 625 ns, which is $\tau_{0.32}$. The dashed line indicates the slope appropriate for square-root scaling. (Reference numbers stated refer to document from which this data was extracted.)

Table 18. Sources and Test Conditions

Pulselength[a]	Laser	Spotsize[b]	Wavelength	PRF
9 ns	XeF excimer (Lumonics 861)	0.44 nm	351 nm	35 pps
26 ns	XeF excimer (Lumonics 861T-4)	0.71 mm	351 nm	35 pps
54 ns	XeF excimer (Lumonics 861T-4)[c]	0.72 mm	351 nm	35 pps
625 ns	Frequency-doubled dye (Candela UV-500)	0.44 mm	355 nm	0.5 pps

[a]FWHM.
[b]Mean diameter @ $1/e^2$ amplitude.
[c]With 10% output coupling.

Table 19. Damage Threshold Scale Factors: 9 to 625 ns

Coating Materials	9 ns Damage Threshold	Scale Factor for 625 ns Threshold		
		Method 1	Method 2	Method 3
Sc_2O_3/SiO_2 (HR)[a]	5.6 J/cm^2	5.0	7.5	6.7
HfO_2/SiO_2 (HR)[a]	3.7 J/cm^2	2.7	2.8	4.3
Al_2O_3/SiO_2 (AR)[b]	1.5 J/cm^2	4.2	5.4	---
HfO_2/SiO_2 (HR)[c]	0.7 J/cm^2	5.6	4.7	4.2
Al_2O_3/SiO_2 (HR)[b]	0.5 J/cm^2	6.6	9.0	3.7
Al on pyrex[d]	0.2 J/cm^2	2.4	2.9	2.9

Method 1. Intercept of linear regression fit.
Method 2. Lowest damaging fluence.
Method 3. Lowest fluence for catastrophic damage.

[a] Interopitcs, Ltd.
[b] Broomer Research Corp.
[c] Laser Optics, Inc.
[d] Newport Corp.

Table 20. Pulse Length Scaling Comparison

Reference		Wavelength (μm)	Pulselength Range (ns)	Scaling Exponent[a]	
				Range	Average
Soileau	[7]	1.05	0.004-0.008	0.0-0.5	0.3
Bliss	[8]	0.69	0.020-23	0.4-0.5	0.4
Newnam	[4]	0.36	0.020-27		0.2
Soileau	[7]	0.53	0.03-0.15	0.1-0.9	0.7
Deaton	[9]	0.27	0.1-0.7	0.0-0.7	0.3
Milam	[10]	1.06	0.17-3.2	0.3-0.5	0.4
Lowdermilk	[11]	1.06	0.17-3.5	0.0-0.5	0.3
Rainer	[6]	0.36	0.6-9	0.1-0.5	0.3
Milam	[12]	1.06	1-9	0.3-0.6	0.6
Newnam	[13]	10.6	1.7-65	0.2-0.3	0.3
Walker	[5]	0.27	5-15	0.0-1.0	0.5
		0.36	5-15	0.0-0.8	0.5
		0.53	5-15	0.0-0.8	0.5
		1.06	5-15	0.0-0.7	0.3
Boyer	[14]	0.25	10-38	0.2-0.5	0.3
This work		0.35	9-625	0.2-0.5	0.4

[a]The value of x in the relationship: threshold fluence $\propto$ (pulse length)^x.
(References in table refer to document from which data was extracted.)

opposed to square root scaling is a more accurate rule of thumb describing the effect of pulse width on damage threshold.

Measured damage thresholds for single film layers of TiO_2, Ta_2O_5, ZrO_2, HfO_2, Al_2O_3 and SiO_2 were compared by Akhtar, et. al. (Ref. 25) with theoretical estimates derived from two models. The first model considered temperature generation due to absorption in the film volume. The second model based damage on inclusions in the film. Absorption and thermal conductivity was experimentally measured.

The results for the six refractory oxides along with the measured damage thresholds are presented in Tables 21 and 22. The damage data was determined using a two stage Nd:YAG laser with a pulse length of 14 nsec and a spot size of 300 microns.

Table 21. Thermal Parameters and Damage Threshold of Oxide Layers

Material	K (bulk) (W/cm°C)	K (film) (W/cm°C)	Absorption Coefficient ∝(1/cm)	Melting Point (°C)	Damage Threshold (J/cm^2)	
					Calculated	Measured
HfO_2	1.7E-1	7.7E-6	0.3	2758	40	41 ± 3
Al_2O_3	2.7E-1	3.3E-1	2.3	2072	38	39 ± 1
ZrO_2	1.1E-1	1.4E-4	2.0	2700	36	34 ± 1
SiO_2	1.4E-2	1.0E-3	0.1	1723	35	34 ± 7
Ta_2O_5	--	2.6E-4	2.4	1918	27	28 ± 2
TiO_2	9.7E-2	1.8E-4	5.9	1775	15	13 ± 1

Table 22. Shows Calculated Values of Temperature Rise in Oxide Films (Equation 4), Damage Thresholds by Inclusion Model (Equation 5), Measured α and E_D

Material	Absorption Coefficient ∝ (1/cm)	Temperature Rise in Film T(°C)	Damage Threshold (J/cm_2)	
			Exp	Cal (Sphere)
HfO_2	0.3	207	41	36
Al_2O_3	2.3	3980	39	1955
ZrO_2	2.0	217	34	43
SiO_2	0.1	25	34	29
Ta_2O_5	2.4	86	28	29
TiO_2	5.9	745	12	32

Equations refer to document from which data was extracted.

Based on results presented in Table 21, absorption coefficient and thermal conductivity have a minor influence on damage but cannot be neglected. Melting point has the main influence, HfO_2 having the highest melting point and the highest damage threshold.

Based on results presented in Table 22, it is clear that damage thresholds predicted by the inclusion model are inconsistent with damage threshold measurements for Al_2O_3 and TiO_2 but are reasonably consistent for other materials. It is concluded that Al_2O_3 and TiO_2 damage due to absorption in the bulk of the film and the other oxides listed damage due to absorption by inclusions in the film.

Damage thresholds were measured by Deaton, et. al. (Ref. 26) for a variety of 1.315 μm reflective coating designs containing oxides, as well as other materials. Each coating was prepared on both Mo and Si substrates. They were characterized to determine the fractional power absorbed at 1.319 μm and the rms roughness at 633 μm before and after coating. The rms roughness, as determined from total integrated scattering measurements was found to be 10 Å uncoated and 50 Å coated for Si substrates and 35 Å uncoated and 40 to 70 Å coated for the Mo substrates.

The damage thresholds are shown in Table 23 for the various coating designs and vendors. The designs containing PbF_2 yielded the lowest damage thresholds and those containing TiO_2/SiO_2 the highest. Films deposited on Si substrates systematically showed higher thresholds than those on Mo substrates although differences in most cases are slight. In all cases, threshold damage consisted of a few randomly distributed micro-pits originating in the first few coating layers.

Measurements were made using a pulsed iodine laser with output energy of 5 joules in a pulse width of approximately 8 microseconds with a spot diameter of 2.8 mm on the sample. All thresholds reported correspond to single shot per site illumination. Damage was determined by white light scattering or Nomarski microscopy. The reported damage threshold is the average of the lowest fluence at which damage occurred in the five shot sequence. The range between the two levels is approximate due to the uncertainty of the peak fluence for a given shot.

The angular dependence of 351 nm laser damage thresholds in HfO_2/SiO_2 multilayer dielectric reflectors was measured by Boyer, et. al. (Ref. 27). Also measured was the 248 nm damage threshold for bare fused silica, evaporated aluminum films and HfO_2/SiO_2 and Al_2O_3/SiO_2 dielectric reflectors for angles out to 85°. Previous work by the author using HfO_2/SiO_2 films had shown that the laser damage threshold for an S-plane polarized beam does not increase with incident angle ($1/\cos\theta$) due to simple geometric fluence dilution and due to decrease in S-polarization electric field within the film as might be expected. A comparison of the measured

Table 23. Iodine Laser Damage Survey

Vendor	Coating Desing	Substrate	Threshold (J/cm^2)
Laser Power Optics	$(PbF_2/ZnS)^4$	Molybdenum	27 ± 7
Laser Power Optics	$(PbF_2/ZnS)^4$	Silicon	17 ± 3
Laser Power Optics	$(ThF_4/ZnS)^4$	Molybdenum	74 ± 10
Laser Power Optics	$(ThF_4/ZnS)^4$	Silicon	85 ± 12
Laser Power Optics	$(PbF_2/ZnS)^4$	Molybdenum	5 ± 2
Laser Power Optics	$(PbF_2/ZnS)^4$	Silicon	11 ± 3
Laser Power Optics	$(ThF_4/ZnS)^4$	Molybdenum	9 ± 2
Laser Power Optics	$(ThF_4/ZnS)^4$	Silicon	13 ± 3
OCLI	$(SiO_2/TiO_2)^8$	Molybdenum	18 ± 3
OCLI	$(SiO_2/TiO_2)^8$	Silicon	24 ± 7
OCLI	$(ZnS/ThF_4)^8$	Molybdenum	117 ± 23
OCLI	$(ZnS/ThF_4)^8$	Silicon	54 ± 8
Spectra Physics	(ZrO_2/SiO_2)28 layers	Molybdenum	47 ± 10
Spectra Physics	(ZrO_2/SiO_2)28 layers	Silicon	55 ± 8
Spectra Physics	(TiO_2/SiO_2)16 layers	Molybdenum	117 ± 17
Spectra Physics	(TiO_2/SiO_2)16 layers	Silicon	32 ± 5
Northrop	$(ThF_4/ZnS)^4$	Molybdenum	92 ± 14
Northrop	$(ThF_4/ZnS)^4$	Silicon	71 ± 10
Northrop	$(Al_2O_3/HfO_2)^5$	Molybdenum	35 ± 7
Northrop	$(Al_2O_3/HfO_2)^5$	Silicon	35 ± 5
Litton	$Al(LH)^7LL$ Run #2	Molybdenum	117 ± 17
Litton	$Al(LH)^7LL$ Run #2	Silicon	80 ± 12
Litton	$Ti(LH)^{10}LL$ Run #1	Molybdenum	50 ± 8
Litton	$Ti(LH)^{10}LL$ Run #1	Silicon	50 ± 8
Coherent	(Gl777)	Molybdenum	95 ± 15
Coherent	(Gl777)	Silicon	144 ± 20
Coherent	(Gl752)	Molybdenum	40 ± 8
Coherent	(Gl752)	Silicon	44 ± 6

damage threshold with the anticipated angular dependence is shown in Figure 54. To better explain the observed angular dependence, a model was proposed in which uniformly absorbing spherical defects (consistent with a 1/cos θ dependence), were replaced by uniformly absorbing cylindrical defects with cylinder axis oriented normal to the film surface. It was further assumed that the total energy absorbed by such defects for damage to occur is a constant independent of the incident angle and that the cylinder height is the thickness of the film. This model is compared with the same damage thresholds in Figure 55 (r/t is the cylinder aspect ratio) and more successfully explains the weak dependence observed.

To test the validity of the model with other materials, damage thresholds were measured as a function of angle at a wavelength of 248 nm on bare fused silica, evaporated aluminum and on HfO_2/SiO_2 and Al_2O_3/SiO_2 multilayers as shown in Figures 56 to 59. The tests were performed using a laser with 23 nsec pulse width and a 50 Hz PRF. The spot size was 0.2 x 0.8 mm at normal incidence. The n on 1 test format used 100 shots per site. For S-polarization experiments, the polarization ratio was 1000:1. Damage diagnostics for the aluminum films was achieved by visual examination with a low power stereoscopic microscope and white light illumination. For the other samples, damage diagnostics were achieved with a telescope and video camera with UV illumination.

All samples were two inches in diameter. Bare evaporated aluminum films on BK-7 glass substrates were chosen to represent the case where damage is expected to occur at the surface due to bulk absorption. Fused silica Corning 7940 was chosen to represent a nonabsorbing bulk material. HfO_2 films are absorbing at 248 nm and do not represent defect dominated laser damage initiation. The HfO_2/SiO_2 films were designed to provide a broad enough reflectance band to provide high reflectance at all test angles. The reflectance of both HfO_2/SiO_2 and Al_2O_3/SiO_2 multilayers were designed for 75°. The Al_2O_3/SiO_2 multilayers were expected to behave at 248 nm as the HfO_2/SiO_2 multilayers did at 351 nm as shown in Figure 54.

Results of normalized damage threshold test on the aluminum films with unpolarized light are presented in Figure 57. At least, a 1/cos θ geometric fluence dilution is apparent. Tests with s-polarized light again show an additional enhancement but with greater scatter in the data. Results of normalized damage threshold tests for the HfO_2/SiO_2 and Al_2O_3/SiO_2 multilayers are shown in Figure 58. All results are for s-polarized light and normalized to make the 60° points fall on the 1/cos θ curve for comparison. The HfO_2 damage thresholds follow the 1/cos θ dependence at 248 nm quite well. The Al_2O_3/SiO_2 threshold values, however, increase more slowly implying a normalization constant that is too large and that eighty five degree thresholds are likely about four

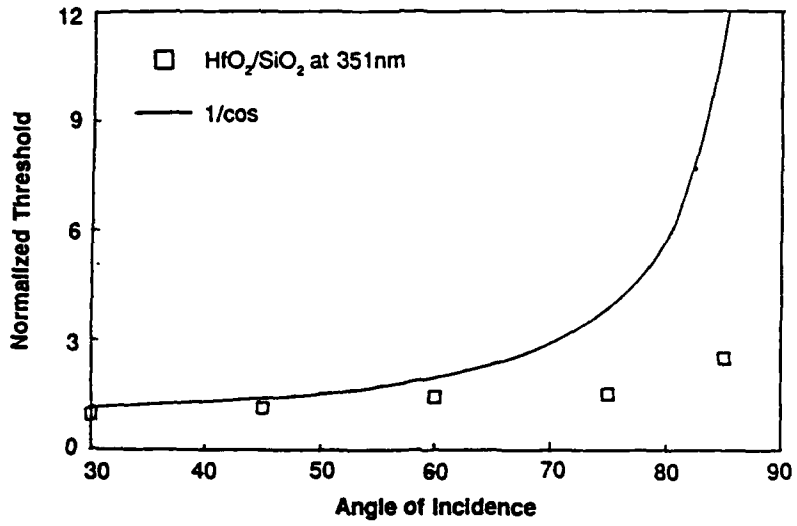

Figure 54. Comparison of the experimental damage threshold values from Reference 1 with the 1/cosθ expected from simple geometric scaling. (Reference 1 refers to the document from which the data was extracted.)

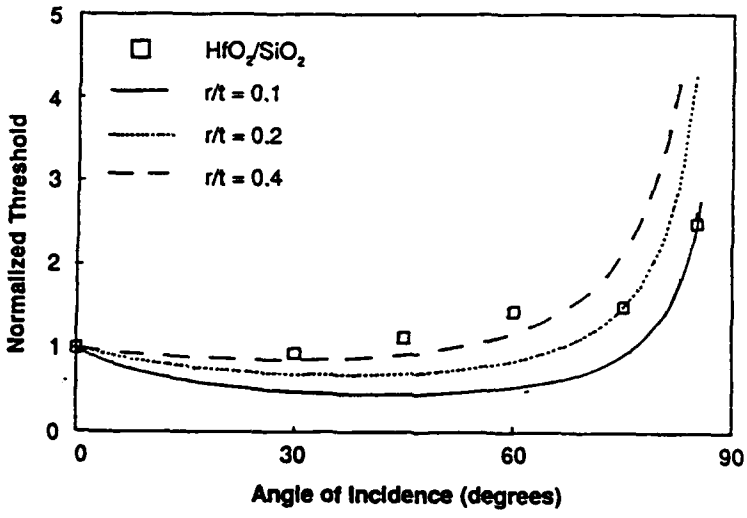

Figure 55. Comparison of the experimental damage threshold values from Reference 1 with the cylindrical defect extension to simple geometric scaling. (Reference 1 refers to the document from which the data was extracted.)

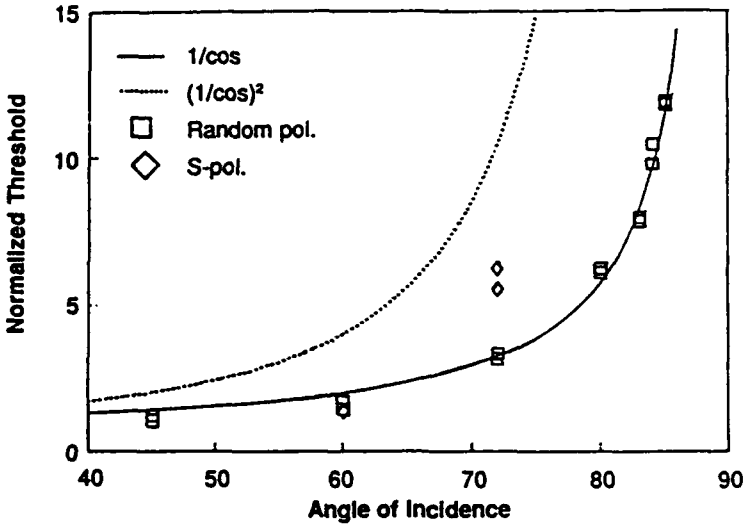

Figure 56. Laser damage threshold values for uncoated Corning 7940 fused silica with random polarization scale as 1/cosθ. The S-polarization results are further enhanced.

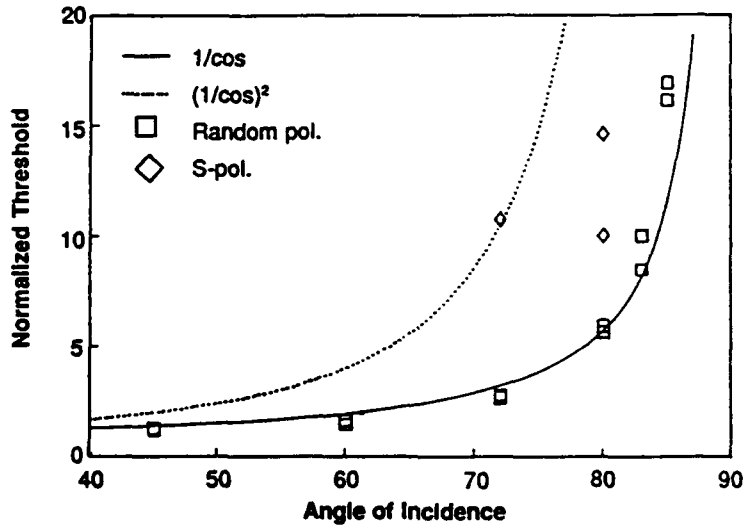

Figure 57. Laser damage threshold values of evaporated aluminum with random polarization scale as 1/cosθ. The thresholds for the S-polarization results are enhanced more than the uncoated fused silica.

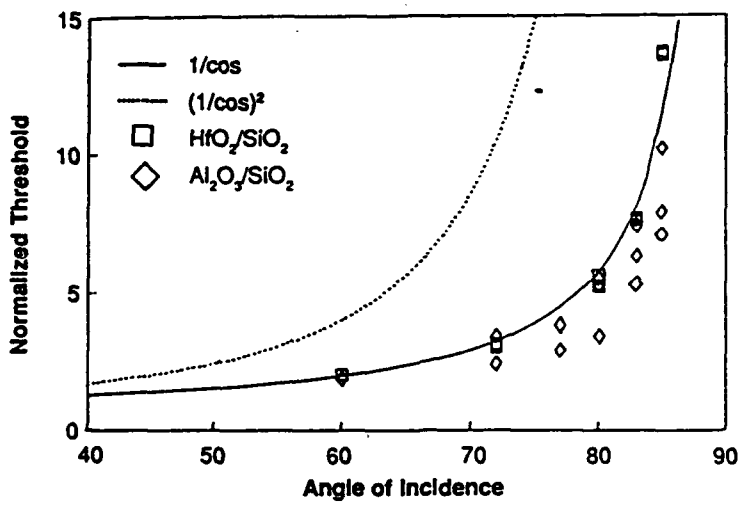

Figure 58. The laser damage threshold values for HfO_2/SiO_2 and Al_2O_3/SiO_2 multilayer dielectric relfectors are compared with $1/\cos\theta$ and $1/\cos^2\theta$.

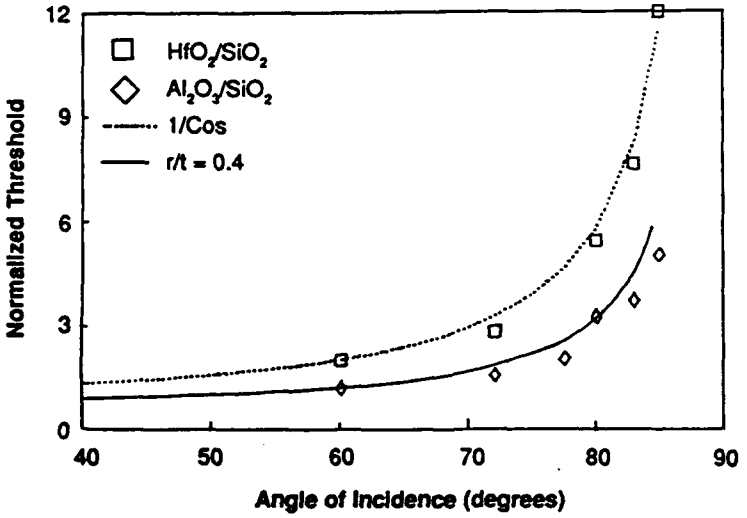

Figure 59. The laser damage threshold values for HfO_2/SiO_2 and Al_2O_3/SiO_2 multilayer dielectric relfectors are compared with $1/\cos\theta$ and the cylindrical defect model with $r/t = 0.4$.

or five times greater than normal incident thresholds. Figure 59 the damage thresholds of the multilayers with spherical and cylindrical defect models. The Al_2O_3/SiO_2 thresholds are normalized so that the value at 60° agrees with the model and the chosen aspect ratio and average values at each angle are plotted for clarity.

It was concluded that damage thresholds for Al_2O_3/SiO_2 multilayers scale less rapidly than $1/\cos\theta$ and are in agreement with a cylindrical model with aspect ratio $r/t = 0.4$. The model and assumptions imply a defect radius of about 10 nm and that melting of the defect would require absorption of about 1% of the incident energy. Aluminum films, bare fused silica and the HfO_2/SiO_2 multilayers, which are absorbing at 248 nm do, however, scale with geometric fluence dilution at the sample surface. For the HfO_2/SiO_2 multilayers and aluminum it is probable that bulk absorption is more important than local defects. The $1/\cos\theta$ scaling of the fused silica damage thresholds implies either the defects are more spherical or the energy absorption mechanism is different in multilayer dielectrics.

3. FLUORIDE AND CHALCOGENIDE COATINGS

3.1 FLUORIDE COATINGS

Fluoride coatings are of interest due to their low indices of refraction and wide spectral transmission bands. The fluorides are also stable in fluorine containing environments and thus prime candidates for use in HF/DF or excimer laser systems. Their water solubility is detrimental, however MgF_2 and CaF_2 are relatively insoluble. Lead fluoride is reasonably insoluble but is a very soft film and thus abrasion susceptible. Fluoride properties are reviewed in Table 24. However, film properties such as moisture resistance and stability of the film are dependent on the deposition technique and its influence on such factors as porosity. The range of properties presented in Table 24 can be extended by alloying two or more of the components. It has been found to be possible to produce epitaxial films of these materials on clean ordered semiconductor substrates at relatively low temperatures (200°C) despite poor lattice match. This is thought to be due to the predominant vapor specie being the undissociated molecule. However, this same absence of dissociation leads to low density polycrystalline films when deposited at room temperature due to absence of an exothermic chemical reaction at the substrate. Density, however, is found to improve with substrate temperature. An alternate technique for providing the additional energy required for adatom mobility is low energy ion bombardment (<250 eV) during film growth. Microstructure may also be improved by ion bombardment resulting in enhanced durability, however, the UV cutoff may be deleteriously shifted to longer wavelengths.

3.2 CHALCOGENIDES AND MULTILAYERS

The chalcogenides and chalcogenide/fluoride multilayer stacks are attractive coating materials from the standpoint of their IR transmittance. The chalcogenides are nonhygroscopic and may be used with the fluorides as a moisture barrier. These materials are deposited by a variety of techniques, including electron beam and thermal evaporation, chemical vapor deposition and molecular beam. Multilayers of $ZnSe/ThF_4$ on Si, Ge and ZnSe substrates have been fabricated as AR and HR coatings for CO_2 laser applications. Multilayers of PbF_2 or ThF_4 with ZnSe or ZnS have been synthesized for CO_2, HF, DF and atomic iodine laser applications. ZnS and ZnSe has been multilayered with BaF_2 for Nd:YAG laser applications. Chalcogenide alloys (ZnS_xSe_{1-x}) have also been investigated for applications at 10.6 micron wavelength.

Table 24. Properties of Fluoride Materials of Interest as Thin Films

Materials	Solubility in Cold Water	Expansion Coefficient (ppm)	Spectral Bandwidth	Refractive Index
NaF	4.22	36	0.15-11	1.33
LiF	0.27	37	0.11-9	1.40
CaF_2	0.0016	18	0.13-12	1.4
SrF_2	0.011	18	0.13-14	1.4
BaF_2	0.12	18	0.14-15	1.45
Cryolite			0.2-14	1.35
AlF_3	0.56		0.2-?	1.35
MgF_2	0.0076	16	0.11-9.7	1.39
PbF_2	0.064	11	0.19-17	1.76
ThF_4	i		0.25-15	1.5

Multilayers of ZnS/BaF_2 have been investigated as thin film distributed Bragg reflectors which, due to fundamental properties of the materials, do not shift under temperature cycling or laser irradiation. Performance is, however, dependent on the degree of film perfection and the control of microstructure and interface diffusion. Both chemical reaction and interface diffusion have been found to contribute to a reduction in reflection band intensity.

Low damage thresholds of the chalcogenides, particularly ZnS coatings on Ge substrates, have been attributed to film porosity and the ingress of water. Increasing substrate temperature during deposition was found to significantly improve the damage threshold. The higher substrate temperature is thought to induce crystallinity by way of increased surface mobility and to desorb water from the substrate surface prior to deposition. This hypothesis is further substantiated by the higher damage threshold exhibited by chalcogenide films deposited by molecular beam. Microscopic examination of these films reveals a complete absence of intragranular voids rendering the films impervious to the ingress of water and other impurities after exposure to the atmosphere. The high purity inherent in films deposited by this process further contributes to their exceptionally high damage threshold. The molecular beam technique allows a high degree of control over the deposition process. The ultra high vacuum condition together with in-situ ion beam cleaning techniques creates an excellent environment for reducing particulate inclusion at the substrate and film interfaces.

Further consideration has been given to controlling film density and eliminating ingress of water in chalcogenide and chalcogenide/fluoride multilayers by a stratified approach in which columnar microstructure would be controlled by alternating the layers of two materials repetitiously through the film thickness. A logical choice of materials, due to their chemical compatibility are ZnSe and ZnS. However, the small difference in lattice mismatch was found to be not great enough to produce propagation of the columnar structure through the interface producing heavily microtwinned material in the ZnS layer. Stratified heterostructures based on combinations such as BaF_2 and ZnS, due to larger lattice mismatch were found to have greater potential for preventing propagation of columnar morphology.

Graded index coatings can be achieved by varying the relative contribution of the two materials to produce AR coatings. However, certain fluorides are more reactive with sulfides which can lead to impurity compound formation at the interfaces and significant absorption effects.

In the following, Section 3.3 reviews work directed at determining damage thresholds for coatings deposited by physical vapor deposition processes. Fluoride coatings were deposited by ionized cluster beam deposition, thermal and E-beam evaporation and ion beam sputtering. Chalcogenides and chalcogenide/fluoride multilayers were deposited by the same process and also by molecular beam. The reader may also wish to review the work of Kardach, et. al. (Ref. 6), discussed in Section 2.1, where fluoride and chalcogenide coating damage thresholds were compared with those of oxides. Section 3.4 examines work done to compare molecular deposited coatings with chemical vapor deposited coatings. Finally, damage threshold is related to the morphology of $ZnSe/ThF_4$ multilayers in Section 3.5. The reader is referred also to Section 2.4 where Gallegos, et. al. (Ref. 23) investigated the application of fluoride as well as oxides to AR coat alexandrite laser rods and Deaton, et. al. (Ref. 26) examined the utility of fluoride/chalcogenide as well as oxide multilayers as coatings for the atomic iodine laser.

As for the oxides, other issues influence the damage thresholds of fluoride and chalcogenide coatings and are discussed at length in the following sections. The principal motivation for organizing the material as presented here has been to preserve the continuity of technical discussion and the background provided by each author to assure the credibility and relevance to the damage threshold data presented in each reference.

3.3 PHYSICAL VAPOR DEPOSITION PROCESS

3.3.1 Fluoride Single Layers

Ionized cluster beam (ICB) deposited BaF_2 films were compared by Waddell, et. al. (Ref. 28) with films deposited by conventional evaporation. The ICB films were deposited on ZnSe substrates as anti-reflection coatings using a box coater equipped with a resistively heated cluster source upon which an electron beam was incident to achieve impact ionization of the BaF_2. Acceleration voltages were applied using a metallic grid structure. The cluster source consisted of a carbon crucible with an orifice. Unlike a Knudsen cell, the cluster source operates in a regime where significant adiabatic cooling of the vapor stream occurs, sufficient to form atomic or molecular aggregates.

The films were deposited under conditions of conventional high vacuum at pressures typically 1 x 10^{-6} mbar. Conventional films of the same material were deposited on ZnSe substrates by replacing the source with a conventional boat. Based on other work it was anticipated that significant effects could be produced on adatom migration, nucleation density, sticking coefficient and enhancement of chemical reactivity. Significant differences in the microstructure of the ICB films were found at different growth temperatures. Films deposited by conventional technique at 200°C were found to have an amorphous structure. Films deposited by ICB showed an oriented growth, particularly at higher accelerating voltage. At 300°C, crystallinity of the ICB films was greatly increased. Conventionally grown films at this temperature showed orientation, but different than that of ICB films. Scattering from conventionally deposited films was found to vary with substrate temperature during deposition, films deposited at 300°C being indistinguishable from the substrate. Scattering was found to be lower for ICB deposited films and to be dependent on both substrate temperature and accelerating voltage. Scatter dropped appreciably at temperatures of 250° and 300°C. It was also found from studying reflectance that a change in growth orientation and film density occurs in the same temperatures range, lower temperatures resulting in films with graded indices and less than theoretical density. The temperature at which the transition occurs was found to be reduced by decreasing the diameter of the orifice of the cluster source.

Damage thresholds for 1.06 micron laser irradiation are compared for conventionally deposited and ICB deposited BaF_2 films on BK-7 glass substrates in Table 25. The pulse width employed in the threshold measurements was 15 nsec FWHM. Damage thresholds for conventionally deposited films were stated to be low, improving somewhat at higher temperature

depositions (300°C substrate temperature). Greater temperature dependence was found for ICB deposited films, a factor of 3 improvement being found for films deposited at 200°C. Higher acceleration voltages, however, were found to reduce damage threshold. Although thick films deposited at 200°C were found not to have high density throughout their thickness, they appear to have a dense layer near the substrate as do thinner films deposited at this temperature, suggesting the dense layer near the substrate is functional in the higher damage threshold.

Table 25. Variation of 1.06 μm LIDT with Film Thickness for ICB BaF_2 Film

Optical Thickness in Units of λ/4	LIDT	(J/cm^2)
1	39.3	18.4
2.4	24.1	--
3.6	18.4	--
10	13.8	9.3
Deposition temperature	200°C	300°C

Table 26 illustrates damage thresholds measured at 10.6 microns for BaF_2 films on ZnSe substrates. Conventionally deposited films were found to have lower damage thresholds than the bare substrates, even when deposited at 300°C. Films deposited by ICB showed significant improvement with values at 300°C similar to values obtained for polycrystalline MBE deposited films. These films are thought to be more dense, approaching bulk properties and therefore do not absorb atmospheric moisture leading to the improved damage thresholds.

Table 26. Laser Damage Thresholds at 10.6 μm

Film/Substrate	Deposition Temperature (°C)	Acceleration Voltage (kV)	LIDT (J/cm^{-2})
U/C ZnSe	--	--	63.9-78.8
BaF_2/ZnSe	250	Conventional	60.5-61.6
	300	Conventional	68.2-74.8
BaF_2/ZnSe	250	0	85.8-86.9
	300	0	107-113

Porous dielectric AR coatings were synthesized by Yoshida, et. al. (Ref. 29), by codeposition of two dielectric materials. the porosity was achieved by preferentially dissolving one material in a chemical solution to produce a graded refractive index. SiO_2 and NaF were deposited from two independent evaporation sources and the NaF subsequently dissolved in ultrapure water. The wavelength of minimum reflectivity is controlled by the film thickness. After processing, the surface roughness was measured and found to be as good as the bare polished borosilicate crown glass (BK-7) substrate which was 11 Å rms. The films were found to be abrasion resistant and withstood the tape peeling test.

Damage threshold of the porous dielectric is compared to multilayer AR coatings and quartz (in Table 27) at three wavelengths: 1.053, 0.527 and 0.355 μm. To achieve the measurements, the output from a Q-switched Nd:YLF laser or an actively mode-locked Nd:YAG laser was amplified by two Nd:glass amplifiers and frequency upconverted by type II KDP crystals. Spot diameter at the sample was 400 mm. Damage was detected with a Nomarski microscope at 200X magnification. "One shot damage," i.e., 1 on 1, as well as n on 1, testing was performed. Results indicated that the porous coating exhibited twice the damage threshold at all tested wavelengths compared to the multilayer AR coatings. The n on 1 tests at fluence levels below the 1 on 1 threshold indicated an increase in threshold from 8 to 11.5 J/cm^2 which is comparable to the bare quartz surface. This is significantly higher than the threshold of a single SiO_2 coating. The damage pattern determined by phase contrast microscopy exhibited small damage pits (~3 μm) with evidence of larger areas being ablated away at higher fluences.

Single layer and multilayer fluoride and oxide coatings were deposited by Kolbe, et. al. (Ref. 30), using evaporation, ion beam sputtering and thermal evaporation in order to compare optical constants, inhomogeneity coefficients and laser damage thresholds for applications in the spectral range between 150 nm and 250 nm. Layers of SiO_2 and Al_2O_3 with thickness of 400 nm were deposited onto fused silica substrates by electron beam evaporation and ion beam sputtering. For the E-beam coatings, the substrate temperature was 300°C and the deposition rate was 0.5 nm/sec with an oxygen back pressure of 2 x 10^{-4} mbars. The vacuum chamber was equipped with an oil diffusion pump and liquid nitrogen Meissner trap. Additional oxide coatings were deposited by ion beam sputtering using a cryo-pumped coating plant. A partial pressure of 10^{-4} mbar oxygen was added to produce fully stoichiometric oxide coatings. Deposition rates were 0.4 nm/sec for silica and 0.3 nm/sec for alumina.

Measurements of optical constants for both Al_2O_3 and SiO_2 films revealed very small deviation from other reported values with the refractive index of the ion beam sputtered coating

Table 27. Comparison of the Damage Threshold Between the Porous Dielectric AR Coating, the Standard AR Coating, and the Quartz at λ=355 nm (τ_p = 0.4 ns), 527 nm (τ_p = 1 ns), and 1053 nm (τ_p = 1 ns), Respectively

AR Coatings	Damage Threshold (J/cm^2)	Laser	Coating Materials and Layers	Test
Multilayer	3-4	1053 nm	No undercoat; TiO_2/SiO_2 2-6, layers	1-on-1
Multilayer	4-8	1 ns	$\lambda/2$ SiO_2 undercoat; TiO_2/SiO_2 3-7, layers	1-on-1
Porous dielectric	12-13			1-on-1
Multilayer	2.5-3.5	527 nm	No undercoat; TiO_2/SiO_2 2-6, layers	1-on-1
Multilayer	4-5	1 ns	$\lambda/2$ SiO_2 undercoat; TiO_2/SiO_2 3-7, layers	1-on-1
Porous dielectric	12			1-on-1
Monolayer	2-4 4.4-6.4		$\lambda/4$ SiO_2 $\lambda/4$ SiO_2	1-on-1 N-on-1
Mixed thin film	2.5-3.2	355 nm	$NaF+SiO_2$	1-on-1
Multilayer	1-3	0.4 ns	$\lambda/2$ SiO_2 undercoat; Al_2O_3/SiO_2, SC_2O_3/SiO_2, 3-7 layers	1-on-1
Porous dielectric	6-9.5 10.5-11.5			1-on-1 N-on-1
Quartz	9.5-16			1-on-1

being slightly higher than those found for the E-beam evaporated films. The extinction coefficient was slightly higher for the Al_2O_3 sputtered film than for the E-beam evaporated Al_2O_3. For the silica films, the extinction coefficient was less than 10^{-4} for both deposition techniques for wavelengths down to 190 nm.

Single layer fluoride coatings of different thicknesses (2, 8, 14, 20, 26, QWOT at about 200 nm) were deposited onto substrates of BK-7 glass, fused silica and calcium fluoride at substrate temperatures between 100°C and 400°C. Deposition rates in nm/sec were: 3 (Al_2O_3), 0.8 (MgF_2), 0.25 (NdF_3), and 0.5 (other materials).

To assess effects of internal stress and scatter loss arising from the microstructure commonly associated with films of these materials, they were examined by visual inspection with

intense white light illumination and by dark field microscopy (magnification 125X). The results are presented in Table 28. A strong dependence on substrate temperature was observed in several properties of the film. In particular, the extinction coefficient dropped significantly with increasing temperature and the inhomogeneity as well as the shift of optical thickness before/after venting increased significantly at low substrate temperature.

Results indicated that deposition of fluoride coatings with low optical losses can be performed only at high substrate temperatures. This may, however, lead to cracking caused by internal stress if the substrate material is not matched to that of the film. Measurements of extinction coefficients of these films were comparable and in some cases (particularly those films deposited by E-beam) were as much as a factor of 2 higher than those documented in other references.

HR quarter wave multilayers were also fabricated. Except for the pure oxide systems, the multilayers were deposited simultaneously onto heated substrates of fused silica, BK-7 glass and calcium fluoride at temperatures between 300°C and 400°C. All systems (except the pure oxides) had cracks when deposited onto fused silica but it was not difficult to deposit coatings without visible defects onto calcium fluoride and BK-7 substrates supporting the hypothesis that internal stresses in fluoride coatings are strongly dependent on the thermal expansion coefficient of the substrate. Performance parameters for Al_2O_3/SiO_2, LaF_3/MgF_2 and LaF_3/AlF_3 agreed well with theoretical values computed from the measured optical constants of the single layers. For the other multilayer combinations, the reflectance was significantly lower than calculated. For LaF_3/AlF_3, GdF_3/AlF_3, NdF_3/AlF_3 and NdF_3/MgF_2 lower reflectance was attributed to design deviations.

For multilayers exhibiting lower reflectance and transmittance, surface roughness of the substrate and its replication at interfaces or interface defects caused by chemical/physical properties of the layer materials were blamed.

Damage threshold measurements were performed with an excimer laser emitting at 193 nm wavelength with pulse length of 25 nsec. The elliptical beam had a cross section of 0.65 mm^2. Damage was detected using an in-situ microscope in connection with digital image processing. Damage threshold of the fluoride and oxide coatings are shown in Figure 60. The low values of the alumina layers are caused by their high absorption loss. Thresholds are generally higher for sputtered coatings than for E-beam coatings which is attributed to their higher packing density and better mechanical stability. The thresholds of the high index fluoride films are much higher than those of the high index oxide films.

Table 28. Morphology of Evaporated Fluoride Single Layers

Material; Substrate Temperature	Layer Quality vs. Layer Thickness [QWOT at 200 nm] 2	8	14	20	26	Substrate Material [F.S.= Fused Silica]	Morphology [Explanations are given below]
NaF; 400°C	-	-	-	-	-	All	Pinholes
NaF; 100°C	-	-	-	-	-	All	Pinholes
AlF_3; 400°C				+		CaF_2	
	+	-	-	-	-	BK-7	Pinholes after aging > 10 days
	+	+	+	+	-	F.S.	Pinholes after aging > 10 days
AlF_3; 100°C				-		CaF_2	Pinholes after aging > 10 days
	+	-	-	-	-	BK-7	Pinholes
	+	+	-	-	-	F.S.	Pinholes after aging > 10 days
MgF_2; 400°C				+		CaF_2	
	+	+	+	+	+	BK-7	
	+	+	-	-	-	F.S.	Cracks (50 l)
MgF_2; 100°C				(+)		CaF_2	
	+	+	(+)	(+)	(+)	BK-7	
	+	+	-	-	-	F.S.	Cracks (10 l)
YF_3; 400°C	(+)	-	-	-	-	All	Pinholes
YF_3; 100°C	(+)	-	-	-	-	All	Pinholes
GdF_3; 400°C				+		CaF_2	
	+	+	+	+		BK-7	
	+	+	-	-		F.S.	Cracks (10l)
GdF_3; 100°C							
	+	+	-	-		BK-7	Hazy
	+	+	-	-		F.S.	Hazy
LaF_3; 400°C				-		CaF_2	Cracks (5 l)
	+	+	-	-	-	BK-7	Cracks (10 l)
	+	+	-	-	-	F.S.	Cracks (5 l)
LaF_3; 100°C				-		CaF_2	Pinholes
	+	+	+	-	-	BK-7	Hazy
	+	+	+	-	-	F.S.	Hazy
NdF_3; 400°C				+		CaF_2	
	+	+	-	-	-	BK-7	Cracks (20 l)
	+	-	-	-	-	F.S.	Cracks (10 l)
NdF_3; 100°C				-		CaF_2	Hazy
	+	+	+	-	-	BK-7	Hazy after aging > 10 days
	+	+	+	-	-	F.S.	Hazy after aging > 10 days

Layers marked with "+" showed no defects
Layers marked with "(+)" were damaged by rubbing with lens tissue and acetone
Layers marked with "-" showed one of the following defects:
--cracks (mean separation is given in brackets)
--extremely high pinhole densities
--hazy appearance without any detectable fine structure.

Damage thresholds for the multilayer coatings are presented in Table 29 and in Figure 61. Those combinations containing Al_2O_3 as the high index material again exhibit low damage thresholds. Also, correlating with the single layer results are the high damage thresholds for NdF_3/MgF_2, LaF_3/AlF_3 and GdF_3/AlF_3. The intermediate thresholds obtained for NdF_3/AlF_3 and GdF_3/AlF_3 do not correlate well with the single layer results. This was attributed to unfavorable deposition conditions with possible improvements by optimizing process parameters.

Table 29. Optical Data of the Deposited Multilayer HR Stacks

Materials	L_c (nm)	No. of layers	R_{exp} (%)	R_{th} (%)	T_{exp} (%)	T_{th} (%)	E_{dam} (J/cm^2)
Al_2O_3/SiO_2	193	61	92.7	93.5	<0.1	0.2	0.26
Al_2O_3/SiO_2 (IBS)	193	41	93.5	94.6	0.2	0.2	---
Al_2O_3/AlF_3	193	39	92.2	97.9	<0.1	<0.1	0.20
Al_2O_3/MgF_2	199	41	96.2	98.4	0.1	<0.1	0.07
NdF_3/AlF_3	193	41	97.6	99.0	0.3	<0.1	0.64
NdF_3/MgF_2	187	39	96.5	98.1	0.3	0.1	1.14
LaF_3/AlF_3	188	41	97.6	98.3	0.5	0.1	1.35
LaF_3/MgF_2	193	41	97.2	97.6	0.5	0.4	1.52
GdF_3/AlF_3	200	41	80.4	98.3	2.1	0.2	0.71

In some cases, the central wavelength λ_c is different from 193 nm. For these coatings, the R and T data were taken at the individual values of λ_c.

3.3.2 Chalcogenide and Chalcogenide/Fluoride Multilayers

A scanning electron microscopy (SEM) was used by Johnson, et. al. (Ref. 31) to identify defects in $ZnSe/ThF_4$ multilayer mirrors which may be responsible for onset of damage. $(ZnSe/ThF_4)^5$ multilayers designed for 3.8 μm reflectance were evaporated on Mo substrates overcoated with Au. The vapor stream was electrostatically filtered for two of the three mirrors studied to reduce the number of particulates in the coating.

In studying the damage morphology, oblong shaped damage sites oriented perpendicular to the electric field of the laser were found to occur in a large erosion pattern which is somewhat bigger than the $^1/e^2$ laser spot size (150 μm). The oblong sites varied with the density of particulates, the orientation effect not occurring in areas where there were no particulates in the damage spot. Particulate density was lower for the electrostatically filtered sample. The oblong

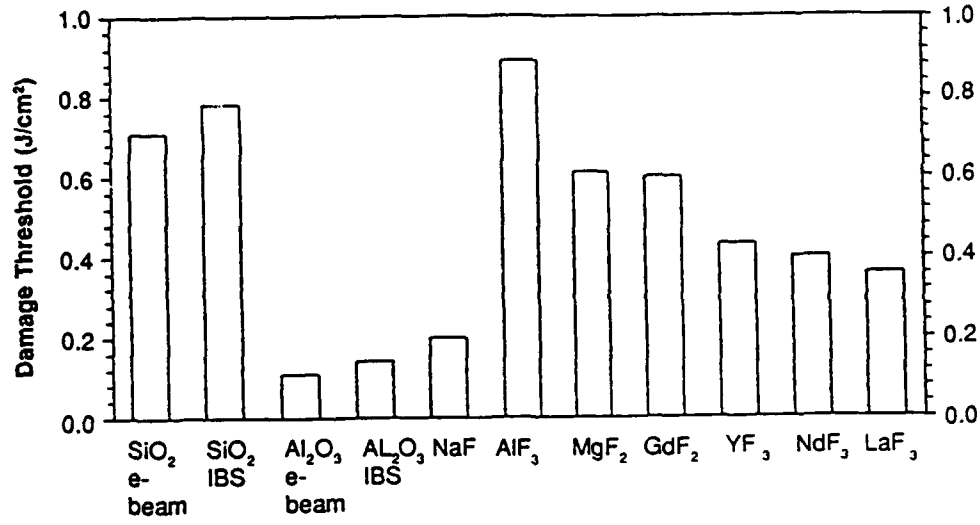

Figure 60. Damage thresholds at 193 nm of single layers (thickness: typically 400 nm).

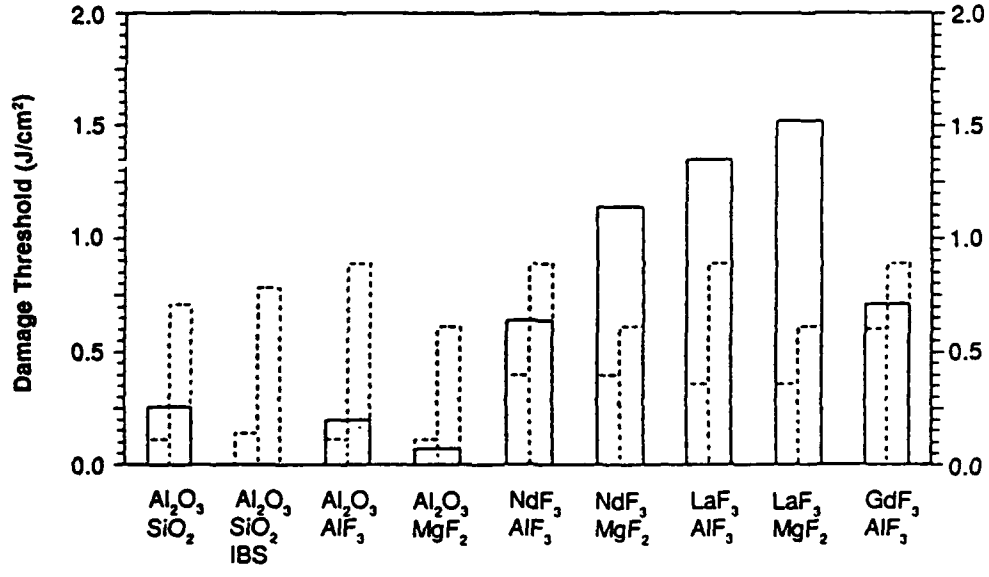

Figure 61. Laser induced damage thresholds at 193 nm of high-reflecting multilayer stacks. The dashed lines indicate the thresholds of the corresponding single layer results.

shaped craters may be due to the interference between the incident laser beam and the scattered waves from the surface particulate.

Another damage morphology observed involved selected erosion at embedded particulates beneath the ZnSe layer. Auger depth profiling indicated the particle was composed of calcium, carbon and oxygen (the bulk ThF_4 may have been stored with a $CaCO_3$ desiccant). Other damage related morphologies observed were pin holes and high stress as indicated by selective crater formation within a larger erosion pattern and cracking at the edges of damage craters.

An HF/DF laser was used for damage testing. In the DF mode (λ = 2.7 μm), the laser did not produce consistently high enough fluence to induce damage. When needed, modes, including HF (λ = 2.7 μm) were used. The spot size for nearly all experiments was 150 μm (500 μm for one damage site) and the pulse length was 1 μsec. Onset of damage is shown in Figures 62 and 63 for low and high defect mirrors, respectively. Tests were performed using one pulse per site with a 0.5 mm separation. The number of pulses at a given fluence was dependent on reducing the uncertainty in the damage frequency below a desired level. A total of 738 pulses was used for Figure 62, and 1010 pulses for Figure 63. The low defect mirror exhibited superior damage resistance relative to the high defect mirror.

Coatings of ZnSe and ZnS were deposited by Lewis, et. al. (Ref. 32) by molecular beam evaporation to assess the improvement in damage threshold achievable by producing films of near theoretical density. ZnSe and ZnS exhibit a columnar polycrystalline morphology which plays an important role in determining resistance to laser induced damage. It is thought that void formation in such structures is enhanced at grain boundaries and that diffusion of impurities, especially water, readily proceeds along such paths. The presence of heterogeneous impurities at such grain boundaries also results in generation of compressive stresses in the film. Such stresses are increased by variations of parameters during deposition which ultimately lead to poor adherence. It is therefore desirable to synthesize films not having polycrystalline columnar morphology. This work examined the limits tc which coatings exhibiting this morphology could be taken. While films deposited by molecular beam evaporation exhibited polycrystalline columnar morphology when examined by cross-section transmission electron microscopy, no voids could be detected. However, a high density of microtwins and stacking faults were evident suggesting further improvements in damage threshold may be feasible.

Substrates were cleaned with solvents prior to loading and further cleaned by Ar^+ beam bombardment in an attached chamber prior to introduction into the ultra high vacuum deposition

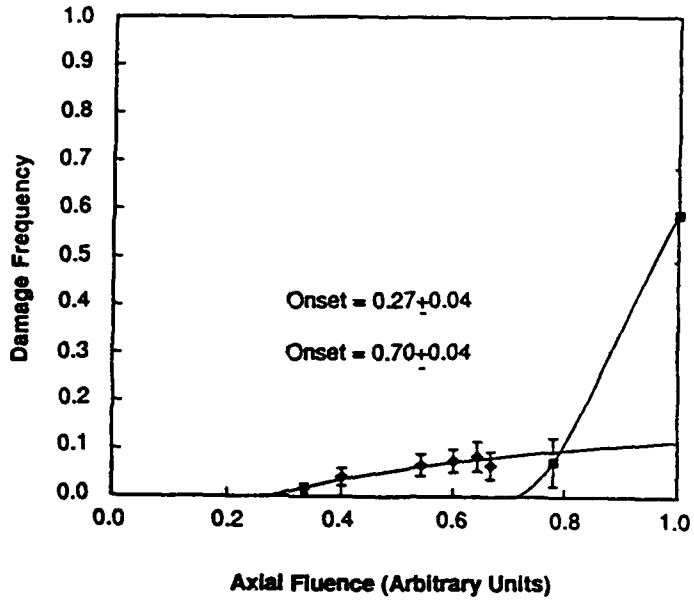

Figure 62. Single-shot laser damage frequency data for the low-defect mirror.

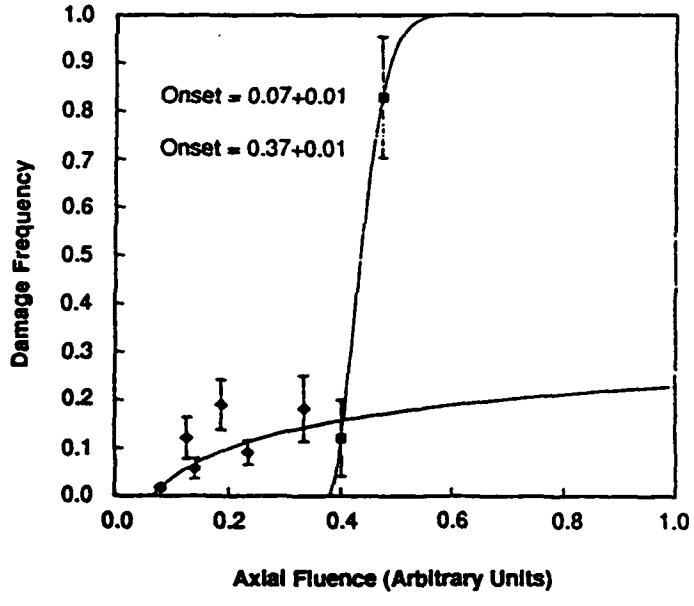

Figure 63. Single-shot laser damage frequency data for the high-defect mirror.

chamber (10^{-11} mbar). The deposition chamber contained Knudsen cells charged with broken lumps of ZnSe (for stoichiometric beams of Zn and Se_2), ZnS (for beams of Zn and S) and AgS (for a S beam). Coatings were deposited on ZnSe, GaAs, Si and Ge substrates. Coatings were mirror smooth replicating the substrate topography.

One micron thick ZnSe films were grown on polycrystalline ZnSe substrates. The ZnSe source temperature was 950°C and the substrate temperature was 175°. The growth rate was 1.2 μm/hour at a partial pressure of $2x10^{-10}$ mbar (H_2O) and $2x10^{-10}$ mbar (CO).

Quarter-wave (λ = 10.6 μm) thick ZnS films were also deposited by the same technique on Ge substrates at 50°C. An S_2 flux (Ag_2S Knudsen source) was used to improve sticking of the ZnS film. Films were deposited under high vacuum and under conditions simulating conventional vacuums: $p(H_2O)$ 2.5 x 10^{-6} mbar, $p(H_2)$ 7 x 10^{-7} mbar, p(CO) 3 x 10^{-7} mbar, and $p(H_2S)$ 4 x 10^{-7} mbar, for comparison of laser induced damage.

Two separate TEA CO_2 lasers were used to examine the dependence of damage threshold on pulse length. One laser provided a 33 nsec FWHM gain switch spike followed by a 1700 nsec tail. The other laser provided a longer pulse comprised of a single, slightly skewed gaussian peak (no tail) of 340 nsec FWHM. The damage threshold for the short pulse and a 102 μm spot size was 60 to 73 J/cm² which exceeds the 50 to 60 J/cm² threshold measured on the uncoated region of the same sample. The difference was attributed to the presence of residual surface impurities on the substrate which had been removed in the coated region by predeposition ion beam cleaning. For the longer pulse length (340 nsec) the damage threshold of the ZnSe coating was found to be 31 to 38 J/cm² for a 180 μm spot size. Micrographs revealed that damage initiated at discrete microscopic inclusions resulted in craters some 10 μm in diameter. The uncoated rear surface of the substrate always damaged at these energy densities.

The damage threshold for the ZnS coatings on Ge substrates were in the range of 15 to 16 J/cm² (33 nsec, 200 μm spot) compared to 16.8 to 24 J/cm² (60 nsec, 140 μm spot) measured by others for clear regions of single layer ZnS/Ge AR coatings. Damage threshold of the Ge substrate was on the order of 25 J/cm². These substrates were observed to contain a great deal of polishing debris and other visible defects. Comparison of ZnS coatings deposited at ultra high vacuum with deposits at conventional pressures exhibited equivalent damage thresholds (16 J/cm²). However, morphology of the damaged film revealed the UHV film adhered more strongly to the substrate.

Damage thresholds of ZnS films on Ge and Si substrates synthesized by thermal evaporation and electron beam evaporation were compared by Gibson, et. al. (Ref. 33). The

principal aims were to identify the sources of damage relative to surface and bulk properties and relate these to the deposition conditions. Attempts were made to identify methods of increasing damage resistance by optimizing deposition conditions. The films were deposited in optical thicknesses of $\lambda/4$, $\lambda/2$, $3\lambda/4$ and λ where $\lambda = 10.6$ μm. The Ge substrates were polished with alumina (Linde A, 0.3 μm). The following sets of films were deposited: (1) thermal evaporation on Ge (120°C), (2) thermal evaporation on Ge (200°C), (3) electron beam evaporation on Ge, (4) $\lambda/4$ thermal evaporation on ZnS (200°C), and (5) $\lambda/4$ thermal evaporation on Si (200°C). A $\lambda/4$ ZnS AR coating was put on the back of the substrate to eliminate coherence effects which would complicate interpretation of measurements made. The following measurements were made on the films: (1) CO_2 laser calorimetry, (2) CO_2 pulsed laser induced desorption spectrometry, and (3) CO_2 laser damage threshold.

Laser damage tests were performed using a CO_2 TEA laser with a 100 nsec spike and 2 μsec tail. Laser damage thresholds were defined to be the peak energy density corresponding to the zero probability of damage. The ratio of coated to uncoated damage thresholds are shown in Tables 30 and 31. As the number of quarter waves deposited increases, more energy is coupled into the substrate surface. For uncoated Ge, transmission is 64%. For $\lambda/4$ and $3\lambda/4$ ZnS on Ge, transmission is 99%, whereas $\lambda/2$ and λ films have transmission of 64%. Consequently, if the damage threshold of the ZnS film on Ge is limited by damage to the substrate, the ratio of coated to uncoated damage thresholds will be 64% for $\lambda/4$ and $3\lambda/4$ films and about 100% for $\lambda/2$ and λ films. Based on Table 30, films thermally evaporated at 200°C and electron beam deposited films are substrate limited while films thermally deposited at 120°C are film limited. This was confirmed studying the damage morphology with a Nomarski microscope.

Table 30. Ratio of Film to Substrate Laser Damage Thresholds for ZnS on Ge

Film Thickness (No. of 1/4 Waves)	LDT (Film)/LDT (Substrate)		
	Thermal "Cold"	Thermal "Hot"	Electron Beam
1	0.26	0.63	0.60
3	0.48	0.65	0.63
2	0.63	0.92	0.99
4	0.66	0.94	1.05
Probable damage source	Film	Substrate	Substrate

Table 31. ZnS Films on High LDT Substrates

	LDT (Jcm^{-2})		LDT Ratio (Coated:Uncoated)	
Substrate Type	Substrate Only	With λ/4 ZnS Film on Both Sides	Experimental	Theoretical if Substrate Limited
Si	66	38	0.58	0.7
ZnS	70	69	0.99	1.00

The effect of prepulsing the ZnS/Ge films deposited at 120°C at fluences below the damage threshold did not increase the damage threshold for the λ/4 film. However, for thicker films deposited at the same temperature, it can be seen from Figure 64 that energy densities in excess of 10 J/cm_2 cause an increase in damage threshold. As can be seen from Figure 65 (d), prepulsing at 11 J/cm^2 decreases probability of damage to values equivalent to films thermally deposited at 200°C or by electron beam evaporation. Since neither the Ge substrate nor films deposited by electron beam nor thermally deposited at the higher temperature showed prepulsing effects, it was surmised that the films deposited at the lower temperature contain a desorbable contaminant limiting their damage threshold. This was confirmed by laser calorimetry and laser induced desorption analysis.

A similar analysis of the films deposited on higher damage resistant substrate (Si and CVD ZnS) at 200°C indicated that ZnS on Si is film limited and ZnS on ZnS is substrate limited. Supporting data is shown in Table 31. Results were again supported by studying the damage morphology. Since damage occurred at the ZnS/Si interface, it is expected that a film substrate reaction may have occurred.

Two component films consisting of ZnS and ZnSe were successively deposited by Lewis, et. al. (Ref. 34) as discrete layers 50 to 300 Å thick with objective of modifying the columnar growth exhibited by the individual components. Since the materials have different lattice constants (5% difference), it was anticipated that epitaxial growth of successive layers onto each other would not be possible suppressing thus propagation of columnar grains at each interface. The expectation was the achievement of more dense films exhibiting higher damage thresholds. The films were grown by molecular beam deposition in an ultra high vacuum deposition system. These two component films were compared to ZnS films on Ge substrates deposited at 50°C. The ZnS films were found to be comparable to the ZnSe films discussed in Reference 32, being very dense and exhibiting no detectable pores. However, unlike ZnSe, the columnar structure of ZnS did not

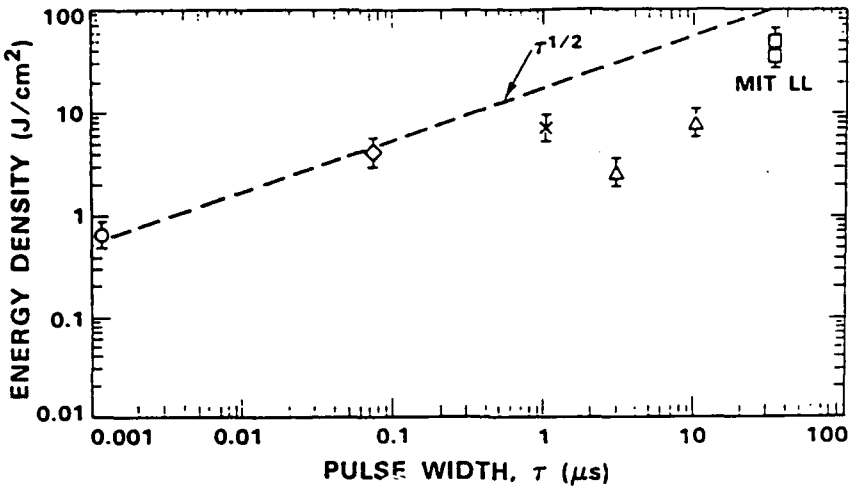

Figure 64. Energy density damage threshold vs. pulse width. The thresholds at 1.2 ns and 70 ns are from References 1 and 2, that at 1 μs is from Reference 3, and those at 3 μs and 10 μs are from Reference 4. (Reference numbers stated refer to document from which this data was extracted.)

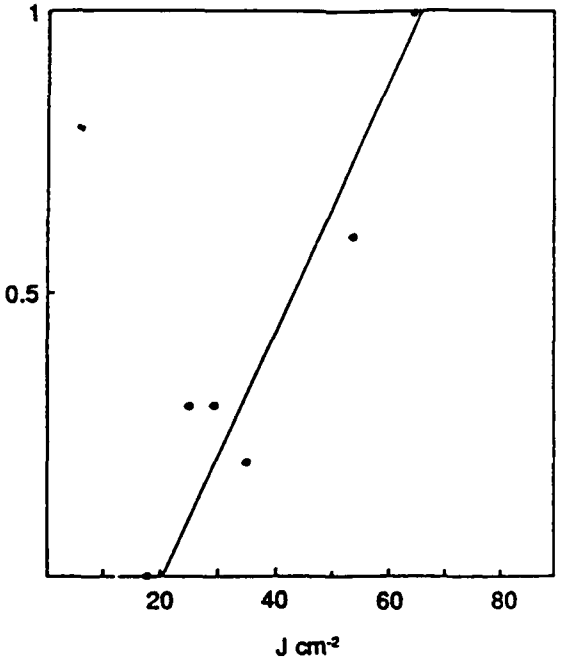

Figure 65. Laser damage probabilities of a ZnS/BaF_2 partial reflector at 1.06 μm.

propagate through the film thickness and the stacking fault contrast within the columnar grain was no longer perpendicular to growth direction. The polycrystalline structure was less ordered and the degree of fiber texture somewhat reduced compared to ZnSe.

Clusters of dislocation loops were observed in the Ge substrate caused by abrasion during polishing and a thin amorphous region was evident at the surface arising from damage induced during ion cleaning.

Microstructure of the two component films ($ZnSe_x S_{1-x}$) deposited on glass coverslips was also similar to that of ZnSe, again exhibiting columnar characteristics. Apparently, the 80 Å thick ZnS sublayer was too thin to prevent propagation of the columnar structure. However, the films had a high degree of interface perfection achieved by the absence of voids and inclusions. Close examination of grain boundary regions showed a similar lack of porosity.

The damage thresholds shown in Table 32 were determined using a short cavity CO_2 TEA laser operating at 10.6 μm wavelength with a 33 nsec FWHM pulse having a tail extending to 1700 nsec. Beam diameter at the sample was 100 μm. Damage was detected using a video camera mounted on a 10X microscope objective close to the sample.

Table 32. Laser Damage Thresholds of Various UHV-Produced Films

Film	Substrate	LIDT/Jcm^{-2}
Uncoated	Ge*	25
ZnS	Ge*	15-16
Uncoated	ZnSe	50-60
ZnSe	ZnSe	60-73
ZnS	ZnSe	79
ZnS_xSe_{1-x}	ZnSe	56-57
$(ZnS/ZnSe)_n$	ZnSe	54-60

All LIDT values determined for pulse lengths of 32 nsec FWHM and $1/e^2$ beam diameters of 100 μm.

*Denotes substrates affected by surface work damage.

The ZnS films on Ge substrates were cross sectioned and their microstructure examined by TEM in the laser damaged regions. Based on this examination, it was argued that damage originated in the regions of high absorption in the Ge surface at dislocation loop clusters caused by

abrasives during polishing. Once heating had been initiated, absorption increased rapidly and the process of thermal runaway ensued resulting in film ablation above the substrate and plasma formation. As a result of this plasma heating, surface melting of the ZnS film was observed at positions away from the damage site center.

Damage thresholds of a 2 μm thick ZnS/ZnSe film of 80 Å and 240 Å layers, respectively, was compared with that of the ZnS_x Se_{1-x} alloyed film on a ZnSe substrate. Damage thresholds were found to be nearly equivalent and within the range measured for the uncoated ZnSe substrate. However, the two component films have slightly lower thresholds than single component ZnS or ZnSe films.

The damage threshold of a variety of AR coatings on CdTe substrates were determined by Eng, et. al. (Ref. 35) using a CO_2 laser with an ultra wide pulse (tens of microseconds). Specifics of the samples tested are summarized in Table 33. The substrates were acquired from two different sources and AR coated by a number of vendors. Coating materials were combinations of ThF_4 and ZnSe. Damage test results are tabulated in Tables 34 to 37. The laser pulse repetition frequency was 1 Hz. The pulse width FWHM was 35 μsec. The spot diameter was 2.73 mm for samples 1 to 4 and 1.06 mm for samples 5 to 48. In tests with the larger spot diameter, it was difficult to achieve damage. Sample CT-2, however, damaged at a rather low level due to a high density of surface defects. For damage test numbers 5 to 8 (sample CT-1), energy density was gradually increased until damage was observed at 30 J/cm^2 after two shots. Similarly, CT-6 (having the same specifications as CT-1) damaged at 30 to 36 J/cm^2 after 60 shots. Other test numbers are representative of conditioning runs with gradually increasing energy density. In Table 35, three damage sites were obtained on sample CT-3 after preconditioning at lower energy densities. Thresholds for the three sites were in the range of 34 to 40 J/cm^2. In Table 36, the laser polarization was purposely changed between tests 29 to 32 and tests 33 to 36 to determine if change in the electric field intensity influences the damage threshold. It was ascertained that 30% change in electric field due to the change in polarization had little effect and it was therefore concluded that damage is mainly thermal in origin. Further results for sample CT-4 in Table 37 indicated a damage threshold of 50 J/cm^2 (test number 43), nearly two orders of magnitude higher than data reported for nanosecond pulses. However, subsequent tests resulted in a threshold of 32 J/cm^2, the reduction thought to be due to surface contamination related to debris from an adjacent damage site from an earlier test.

Energy density damage thresholds as a function of pulse width, based on other studies, are shown in Figure 64. Observed thresholds relative to short pulses are more than an order of

Table 33. CdTe Test Sample Specifications

Sample Number	CT-1	CT-2	CT-3	CT-4	CT-5
Crystal Surface	Polycrystal	Polycrystal	(111) or (110)	(111) or (110)	(111) or (110)
Crystal Growth	II-VI Inc.[a]	Unknown	II-VI Inc.[a]	II-VI Inc.[a]	II-VI Inc.[a]
AR-Coat Type	ThF_4/ZnSe	ThF_4	ZnSe/ThF_4/ZnSe	ThF_4/ZnSe	ThF_4/ZnSe
Final Mechan. Polish	0.3 lm	Ultrafine (mm)	0.3 lm	0.3 lm	0.3 lm
Chem/RF Cleaning	Yes/No	No/Yes	Yes/Yes	Yes/No	Yes/No
Evaporation	Thermal	E-beam	Thermal	E-beam	Thermal
Substrate Temp., °C	150	100	200-250	150	200

[a] Modified Bridgeman method within doping.

Table 34. Damage Test Results on CdTe Samples

Damage Test Number	Sample Number[a]	Peak Energy Density (J/cm^2)	Number of Shots	Polarization	Results[a]
1	CT-1	7.4-9.6	900	Linear	ND
2	CT-1	5.1-6.7	3600	Linear	ND
3	CT-2	3.9-5.3	900	Linear	ND
4	CT-2	5.3	300	Linear	D
5	CT-1	6-8	600	Linear	ND
6	CT-1	12-16	600	Linear	ND
7	CT-1	20-25	600	Linear	ND
8	CT-1	30	2	Linear	D
9	CT-6[b]	8-10	1200	Linear	ND
10	CT-6	18-22	600	Linear	ND
11	CT-6	24-30	600	Linear	ND
12	CT-6	30-36	60	Linear	D

[a] ND = no damage; D = damage.
[b] The fabrication process for sample CT-6 is the same as that for CT-1.

Table 35. Damage Test Results on CdTe Samples

Damage Test Number	Sample Number[a]	Peak Energy Density (J/cm^2)	Number of Shots	Polarization	Results[b]
13	CT-3(111)	16-22	600	Linear	ND
14	CT-3(111)	22-26	600	Linear	ND
15	CT-3(111)	26-30	600	Linear	ND
16	CT-3(111)	32-34	5	Linear	D
17	CT-3(110)	8-10	600	Linear	ND
18	CT-3(110)	16-20	600	Linear	ND
19	CT-3(110)	26-32	600	Linear	ND
20	CT-3(110)	38-40	5	Linear	D
21	CT-3(110)	10-16	600	Linear	ND
22	CT-3(110)	16-22	3600	Linear	ND
23	CT-3(110)	26-32	600	Linear	ND
24	CT-3(110)	38	5	Linear	D

[a] Numbers within parentheses denote crystal surface.
[b] ND = no damage; D = damage.

Table 36. Damage Test Results on CdTe Samples

Damage Test Number	Sample Number[a]	Peak Energy Density (J/cm^2)	Number of Shots	Polarization	Results[b]
25	CT-3(110)	10-16	600	Linear	ND
26	CT-3(110)	16-22	3600	Linear	ND
27	CT-3(110)	26-32	600	Linear	ND
28	CT-3(110)	38	5	Linear	D
29	CT-1	6-8	600	Linear	ND
30	CT-1	12-16	600	Linear	ND
31	CT-1	28-32	600	Circular	ND
32	CT-1	34	20	Circular	D
33	CT-3(110)	7-10	1200	Linear	ND
34	CT-3(110)	18-22	600	Linear	ND
35	CT-3(110)	26-32	600	Circular	ND
36	CT-3(110)	34-36	300	Circular	D

[a] Numbers within parentheses denote crystal surface.
[b] ND = no damage; D = damage.

Table 37. Damage Test Results on CdTe Samples

Damage Test Number	Sample Number[a]	Peak Energy Density (J/cm^2)	Number of Shots	Polarization	Results[b]
37	CT-4(110)	6-8	600	Linear	ND
38	CT-4(110)	8-12	600	Linear	ND
39	CT-4(110)	12-16	600	Linear	ND
40	CT-4(110)	16-21	600	Linear	ND
41	CT-4(110)	24-30	600	Linear	ND
42	CT-4(110)	30-40	600	Linear	ND
43	CT-4(110)	45-50	5	Linear	D
44	CT-4(110)	6-8	600	Linear	ND
45	CT-4(110)	16-20	600	Linear	ND
46	CT-4(110)	20-24	600	Linear	ND
47	CT-4(110)	24-28	600	Linear	ND
48	CT-4(110)	30-32	15	Linear	D

[a] Numbers within parentheses denote crystal surface.
[b] ND = no damage; D = damage.

magnitude higher. The damage thresholds for long pulses fall below the square root of pulse width line extrapolated from short pulse data.

Work performed by Lewis, et. al. (Ref. 36) had the objective of assessing the role of interfaces in multilayers in contributing to laser induced damage. While past work has indicated that the electric field distribution in the multilayer is an important factor in determining the damage threshold, as is the laser pulse width, dependence as exhibited by experiments may be masked by coating defects. Defects due to contamination are most likely to occur at interfaces, particularly at the substrate interface. Since the peak electric field in $\lambda/4$ multilayers also occurs at these interfaces, it is often not clear which is the predominating cause of failure. The distributed Bragg reflector (DBR) design was selected as a candidate for distinguishing electric field and interface effects within the multilayer structure. The particular DBR structure used in this work was characterized by an essentially uniform refractive index with very thin sharp discontinuities at $\lambda/2n$ intervals. The peak electric field in this structure is in the high index layers ($n = 2.2$) which are separated by thin low index layers ($n = 1.5$). The substrate index is also 1.5. The relative position of the peak in the high index layer can be shifted simply by altering the phase of the

structure by adding to or subtracting from multilayer material at the air/film interface. The peak field can be placed close to an interface allowing its effect on damage threshold to be assessed. Alternatively, the peak field may be allowed to remain close to the center of the high index layer to explore the effect on laser damage threshold of incorporating a few atomic layers of different material at this position. Total reflectance and bandwidth can be varied by selecting the number of layers and the index difference. Similar effects can be achieved with the reverse structure of thicker low index films separated by thin high index layers. The design has the added advantage of allowing use of techniques for preventing propagation of columnar microstructure.

HR coatings using these design principles were made by molecular beam epitaxy. Substrates were cleaned prior to deposition using a raster scanned argon ion beam. Two types of multilayers were deposited to assess interface perfection. In the first, a BaF_2/ZnSe multilayer was deposited with each layer 10 nm thick. This was ion beamed to determine the chemical composition of the layers at discrete intervals. At the ZnSe/BaF_2 interface, chemical reactivity was indicated by the presence of Zn in ZnF_2. The second type of multilayer involved fabricating designs with increasingly thinner $\lambda/2$ distributed layers. Comparison of measured reflectance with matrix technique calculations indicated a diffused interface between layers based on lower reflectance than expected as may result from chemical reaction or diffusion. XTEM micrographs revealed interface roughness on the order of 25 Å with a period of 150-300 Å. This is fixed largely by crystallite diameters of ZnS layers of about 100 Å. Based on the similar morphology and growth behavior of ZnSe it was assumed that an interface spread of 25 Å also occurs for ZnSe/BaF_2 structures. Models assuming a linear gradation of index over 25 Å provided agreement with spectral results implying a high degree of chemical reaction between the material.

Some improvement was noted for PbF_2/ZnS because of the higher mobility of PbF_2 during growth. The measured optical density at the reflection maximum slightly exceeding theoretical prediction suggests lower interdiffusion and reaction than for ZnS/BaF_2.

Based on shifts in the reflectance peak to longer wavelengths when heated, it was deduced that water was not liberated and the films were not porous.

Laser damage threshold measurements were made using a Nd:YAG laser (λ = 1.06 μm) with a 10 nsec pulse width. Spot size was 59 μm. Measurements were made on a single shot basis.

Damage probabilities determined in 1 on 1 experiments at λ = 1.06 μm are shown in Figures 65 and 66 for a DBR designed to have peak reflectivity of 60% at 1.06 μm. The zero

probability threshold is close to 20 J/cm^2, similar to values obtained on films of the component materials. Damage initiated at the glass substrate in all cases implying that high peak fields within the $\lambda/2$ ZnS layers do not themselves appear to initiate damage. This may be a consequence of the relatively higher perfection of the MBE grown structures with high crystallinity and absence of absorbing inclusions.

3.4 COMPARISON OF MBE AND CVD DEPOSITION PROCESSES

BaF_2 and PbF_2 were examined as components in multilayers with ZnS and ZnSe by Lewis, et. al. (Ref. 37). The fluoride coatings were deposited in ultra-high vacuum from Knudsen sources, the coating materials contained in high purity graphite crucibles carefully out gassed following baking of the chamber at 180°C. Deposition rates ranged from 0.1 to 1 micron per hour. ZnSe and ZnS films were deposited from high purity source materials prepared by CVD and contained in graphite and pyrolytic boron nitride crucibles, respectively. Substrate temperatures ranged from 40 to 350°C. Substrates were Si, ZnSe, ZnS or glass.

The surface morphology of the room temperature deposited BaF_2 films was found to be rough and the films exhibited poor durability. High optical scattering was observed varying approximately linearly with film thickness. As the deposition temperature increased, the microstructure became more crystalline (250°C) and the films became exceptionally smooth and quite hard (350°C). Refractive index measurements (measured at 400 nm wavelength) suggested that film density increased at higher deposition temperatures (350°C). Cross sectional morphology indicated a change from no columnar growth at room temperature to a dense columnar film with increased crystallite sizes due to increased adatom mobility for films deposited at 350°C.

Barium fluoride/lead fluoride mixtures were deposited by varying the source temperatures of the two evaporants. The change in adatom mobility achieved by the joint deposition on a 40°C substrate lead to quite smooth films for BaF_2 concentrates as high as 77%.

The film microstructure was synthetically controlled by repetitively depositing a composite built up from 75 Å of BaF_2 interspersed between 115 Å of ZnS producing crystallite blocks about 80 Å in dimension. This substantially reduced porosity increased the density of the film. This technique was extended to create graded refractive index AR coatings with exceptionally wide bandwidths by varying the relative contributions of BaF_2 and ZnS as the deposition proceeds. This technique was used to deposit 2 micron thick films with index linearly graded from 1.7 to 2.4. The film consisted of 240 discrete layers with thickness varying from 2 Å to 240 Å.

Interface absorption in multilayers of PbF_2 and ZnS was considered problematic from the standpoint of a solid state reaction producing PbS, a narrow bandgap material (0.29 eV) which would seriously degrade transmission. For PbF_2/ZnS digital graded hetrostructures, significant absorption was found to commence at wavelengths as high as 1900 nm. Such absorption was found to be suppressed by a 20 to 30 Å layer of BaF_2 at the PbF_2 and ZnS interface. While BaS may form, it has a relatively wide bandgap, and does not produce deleterious loss in the visible spectrum.

The effects of film roughness on damage threshold for BaF_2 films on ZnSe and Si substrates were determined. Also damage thresholds were determined for alloyed film $(BaPb)F_2$, graded digital coatings, digital coatings and graded buffered digital coatings. Damage thresholds were measured at a wavelength of 10.6 microns using a short cavity CO_2 TEA laser with a pulse length of 33 nsec with the beam focused to a 100 micron diameter spot. Ten separate irradiations were carried out at each nominal value of incident energy in a matrix pattern. Damage was assessed by a 400X optical microscope. Damage thresholds were determined from statistical probability plots produced from up to 80 separate irradiations. A typical statistical plot is shown in Figure 67 corresponding to a BaF_2 film deposited on a ZnSe substrate at room temperature. The minimum energy required to just produce damage is defined as LD_0 and the maximum energy to produce damage on every spot is defined as LD_{100}. These values are listed in Table 38 for BaF_2 coatings on ZnSe substrates deposited at different temperatures and thus having different degrees of scatter (surface roughness). The value of LD_0 is found to be approximately constant while LD_{100} is found to increase with surface roughness. It is hypothesized that rougher surfaces redistribute the electric field intensity, increasing the damage threshold.

Table 38. Laser Damage Thresholds of Barium Fluoride Films on ZnSe Substrates at 10.6 μm

Thickness (μm)	Growth Temperature (°C)	Damage Threshold (J/cm^2)		Normalized 250 nm Scatter for 1 μm Film Thickness, i.e., %/μm
		LD(0)	LD(100)	
Uncoated	---	49	74	2.0
1.7	40	46	104	7.7
3.0	116	41	79	9.8
1.4	250	40	60	12.8
1.8	350	44	48	5.2

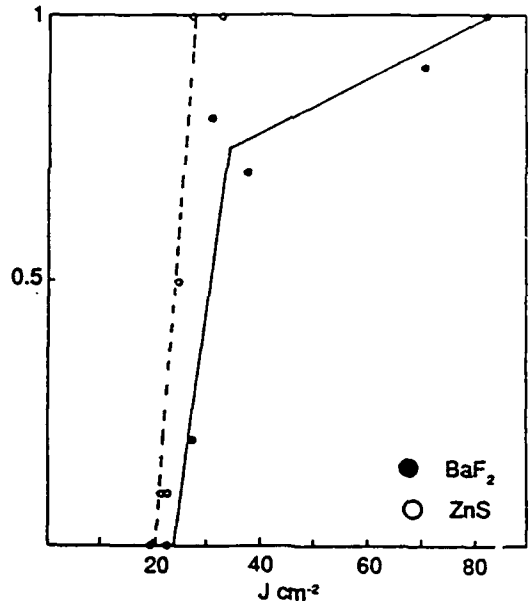

Figure 66. Laser damage probabilities of thin films of the component materials of the design used for the tests in Figure 65.

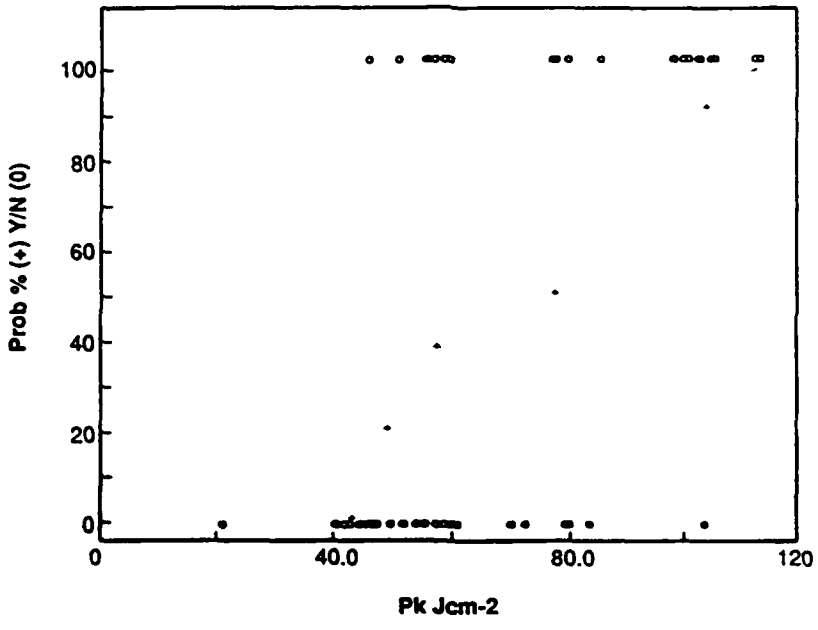

Figure 67. Typical damage probability plot determined for a film of barium fluoride deposited on ZnSe at ambient temperature.

Table 39 presents data on more dense BaF_2 films on ZnSe and Si substrates. It is clear from the data that thresholds vary significantly and are not correlated to the refractive index, (an indicator of density of the film). The thresholds for the mixed alloy films are somewhat intermediate between PbF_2 and BaF_2 deposited at room temperature and identical to digital PbF_2/BaF_2 hetrostructures. The digital hetrostructure containing PbF_2 with ZnSe or ZnS, whether graded or not, has a damage threshold equivalent to PbF_2. Since this threshold is not intermediate between that of PbF_2 and ZnSe or ZnS it is suggested that PbF_2 is the damage controlling component. This is thought to be due to the non-stoichiometric character of the material. Contrastingly, the damage threshold of digitally graded hetrostructures containing BaF_2 are exceptionally high.

3.5 OTHER RELEVENT ISSUES

Several different thin film designs using $ZnSe/ThF_4$ on Si, Ge and ZnSe substrates were exposed to CO_2 laser irradiation by Deng, et. al. (Ref. 38) to determine damage threshold. Designs tested were standard two layer "V" coats with thin air interface layers for AR, partial reflectors and high or total reflectors. Analysis showed a 25% increase in the peak electric field at the air interface for the AR coatings relative to the other designs with the field remaining high through the next interface. The high field at the interface connected with the potential for contaminants, nucleation defects and mixing via diffusion was identified as a potential cause of lower damage threshold that could be improved by redesign.

Thin film morphology was assessed by Nomarski microscopy showing rises and pits in the coatings at about 100/micron spacings and by visible light scattering (λ = 0.5145 μm) indicating discrete scattering sites at a spacing of about 0.5 mm. Scattering sites were widely spaced relative to the beam diameter with no attempt to include or not include a site in the test beam.

Damage thresholds shown in Tables 40 and 41 were measured using a CO_2 laser operated in the TEM_{00} mode, intensity on the sample being controlled by a single wire grid polarizer. A ZnSe lens focused the beam to a 60 μm spot on the sample. Pulse duration was 230 nsec. Damage threshold was taken to be the intensity midway between the lowest intensity at which damage always occurred and the highest at which it never occurred. Damage thresholds of the reflective coatings was found to be independent of the reflectance and the substrate. The defect density average threshold for the reflective coatings was 90 J/cm^2 or 150 MW/cm^2.

Table 39. Laser Damage Thresholds of Fluoride Thin Films and Multilayers

Film	Substrate	Composition %(Ba)	Refractive Index	Damage Threshold (J/cm^2)	
				LD(0)	LD(100)
	ZnSe			49	74
	Si			67	98
BaF_2	Si		1.52	68	83
BaF_2	ZnSe			68	89
PaF_2	ZnSe		1.64	22	32
PbF_2/ZnSe	ZnSe		1.73	24	74
PbF_2	ZnSe		1.85	4	35
PbF_2	ZnSe		1.89	6	46
PbF_2	Zns		1.89	51	90
$(BaPb)F_2$	Si	19.4		31	46
$(BaPb)F_2$	ZnSe	56.0	1.59	33	60
$(BaPb)F_2$	Si	77.0	1.60	27	49
d-PbF_2/BaF_2	ZnSe		(1.84)	31	47
d-PbF_2/ZnSe	ZnSe		(2.02)	21	41
d-PbF_2/ZnSe	ZnSe		(1.63)	58	89
gd-BbF_2/ZnS	ZnS			58	120
gd-PbF_2/ZnS	ZnS			27	42
gd-PbF_2/ZnS	ZnS			26	33

NOTES: Alloys denoted by eg $(BaPb)F_2$
d = digital coating
gd = graded digital coating

Table 40. Damage Thresholds of 10.6 μm Coatings

Substrate	Reflectance	Nomarski Defect Density (mm^{-2})	Energy Density (J/cm^2)	Intensity (MW/cm^2)
Si	100%	37	91 ± 18	371 ± 74
Si	100%	54	84 ± 22	359 ± 100
Si	100%	--	80 ± 31	342 ± 132
Si	100%	39	100 ± 21	410 ± 86
Ge	99.3%	23	99 ± 19	404 ± 76
Ge	99.3%	18	96 ± 21	392 ± 84
ZnSe	60%	18	86 ± 58	345 ± 58
ZnSe	85%	25	88 ± 12	361 ± 49
ZnSe	AR	27	41 ± 12	169 ± 48
ZnSe	AR	32	30 ± 9	123 ± 37

Table 41. Comparison of 0.5145 μm Scatter and 10.6 μm Damage Threshold

Type & Manufacturer	Scatter	Threshold
AR on ZnSe:		
II-VI	Low	Comparable (30 J/cm^2)
L.P.O.	High	Comparable (34 J/cm^2)
Partial Reflectors:		
II-VI	Low	Comparable (86 J/cm^2)
L.P.O.	Low	Comparable (86 J/cm^2)
100% R Coatings on Si:		
II-VI	Average	Comparable (91 J/cm^2)
L.P.O.	Average	Comparable (100 J/cm^2)

REFERENCES

1. Faizullov, F.S., et.al., "Optical Coatings for High Power Nd Lasers," NIST Special Publication 756, Laser Induced Damage In Optical Materials: 1987, pp. 440-449.

2. Zhouling, Wu, et.al., "Damage Threshold Dependence On Film Thickness," NIST Special Bulletin 775, Laser Induced Damage In Optical Materials: 1988, pp. 321-327.

3. Ghansyam Krishna, M., et.al., "Optical Properties of Low Energy Ion Assisted Deposited TiO_2 Films," NIST Special Publication 756, Laser Induced Damage In Optical Materials: 1987, pp. 280-285.

4. Zhengxiu, F., et.al., "Free Vibration Pulse Laser Induced Damage In Optical Thin Films," NIST Special Publication 775, Laser Induced Damage In Optical Materials: 1988, pp. 361-365.

5. Guenther, K. H., et. al., "Laser Damage Thresholds of Dielectric Multilayers Produced by Reactive Ion Plating Deposition," NIST Special Publication 775, Laser Induced Damage In Optical Materials: 1988, p. 320.

6. Kardach, J. A., et. al., "Photon Induced Desorption and Emission from Thin Film Dielectric Surfaces," NIST Special Publication 752, Laser Induced Damage In Optical Materials: 1986, pp. 488-504.

7. Carniglia, C. K., et. al., "Effect of Overcoats On 355 nm Reflectors," NBS Special Publication 727, Laser Induced Damage In Optical Materials: 1984, pp. 285-290.

8. Wolfe, C. R., et. al., "Laser Conditioning of Optical Thin Films," NIST Special Publication 801, Laser Induced Damage In Optical Materials: 1989, pp. 360-375.

9. Kozlowski, M. R., et. al., "Large Area Laser Conditioning of Dielectric Thin Film Mirrors," NIST Special Publication 801, Laser Induced Damage In Optical Materials: 1989, pp. 376-390.

10. Mordaunt, D. W., et. al., "Population Distribution of Conditioned Damage Thresholds On AR Coated BK-7 Glass With Varying Laser Spot Size," NIST Special Publication 801, Laser Induced Damage In Optical Materials: 1989, pp. 383-402.

11. Wilder, J. G., et. al., "Effect Of n on 1 Laser Treatment On Damage Thresholds of Selected Optical Coatings," NIST Special Publication 775, Laser Induced Damage In Optical Materials: 1988, pp. 259-264.

12. Thomas, I. M., et. al., "HR Coatings Prepared from Colloidal Suspensions," NIST Special Publication 756, Laser Induced Damage In Optical Materials: 1987, pp. 286-289.

13. Floch, H., et. al., "1064 nm and 350 nm Radiation Stability of Low Density ThO_2-SiO_2 High Reflective Coatings Deposited from Sols," NIST Special Publication 756, Laser Induced Damage In Optical Materials: 1987, pp. 290-299.

14. Brusasco, R., et. al., "Oxide Optical Coatings Prepared by Metal Organic Vapor Deposition," NIST Special Publication 756, Laser Induced Damage In Optical Materials: 1987, pp. 300-307.

15. Pond, B. J., et. al., "Stress Reduction of Ion Beam Sputtered Mixed Oxide Coatings by Baking," NIST Special Publication 756, Laser Induced Damage In Optical Materials: 1988, pp. 311-319.

16. Thomas, I., et. al., "Influence of Post-deposition Treatment by UV Light and Oxygen (ozone) on 350 nm Damage Thresholds of SiO_2 Films Deposited from Sols," NIST Special Publication 752, Laser Induced Damage In Optical Materials: 1986, pp. 297-299.

17. Wilder, J., et. al., "Chemical Vapor Deposition of TiO_2 Thin Films at Room Temperature," NIST Special Publication 752, Laser Induced Damage In Optical Materials: 1986, pp. 387-391.

18. Stewart, A. F., et. al., "The Properties of Laser Annealed Dielectric Films," NIST Special Publication 756, Laser Induced Damage In Optical Materials: 1987, pp. 369-387.

19. Rainer, F., et. al., "Database of Average-Power Damage Thresholds at 1064 nm," NIST Special Publication 756, Laser Induced Damage In Optical Materials: 1987, pp. 410-418.

20. Campbell, J. H., et. al., "Damage Resistant Optical Coatings Prepared Using High Temperature, Plasma Chemical Vapor Deposition," NIST Special Publication 801, Laser Induced Damage In Optical Materials: 1989, pp. 426-442.

21. Thomas, I. M., et. al., "High Damage Threshold AlO.OH-SiO_2 HR Coatings Prepared by the Sol-Gel Process," NIST Special Publication 801, Laser Induced Damage In Optical Materials: 1989, pp. 484-489.

22. Floch, H. G., et. al., "1-on-1 And n-on-1 Laser Strength of Binder Aided ZrO_2 and ZrO_2-SiO_2 Reflective Sol-Gel Coatings," NIST Special Publication 801, Laser Induced Damage In Optical Materials: 1989, pp. 490-508.

23. Gallegos, G., et. al., "Damage Thresholds of Antireflectron Coatings at 790 nm," NIST Special Publication 752, Laser Induced Damage In Optical Materials: 1986, pp. 484-487.

24. Foltyn, S. R., et. al., "Long Range Pulse Width Scaling of 351 nm Laser Damage Thresholds," NIST Special Publication 752, Laser Induced Damage In Optical Materials: 1986, pp. 336-343.

25. Akhtar, S. M. J., et. al., "Thermal Conductivity of Dielectric Films and Correlation To Damage Threshold at 1064 nm," NIST Special Publication 752, Laser Induced Damage In Optical Materials: 1986, pp. 345-351.

26. Deaton, T. F., et. al., "Survey of Laser Damage Thresholds for High Reflector Films at 1.315 Microns," NBS Special Publication 727, Laser Induced Damage In Optical Materials: 1984, pp. 352-355.

27. Boyer, J. D., et. al., "Angular Dependence of Thin Film Dielectric Coating Damage Thresholds Revisited," NIST Special Publication 801, Laser Induced Damage In Optical Materials: 1989, pp. 417-424.

28. Waddell, E. M., et. al., "Cluster Beam Deposition for Optical Thin Films," NIST Special Publication 756, Laser Induced Damage In Optical Materials: 1987, pp. 309-319.

29. Yoshida, K., et. al., "Highly Damage Resistant Porous Dielectric Coating for High Power Lasers In the Ultraviolet to Near Infrared Region," NBS Special Publication 746, Laser Induced Damage In Optical Materials: 1985, pp. 350-354.

30. Kolbe, J., et. al., "Laser Induced Damage Thresholds of Dielectric Coatings At 193 nm and Correlations To Optical Constants and Process Parameters," NIST Special Publication 801, Laser Induced Damage In Optical Materials: 1989, pp. 404-416.

31. Johnson, L. F., et. al., "Scanning Electron Microscopy Studies of Laser Damage Initiating Defects In $ZnSe/ThF_4$ and SiH/SiO_2 Multilayer Coatings," NBS Special Publication 727, Laser Induced Damage In Optical Materials: 1984, pp. 356-370.

32. Lewis, K. L., et. al., "Assessment of Optical Coatings Prepared by Molecular Beam Techniques," NBS Special Publication 727, Laser Induced Damage In Optical Materials: 1984, pp. 162-170.

33. Gibson, D. R., et. al., "CO_2 Laser Induced Damage In A Model Thin Film System," NBS Special Publication 746, Laser Induced Damage In Optical Materials: 1985, pp. 460-471.

34. Lewis, K. L,, et. al., "Laser Induced Damage In Dense Optical Thin Films," NBS Special Publication 746, Laser Induced Damage In Optical Materials: 1985, pp. 472-479.

35. Eng, R. S., et. al., "Measurements of Ultra-wide Pulse Damage Thresholds of Anti-Refection Coated IR Materials at 10.6 μm," NIST Special Publication 756, Laser Induced Damage In Optical Materials: 1987, pp. 451-461.

36. Lewis, K. L., et. al., "Some Studies of Thin Film Distributed Bragg Reflectors," NIST Special Publication 775, Laser Induced Damage In Optical Materials: 1988, pp. 400-413.

37. Lewis, K. L., et. al., "Fabrication of Fluoride Thin Films Using Ultra-High Vacuum Techniques," NIST Special Publication 752, Laser Induced Damage In Optical Materials: 1986, pp. 365-386.

38. Deng, H., et. al., "Single Pulsed Laser Induced Damage In IR Coatings at 10.6 μm," NBS Special Publication 727, Laser Induced Damage In Optical Materials: 1984, pp. 371-376.

THE TACTICAL WEAPON GUIDANCE AND CONTROL INFORMATION ANALYSIS CENTER (GACIAC)

GACIAC is a DoD Information Analysis Center operated by IIT Research Institute under the technical sponsorship of the Joint Service Guidance and Control Committee with members from OSD, Army, Navy, Air Force, and DARPA. The AMC Smart Weapons Management Office of the U.S. Army Missile Command provides the Contracting Officer's Technical Representative. GACIAC's mission is to assist the tactical weapon guidance and control community by encouraging and facilitating the exchange and dissemination of technical data and information for the purpose of effecting coordination of research, exploratory development, and advanced technology demonstrations. To accomplish this, GACIAC's functions are to:

1. Develop a machine-readable bibliographic data base -- currently containing over 40,000 entries;

2. Collect, review, and store pertinent documents in its field of interest -- the library contains over 14,000 reports;

3. Analyze, appraise, and summarize information and data on selected subjects;

4. Disseminate information through the GACIAC Bulletin, bibliographies, state-of-art summaries, technology assessments, handbooks, special reports, and conferences;

5. Respond to technical inquiries related to tactical weapon guidance and control; and

6. Provide technical and administrative support to the Joint Service Guidance and Control Committee (JSGCC).

The products and services of GACIAC are available to qualified industrial users through a subscription plan or individual sales. Government personnel are eligible for products and services under block funding provided by the Army, Navy, Air Force and DARPA. A written request on government stationery is required to receive all the products as a government subscriber.

Further information regarding GACIAC services, products, and participation plan, or additional copies of this State of the Art Review may be obtained by writing or calling: GACIAC, IIT Research Institute, 10 West 35th Street, Chicago, Illinois 60616-3799, Area code 312, 567-4526.

JSGCC

JOINT SERVICE GUIDANCE AND CONTROL COMMITTEE